



AFTAC Project No. VT/1705

PRELIMINARY EVALUATION OF THE NORWEGIAN  
SHORT PERIOD ARRAY

SPECIAL REPORT NO. 6  
EXTENDED ARRAY EVALUATION PROGRAM

Prepared by  
Thomas E. Barnard and Richard L. Whitelaw

T. W. Harley, Program Manager  
Area Code 703, 836-3882 Ext. 300

TEXAS INSTRUMENTS INCORPORATED  
Services Group  
P.O. Box 5621  
Dallas, Texas 75222

Contract No. F33657-71-C-084  
Amount of Contract: \$511,580  
Beginning 1 April 1971  
Ending 31 March 1972

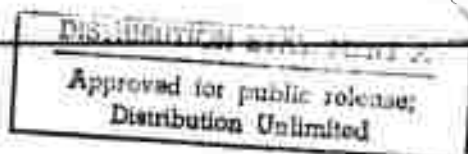
Prepared for  
AIR FORCE TECHNICAL APPLICATIONS CENTER  
Washington, D.C. 20333

Sponsored by  
ADVANCED RESEARCH PROJECTS AGENCY  
Nuclear Monitoring Research Office  
ARPA Order No. 1714  
ARPA Program Code No. 1F10

Reproduced by  
NATIONAL TECHNICAL INFORMATION SERVICE  
U.S. Department of Commerce  
Springfield VA 22151  
30 April 1972



Acknowledgement: This research was supported by the Advanced Research Projects Agency, Nuclear Monitoring Research Office, under Project VELA-UNIFORM, and accomplished under the technical direction of the Air Force Technical Applications Center under Contract No. F33657-71-C-0843.



services group

103  
N/A #14 - SEE AD 745199

AD 745198

DOCUMENT CONTROL DATA - R & D

(Security classification of title, body of abstract and indexing annotation must be entered when the overall report is classified)

1. ORIGINATING ACTIVITY (Corporate author) Texas Instruments Incorporated Services Group P.O. Box 5621, Dallas, Texas		2a. REPORT SECURITY CLASSIFICATION <b>UNCLASSIFIED</b>	
		2b. GROUP	
3. REPORT TITLE Preliminary Evaluation of the Norwegian Short Period Array, Special Report No. 6, Extended Array Evaluation Program			
4. DESCRIPTIVE NOTES (Type of report and inclusive dates) Special			
5. AUTHOR(S) (First name, middle initial, last name) Thomas E. Barnard and Richard L. Whitelaw			
6. REPORT DATE 30 April 1972		7a. TOTAL NO. OF PAGES 100	7b. NO. OF REFS 4
8a. CONTRACT OR GRANT NO. Contract No. F33657-71-C-0843		9a. ORIGINATOR'S REPORT NUMBER(S) Special Report No. 6	
b. PROJECT NO. AFTAC Project No. VT/1705		9b. OTHER REPORT NO(S) (Any other numbers that may be assigned this report)	
c.			
d.			
10. DISTRIBUTION STATEMENT APPROVED FOR PUBLIC RELEASE; DISTRIBUTION UNLIMITED			
11. SUPPLEMENTARY NOTES		12. SPONSORING MILITARY ACTIVITY Advanced Research Projects Agency Department of Defense The Pentagon, Washington, D.C. 20301	
13. ABSTRACT This report presents results from the preliminary evaluation of the Norwegian short-period Seismic Array. A description of the array itself and the data base for the evaluation is followed by discussion of noise characteristics, signal characteristics, array processing performance, detection capability, and discriminant performance.			





AFTAC Project No. VT/1705

PRELIMINARY EVALUATION OF THE NORWEGIAN  
SHORT PERIOD ARRAY

SPECIAL REPORT NO. 6  
EXTENDED ARRAY EVALUATION PROGRAM

Prepared by  
Thomas E. Barnard and Richard L. Whitelaw

T. W. Harley, Program Manager  
Area Code 703, 836-3882 Ext. 300

TEXAS INSTRUMENTS INCORPORATED  
Services Group  
P.O. Box 5621  
Dallas, Texas 75222

Contract No. F33657-71-C-0843  
Amount of Contract: \$511,580  
Beginning 1 April 1971  
Ending 31 March 1972

Prepared for  
AIR FORCE TECHNICAL APPLICATIONS CENTER  
Washington, D.C. 20333

Sponsored by  
ADVANCED RESEARCH PROJECTS AGENCY  
Nuclear Monitoring Research Office  
ARPA Order No. 1714  
ARPA Program Code No. 1F10

30 April 1972

Acknowledgement: This research was supported by the Advanced Research Projects Agency, Nuclear Monitoring Research Office, under Project VELA-UNIFORM, and accomplished under the technical direction of the Air Force Technical Applications Center under Contract No. F33657-71-C-0843.

## ABSTRACT

This report presents results from the preliminary evaluation of the performance of the Norwegian short-period Seismic Array. A description of the array itself and the data base for the evaluation is followed by discussion of noise characteristics, signal characteristics, array processing performance, detection capability, and discriminant performance.

Neither the Advanced Research Projects Agency nor the Air Force Technical Applications Center will be responsible for information contained herein which has been supplied by other organizations or contractors, and this document is subject to later revision as may be necessary. The views and conclusions presented are those of the authors and should not be interpreted as necessarily representing the official policies, either expressed or implied, of the Advanced Research Projects Agency, the Air Force Technical Applications Center, or the US Government.

# TABLE OF CONTENTS

SECTION	TITLE	PAGE
	ABSTRACT	iii
I.	INTRODUCTION	I-1
II.	NOISE ANALYSIS	II-1
	A. INTRODUCTION	II-1
	B. SPECTRAL CONTENT	II-1
	C. RMS NOISE LEVELS AND TIME VARIABILITY	II-3
	D. MULTIPLE COHERENCE	II-13
III.	SIGNAL ANALYSIS	III-1
	A. INTRODUCTION	III-1
	B. SIGNAL SIMILARITY	III-1
	C. SUBARRAY BEAM AMPLITUDE VARIATIONS	III-3
	D. SIGNAL SPECTRAL CONTENT	III-9
	E. TIME DELAY ANOMALIES	III-12
	F. COMPARISON OF NORSAR $m_b$ VALUES WITH PDE AND LASA $m_b$ 's	III-19
IV.	ARRAY BEAMFORMING RESULTS	IV-1
	A. INTRODUCTION	IV-1
	B. NOISE REDUCTION	IV-1
	C. SIGNAL DEGRADATION	IV-4
	D. SIGNAL-TO-NOISE IMPROVEMENT	IV-7
V.	PRELIMINARY ESTIMATE OF THE NORSAR SHORT-PERIOD TELESEISMIC DETECTION THRESHOLD	V-1

TABLE OF CONTENTS  
(continued)

SECTION	TITLE	PAGE
VI.	SHORT-PERIOD DISCRIMINATION	VI-1
	A. DEFINITION OF DISCRIMINANTS	VI-1
	B. NORSAR SHORT-PERIOD DISCRIMINATION RESULTS	VI-2
VII.	CONCLUSIONS AND FUTURE PLANS	VII-1
	A. CONCLUSIONS	VII-1
	B. FUTURE PLANS	VII-5
VIII.	REFERENCES	VIII-1

## LIST OF FIGURES

FIGURE	TITLE	PAGE
I-1	NORSAR SHORT PERIOD ARRAY	I-3
II-1	AVERAGE SIGNLE SENSOR AVERAGE SUBARRAY BEAM AND ARRAY BEAM NOISE POWER SPECTRA FOR GREECE NOISE SAMPLE	II-2
II-2	SINGLE SENSOR NOISE SPECTRAL RATIO VARIATIONS GREECE NOISE SAMPLE	II-4
II-3	SUBARRAY BEAM NOISE SPECTRAL RATIO VARIATIONS GREECE NOISE SAMPLE	II-5
II-4	FREQUENCY RESPONSE OF STANDARD FILTER AND SDL FILTER	II-7
II-5	HISTOGRAM OF SINGLE SENSOR NOISE LEVELS FOR THREE NOISE SAMPLES	II-8
II-6	REFERENCE SUBARRAY RMS NOISE LEVELS	II-9
II-7	ADJUSTED-DELAY ARRAY BEAM P.MS NOISE LEVELS	II-11
II-8	MULTIPLE COHERENCE FOR SUBARRAY 10 NOISE FIELD GREECE NOISE SAMPLE	II-14
II-9	MULTIPLE COHERENCE BETWEEN THE REFERENCE SENSOR OF SUBARRAY 1 AND THE REFERENCE SENSORS OF SUBARRAYS 2, 3, 4, 6, AND 8 GREECE NOISE SAMPLE	II-15
III-1	SELECTED SUBARRAY BEAM AND SINGLE SENSOR TRACES OF EVENT IRA/221/02N SCALE FACTOR = 0.0002 INCHES/COUNT	III-2
III-2	SELECTED SUBARRAY BEAM AND SINGLE SENSOR TRACES OF EVENT KAZ/115/03N SCALE FACTOR = 0.00005 INCHES/COUNT	III-4
III-3	SUBARRAY SIGNAL AMPLITUDES FOR GRE/068/04N	III-5
III-4	SUBARRAY SIGNAL AMPLITUDES FOR URA/082/06N	III-6

LIST OF FIGURES  
(continued)

FIGURE	TITLE	PAGE
III-5	REFERENCE SUBARRAY AND ARRAY BEAM SIGNAL SPECTRA OF EVENT URA/082/06N	III-10
III-6	REFERENCE SUBARRAY AND ARRAY BEAM SIGNAL SPECTRA OF EVENT KAZ/115/03N	III-11
III-7	REFERENCE SUBARRAY AND ARRAY BEAM SIGNAL SPECTRA OF EVENT KIR/082/20N	III-13
III-8	REFERENCE SUBARRAY AND ARRAY BEAM SIGNAL SPECTRA OF EVENT TSI/083/13N	III-14
III-9	REFERENCE SUBARRAY AND ARRAY BEAM SIGNAL SPECTRA OF EVENT NEV/189/14N	III-15
III-10	NORSAR MAGNITUDE VERSUS PDE OR LASA MAGNITUDE	III-21
III-11	HISTOGRAM OF DIFFERENCES BETWEEN NORSAR AND PDE OR LASA $m_b$ FOR 85 EVENTS	III-23
IV-1	SINGLE SENSOR TO SUBARRAY NOISE REDUCTION FOR NOISE SAMPLE BEFORE EVENT NEC/156/10N	IV-2
IV-2	SUBARRAY TO ARRAY NOISE REDUCTION FOR NOISE SAMPLE BEFORE EVENT NEC/156/10N	IV-3
IV-3	NOISE REDUCTION FROM REFERENCE SUBARRAY TO ADJUSTED-DELAY BEAM (0.55 TO 1.5 Hz)	IV-5
IV-4	SIGNAL-TO-NOISE RATIO IMPROVEMENT OF ADJUSTED-DELAY BEAM RELATIVE TO AVERAGE SUBARRAY BEAM (DATA PRO- CESSED THROUGH STANDARD FILTER)	IV-10
IV-5	SIGNAL-TO-NOISE RATIO IMPROVEMENT OF ADJUSTED-DELAY BEAM RELATIVE TO REFERENCE SUBARRAY BEAM (DATA PASSED THROUGH STANDARD FILTER)	IV-12

LIST OF FIGURES  
(continued)

FIGURE	TITLE	PAGE
IV-6	SIGNAL-TO-NOISE RATIO IMPROVEMENT OF DIVERSITY-STACK BEAM RELATIVE TO ADJUSTED-DELAY BEAM (DATA PASSED THROUGH STANDARD FILTER)	IV-13
V-1	NORSAR P WAVE DETECTIONS/MISSES vs. $m_b$ AND EPICENTRAL DISTANCE	V-2
V-2	HISTOGRAM OF P WAVES PROCESSED AND DETECTED BY THE NORSAR SHORT- PERIOD ARRAY	V-4
V-3	INCREMENTAL DETECTION PROBABILITY OF THE NORSAR SHORT-PERIOD ARRAY	V-5
VI-1	REFERENCE SUBARRAY P30 MEAN SQUARE DISCRIMINANT	VI-4
VI-2	ADJUSTED-DELAY BEAM P30 MEAN SQUARE DISCRIMINANT	VI-5
VI-3	REFERENCE AUTOCORRELATION MEAN SQUARE	VI-6
VI-4	ADJUSTED-DELAY BEAM AUTOCORRELA- TION MEAN SQUARE	VI-7
VI-5	REFERENCE ENVELOPE DIFFERENCE (COUNTS SQUARED)	VI-8
VI-6	ADJUSTED-DELAY BEAM ENVELOPE DIFFERENCE (COUNTS SQUARED)	VI-9
VI-7	REFERENCE DOMINANT PERIOD (SECONDS)	VI-10
VI-8	ADJUSTED-DELAY BEAM DOMINANT PERIOD (SECONDS)	VI-12
VI-9	REFERENCE SPECTRAL RATIO [ (0.3-0.8)/(1.4-1.8) ] (dB)	VI-13
VI-10	ADJUSTED-DELAY BEAM SPECTRAL RATIO [ (0.3-0.8)/(1.4-1.8) ] (dB)	VI-14
VI-11	REFERENCE SPECTRAL RATIO [ (1.5-5)/(0.55-1.5) ] (dB)	VI-15

LIST OF FIGURES  
(continued)

FIGURE	TITLE	PAGE
VI-12	ADJUSTED-DELAY BEAM SPECTRAL RATIO [(1.5-5)/(0.55-1.5)] (dB)	VI-16
VI-13	MAGNITUDE 5.3 EVENT FROM WESTERN RUSSIA (DAY 295 OF 1971, 05:00:00)	VI-17
VI-14	MAGNITUDE 5.4 EVENT FROM EASTERN KAZAKH (DAY 181 OF 1971, 03:56:57)	VI-19

# LIST OF TABLES

TABLE	TITLE	PAGE
I-1	EVENT PARAMETERS	I-4
III-1	MAXIMUM VARIATION OF SUBARRAY BEAM SIGNAL RMS LEVELS ACROSS NORSAR	III-7
III-2	DELAY ANOMALIES FOR FOUR SOUTH CENTRAL RUSSIAN EVENTS	III-17
III-3	DELAY ANOMALIES FOR FOUR MEDITERRANEAN EVENTS	III-18
III-4	DISTANCE FACTOR (B) FOR COMPUTING NORSAR $m_b$ VALUES	III-20
IV-1	SUBARRAY-LEVEL AND ARRAY-LEVEL SIGNAL DEGRADATION (FROM HAND MEASUREMENTS)	IV-6
IV-2	SIGNAL DEGRADATION FROM AVERAGE SUBARRAY BEAM TO ADJUSTED-DELAY BEAM	IV-8

## SECTION I

### INTRODUCTION

This report presents the results of a preliminary evaluation of the Short-Period (SP) Norwegian Seismic Array (NORSAR), using seismic data recorded during 1970, 1971, and 1972. The overall objectives of the NORSAR SP evaluation are:

- Determine the best processing methods for enhancing the signal-to-noise ratio of Eurasian events
- Determine the array detection capability for Eurasian events
- Evaluate the performance of short-period discriminants at NORSAR
- In conjunction with the long-period NORSAR data, determine the detection and discrimination capability of NORSAR for Eurasian events.

Substantial progress has been made toward achieving the first three objectives; future analysis will be directed toward improving the preliminary results presented in this report and meeting the fourth objective.

Five analysis tasks were undertaken in order to meet the first three objectives stated above:

- Noise analysis
- Signal analysis
- Array processing effectiveness
- Preliminary detection threshold estimation
- Behavior of SP discriminants

Results of each task are presented in subsequent sections of this report.

The NORSAR SP array, centered about 100 km due north of Oslo, Norway, consists of 132 short-period seismometers and has an aperture of about 100 km. The sensors are grouped into 22 six-element subarrays; each subarray has a center sensor and a five-sensor ring and is about 7 km in diameter (Figure I-1). In this report subarray 1 refers to subarray 01A, subarrays 2 through 8 to subarrays 01B through 07B, and subarrays 9 through 22 to subarrays 01C through 14C. Within a subarray, sensors 0 through 4 refer to sensors in the surrounding ring, starting with the first sensor east of a north ( $0^{\circ}$ ) azimuth, and proceeding clockwise around the ring. Sensor 5 refers to the central sensor of a subarray. Thus, sensor 0 of subarray 1 is sensor 01A01 in the official nomenclature, and sensor 5 of subarray 22 is sensor 14C00.

The results presented in the following sections are based primarily on analysis of events located on the Eurasian continent. A total of 102 events have been analyzed; Table I-1 lists the event parameters.

Geographically, the events are concentrated principally in the Northwestern Pacific (from Kamchatka to Taiwan) and in south central Asia (north and west of the Himalayan system). There are five events from the Ural Mountain region, three from continental North America, two from as far west in Europe as Greece, two from the Arctic Ocean and one from the Aleutian Islands. Ninety percent of the events are either shallow ( $\leq 100$  km) focus or have unknown depths. Twelve events are signals from known test areas, including six from Eastern Kazakh, one from Novaya Zemlya, two from the Ural Mountains, one from the Aleutian Islands and two from Nevada.

For 72 of the signals an associated 320-second noise sample taken just prior to the signal was edited and processed, these samples were used to obtain the noise analysis results reported in Section II of this report.

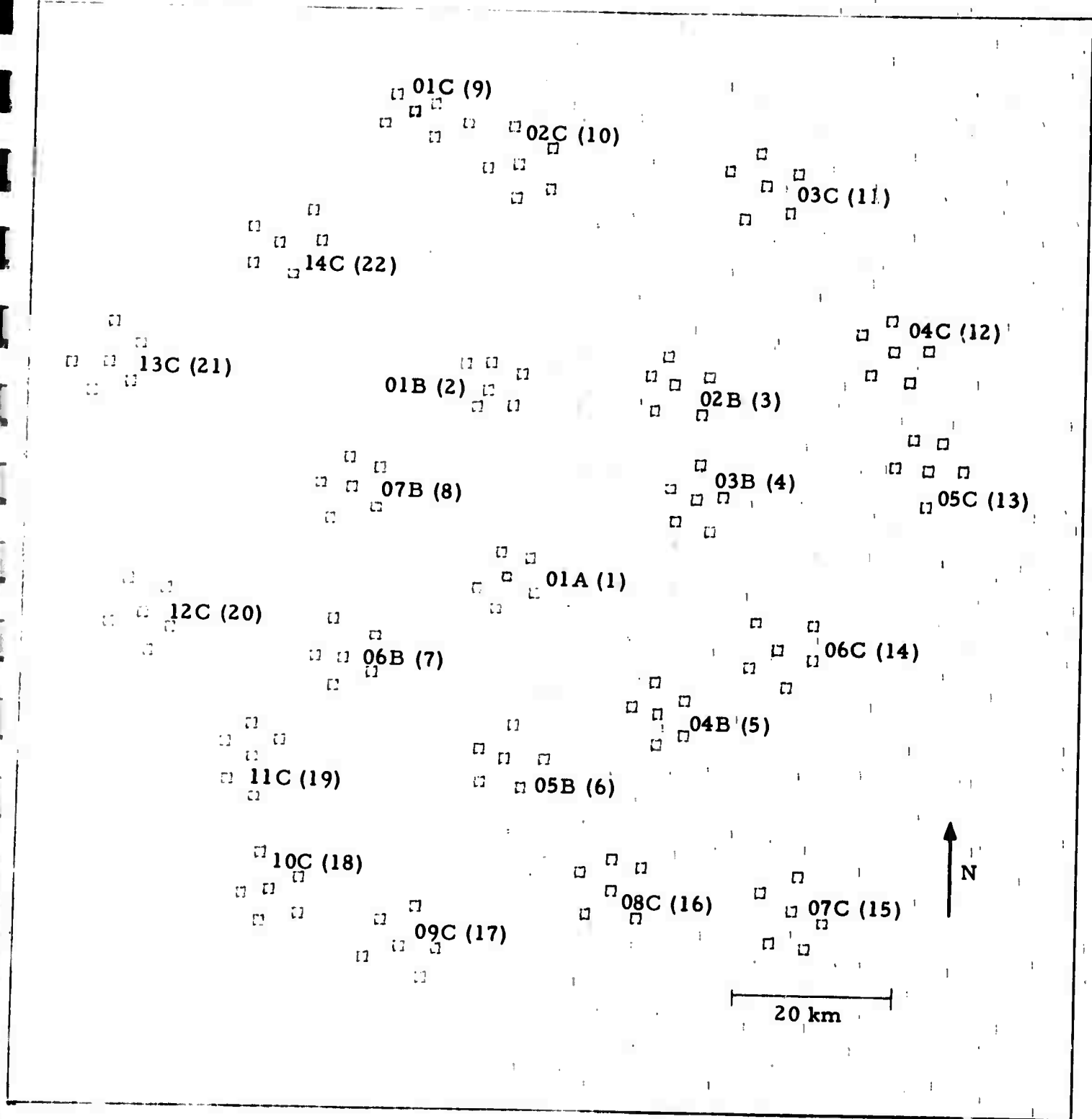


FIGURE I-1  
NORSAR SHORT PERIOD ARRAY

TABLE I-1  
EVENT PARAMETERS

Designation	Date	Origin Time	Lat.	Long.	$m_b$	Depth	Source Bulletin	Comment
KUR/060/07N	03/01/71	06.53.32	50.7N	154.5E	4.3	190	P	ND
TAI/062/04N	03/03/71	04.01.45	26.8N	125.9E	4.5	167	P	
JAP/063/07N	03/04/71	07.48.39	40.7N	143.5E	5.2	37	P	
MED/063/08N	03/04/71	08.58.29	33.5N	28.3E	4.0	N	S	
JAP/065/11N	03/06/71	11.49.40	33.1N	142.0E	4.1	50	S	
UZB/065/23N	03/06/71	23.02.02	40.8N	68.6E	4.6	185	S	
JAP/066/02N	03/07/71	02.50.02	43.0N	145.8E	3.8	50	S	
TAL/066/21N	03/07/71	21.55.17	4.3N	127.1E	4.9	99	P	
TUR/067/23N	03/08/71	22.44.47	37.5N	29.7E	4.7	21	P	
GRE/068/04N	03/09/71	04.58.38	38.7N	20.3E	4.8	16	P	
CAL/068/15N	03/09/71	15.35.16	36.8N	122.2W	4.8	11	P	
JAP/068/21N	03/09/71	12.19.52	36.6N	142.1E	4.4	64	P	
KUR/069/05N	03/10/71	05.21.03	45.4N	151.2E	4.3	60	P	
SZE/070/04N	03/11/71	04.43.37	28.7N	103.7E	5.1	56	P	
KIR/070/24N	03/11/71	23.59.46	40.1N	77.1E	4.4	N	P	MBN
ALI/071/08N	03/12/71	08.24.47	51.5N	177.4E	4.0	N	S	ND
MON/071/08N	03/12/71	08.56.04	47.7N	113.9W	4.3	32	P	ND
RYU/072/03N	03/13/71	02.37.40	26.8N	129.8E	4.4	35	P	MBN
JAP/072/03N	03/13/71	02.59.38	40.1N	142.4E	5.1	57	P	
RYU/072/03N	03/13/71	03.32.20	26.8N	129.7E	4.3	N	P	
VAN/072/23N	03/13/71	23.51.35	50.6N	129.9N	5.7	N	P	
SAK/073/07N	03/14/71	06.41.10	46.3N	142.3E	4.5	257	P	
KM1/073/12N	03/14/71	12.15.14	53.9N	160.5E	5.3	35	P	
KM2/073/12N	03/14/71	12.24.04	54.0N	160.6E	4.8	N	P	

TABLE I-1

(Continued)

Designation	Date	Origin Time	Lat.	Long.	m <sub>b</sub>	Depth	Source Bulletin	Comment
JAP/074/14N	03/15/71	14.12.10	31.1N	141.8E	4.8	N	P	ND
GRE/074/15N	03/15/71	15.23.17	37.2N	24.0E	4.8	32	P	
SIN/075/22N	03/16/71	22.28.33	39.1N	75.7E	4.5	N	P	
TAI/075/22N	03/16/71	22.52.09	23.8N	121.6E	4.6	40	P	
SWR/076/02N	03/17/71	02.15.46	46.0N	45.4E	4.1	N	S	ND
KUR/077/03N	03/18/71	03.13.15	49.2N	156.3E	5.1	N	P	
KUR/077/08N	03/18/71	08.11.04	49.3N	155.3E	3.9	60	S	
KAZ/081/04N	03/22/71	04.32.57	49.7N	78.2E	5.8	0	P	
URA/082/06N	03/23/71	06.59.56	61.3N	56.5E	5.6	0	P	
KIR/082/09N	03/23/71	09.52.12	41.5N	79.3E	5.7	N	P	
KIR/082/20N	03/23/71	20.47.17	41.5N	79.3E	6.0	N	P	
TSI/083/13N	03/24/71	13.54.17	35.5N	98.2E	5.8	13	P	
KIR/083/20N	03/24/71	20.54.28	41.5N	79.5E	5.3	18	P	
AND/087/08N	03/28/71	08.23.19	11.8N	95.1E	5.5	N	P	
SIN/090/20N	03/31/71	20.00.31	39.6N	74.8E	4.8	38	P	
TIB/093/07N	04/03/71	07.34.50	32.2N	95.1E	5.1	N	P	
TAD/094/01N	04/04/71	01.35.23	38.4N	73.3E	4.8	N	P	
KUR/095/00N	04/05/71	00.00.04	44.1N	147.4E	4.2	N	S	
KUR/095/17N	04/05/71	16.49.08	45.5N	151.9E	5.1	N	P	
KUR/098/03N	04/08/71	03.23.50	46.9N	151.3E	3.8	N	S	
KUR/099/04N	04/09/71	03.56.07	43.4N	147.6E	4.8	50	P	
KAM/099/08N	04/09/71	08.33.20	56.3N	162.7E	4.9	45	P	
KUR/099/15N	04/09/71	15.08.09	44.3N	147.0E	5.1	126	P	
YUG/100/02N	04/10/71	02.58.05	42.5N	20.1E	4.6	21	P	

TABLE I-1  
(Continued)

Designation	Date	Origin Time	Lat.	Long.	m <sub>b</sub>	Depth	Source Bulletin	Comment
OKH/101/02N	04/11/71	02.36.53	59.0N	157.3E	4.0	N	S	ND
KUR/101/08N	04/11/71	08.42.05	46.2N	153.0E	4.5	N	P	
KUR/102/18N	04/12/71	18.06.32	43.4N	147.3E	4.1	35	S	
IRA/102/19N1	04/12/71	19.03.25	28.3N	55.6E	6.0	44	P	
SIB/105/18N	04/15/71	18.53.57	70.1N	155.0E	3.5	N	S	ND
KAZ/108/23N	04/18/71	23.14.19	45.8N	76.1E	4.5	N	S	
GRE/109/02N	04/19/71	02.43.52	39.0N	20.5E	5.1	16	P	
TAD/110/03N	04/20/71	03.48.27	38.3N	73.5E	4.9	130	P	
KAZ/115/03N	04/25/71	03.32.58	49.8N	78.1E	5.9	0	P	
HIN/121/19N	05/01/71	18.58.11	36.3N	70.3E	4.5	230	P	
TIB/123/00N	05/03/71	00.33.22	30.8N	84.5E	5.4	16	P	
CAS/135/04N	05/15/71	04.53.05	38.1N	49.1E	4.6	N	P	
URA/136/07N	05/16/71	06.59.33	52.0N	56.0E	3.8	N	S	ND
YUN/141/02N	05/21/71	02.58.37	26.7N	101.8E	4.9	45	P	
KUR/142/12N	05/22/71	12.59.53	49.0N	154.0E	3.8	N	S	ND
KAZ/145/04N	05/25/71	04.02.57	49.8N	78.2E	5.2	0	P	
TAD/147/00N	05/27/71	00.30.27	38.3N	69.0E	4.8	36	P	
TIB/155/14N	06/04/71	14.10.46	32.2N	95.2E	5.0	N	P	
SZM/155/09N	06/04/71	09.10.02	84.6N	108.0E	5.1	N	P	
NEC/156/10N	06/05/71	10.21.28	37.3N	113.7E	4.7	N	P	
KAZ/157/04N	06/06/71	04.02.57	50.0N	77.6E	5.5	0	P	
NEV/167/14N	06/16/71	14.50.00	37.0N	116.0W	4.9	0	P	
KAZ/170/04N	06/19/71	04.03.57	50.0N	77.7E	5.5	0	P	
KAZ/181/04N	06/30/71	03.56.57	50.0N	79.1W	5.4	0	P	

TABLE I-1

(Continued)

Designation	Date	Origin Time	Lat.	Long.	$m_b$	Depth	Source Bulletin	Comment
KIR/184/04N	07/03/71	04.26.22	41.3N	79.3E	4.9	17	P	
KUR/185/15N	07/04/71	15.29.21	43.7N	147.5E	4.4	N	P	
TAD/188/04N	07/07/71	03.52.53	38.6N	73.1E	4.5	62	P	
NEV/189/14N	07/08/71	14.00.00	37.4N	117.1W	5.5	0	P	
KUR/191/02N	07/10/71	02.04.28	51.0N	153.0E	3.6	N	S	
KUR/191/14N	07/10/71	14.28.56	43.5N	147.8E	4.8	55	P	
URA/141/16N	07/10/71	16.59.59	64.2N	55.2E	5.3	0	P	
KUR/193/06N	07/12/71	06.08.15	45.0N	149.0E	4.6	N	S	
KUR/199/12N	07/18/71	12.32.38	51.0N	157.0E	4.3	N	S	ND
KAM/201/05N	07/20/71	05.33.24	56.0N	161.0E	3.7	N	S	
WRS/202/15N	07/21/71	15.49.27	52.0N	54.0E	3.8	N	S	ND
KUR/202/23N	07/21/71	23.50.14	47.0N	147.0E	3.8	N	S	ND
HOK/203/16N	07/22/71	16.04.16	41.0N	147.0E	3.6	N	S	ND
KUR/204/12N	07/23/71	12.45.12	46.0N	150.0E	3.7	N	S	ND
KUR/205/04N	07/24/71	04.19.41	45.0N	147.0E	3.6	N	S	ND
SWR/205/11N	07/24/71	11.11.42	48.0N	28.0E	3.5	N	S	
KUR/206/00N	07/25/71	00.41.26	50.0N	154.0E	4.1	N	S	ND
KAM/206/01N	07/25/71	01.23.19	55.0N	163.0E	4.0	N	S	ND
KAM/206/08N	07/25/71	08.12.34	53.0N	160.0E	3.7	N	S	
KUR/206/08N	07/25/71	08.35.19	44.0N	147.0E	4.0	N	S	
SIN/207/01N	07/26/71	01.48.33	39.9N	77.2E	6.0	N	P	
BLS/210/19N	07/29/71	19.40.10	39.6N	30.4E	4.5	N	P	
KUR/213/02N	08/01/71	02.06.06	50.4N	156.8E	5.6	20	P	
KUR/214/02N	08/02/71	02.57.24	50.8N	158.1E	3.6	N	S	ND
KYU/214/13N	08/02/71	13.59.41	33.0N	130.9E	3.6	N	S	

TABLE I-1  
(Continued)

Designation	Date	Origin Time	Lat.	Long.	m <sub>b</sub>	Depth	Source Bulletin	Comment
KAM/217/01N	08/05/71	01.05.57	50.0N	156.8E	3.7	N	S	ND
SIN/221/01N	08/09/71	01.03.16	42.1N	83.4E	4.2	N	P	
IRA/221/02N	08/09/71	02.54.37	36.2N	52.7E	5.2	27	P	
SAK/248/18N	09/05/71	18.55.57	48.0N	143.0E	4.3	N	S	
TUR/252/15N	09/09/71	15.10.03	37.3N	30.2E	5.3	23	P	
NZM/270/06N	09/27/71	05.59.55	73.4N	55.1E	6.4	0	P	
WRS/277/10N	10/04/71	10.00.02	61.6N	47.1E	5.1	13	P	
WRS/295/05N	10/22/71	05.00.00	51.6N	54.5E	5.3	6	P	
CAN/310/22N	11/06/71	22.00.00	51.5N	179.1E	6.8	2	P	

Abbreviations:

S SAAC/LASA Bulletin  
P PDE Bulletin  
ND NONDETECTION  
MNB NORSAR Magnitude

Data quality was excellent; about one-half of the time all 132 sensors were operational. In most of the other cases one subarray (six sensors) was dead; the worst data loss was 19 sensors. With the exception of one event, there were essentially no spikes in the data. We do not have individual seismometer response curves, however, based on results of the signal and noise analysis it appears that the seismometers are reasonably well equalized across the array.

## SECTION II

### NOISE ANALYSIS

#### A. INTRODUCTION

Seventy-two 320-second (5 minutes, 20 seconds) noise samples spread over 1971 were analyzed to determine the NORSAR short period noise characteristics; all noise samples preceded events and were selected to end 25 seconds before the predicted P-wave arrival time.

The following calculations were made during the analysis:

- Spectral content and variability across the array for single sensors and subarray beams
- RMS noise levels for selected bandpasses for the single sensors, subarray beams and the array beam
- Variability with time
- Multiple coherences both within a subarray and between subarrays.

The noise data, with the exception of level as a function of time, were very similar sample-to-sample. Thus the selected data presented in this report is representative of the entire 72-sample ensemble.

#### B. SPECTRAL CONTENT

The average single sensor spectrum, average subarray beam spectrum, and array beam spectrum for the noise sample preceding the Greece event (9 March 1971) are shown in Figure II-1. It should be noted that the Greece sample has higher than average noise levels. The system response has not been removed, but the spectra are normalized to  $1(m\mu)^2/\text{Hz}$  at 1.0 Hz. The spectra are very simple, with a peak at .16 to .33 Hz (6 to 3 seconds) and a rapid decrease in spectral density with increasing frequency. There appears to be a weak secondary

Noise Power Density (dB relative to  $1 \text{ (m}\mu\text{)}^2/\text{Hz}$  at 1.0 Hz)

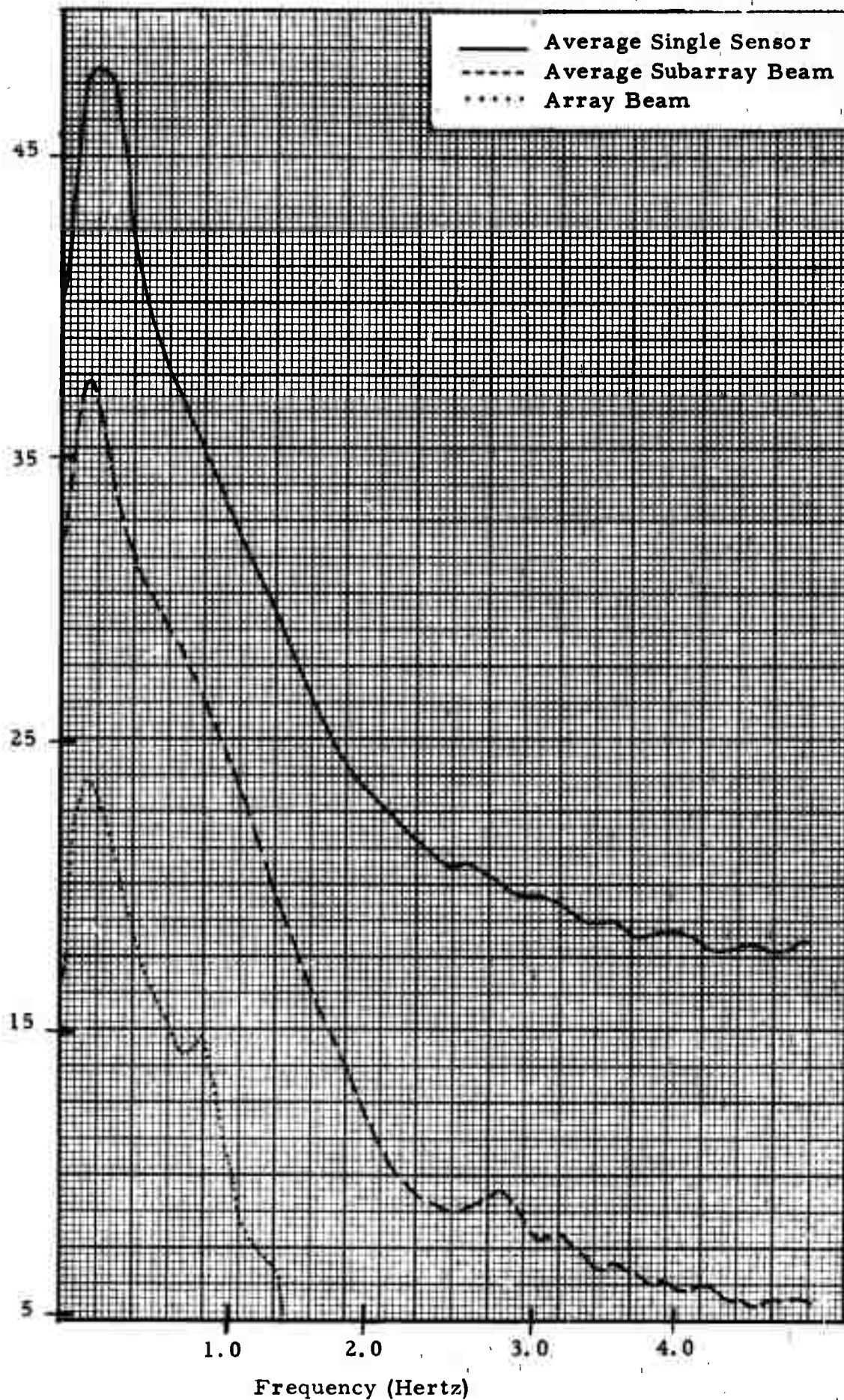


FIGURE II-1

AVERAGE SINGLE SENSOR AVERAGE SUBARRAY BEAM AND ARRAY BEAM  
NOISE POWER SPECTRA FOR GREECE NOISE SAMPLE

peak (best seen on the array beam spectrum) at about 0.8 Hz, however this peak is more than 10 dB down from the low-frequency peak.

The single sensor power spectra variations are summarized in Figure II-2, which shows a typical sensor to average single sensor spectral ratio, the maximum positive ratio (sensor 3 of subarray 10) and the maximum negative ratio (sensor 2 of subarray 11). Figure II-2 shows that the 132 single sensor power spectra are very similar; the maximum positive or negative variation is about 5 dB, and for most sensors it is less than 2 dB at all frequencies.

Only one anomaly was noted in the single sensor power spectra; sensors 0 and 1 of subarray 22 had a spectral line at 2.8 Hz. This anomaly was observed in most of the remaining noise samples

Variations in the noise spectra of the subarray beams were examined by comparing the ratio of each subarray beam to the average subarray beam. In the region of significant power density (0 to 2.0 Hz) all subarrays were within 4 dB of the average subarray spectrum (Figure II-3). At higher frequencies variations sometimes were larger, apparently because subarray system noise levels are different.

In summary, the NORSAR short-period noise spectra are very simple and very similar (except in level) from sample to sample. No significant variations either in spectral shape or across the array have been observed.

#### C. RMS NOISE LEVELS AND TIME VARIABILITY

Wideband RMS noise levels for the single sensors, subarray beams and array beam were computed for all noise samples. In addition, for the reference\* subarray and adjusted delay array beams\*\* RMS calculations were made

---

\* The reference subarray beam is the subarray beam selected as reference for the associated event; it is the subarray with the largest signal amplitudes.

\*\* The adjusted-delay array beam is the array beam formed with time delay anomalies appropriate for the associated event.

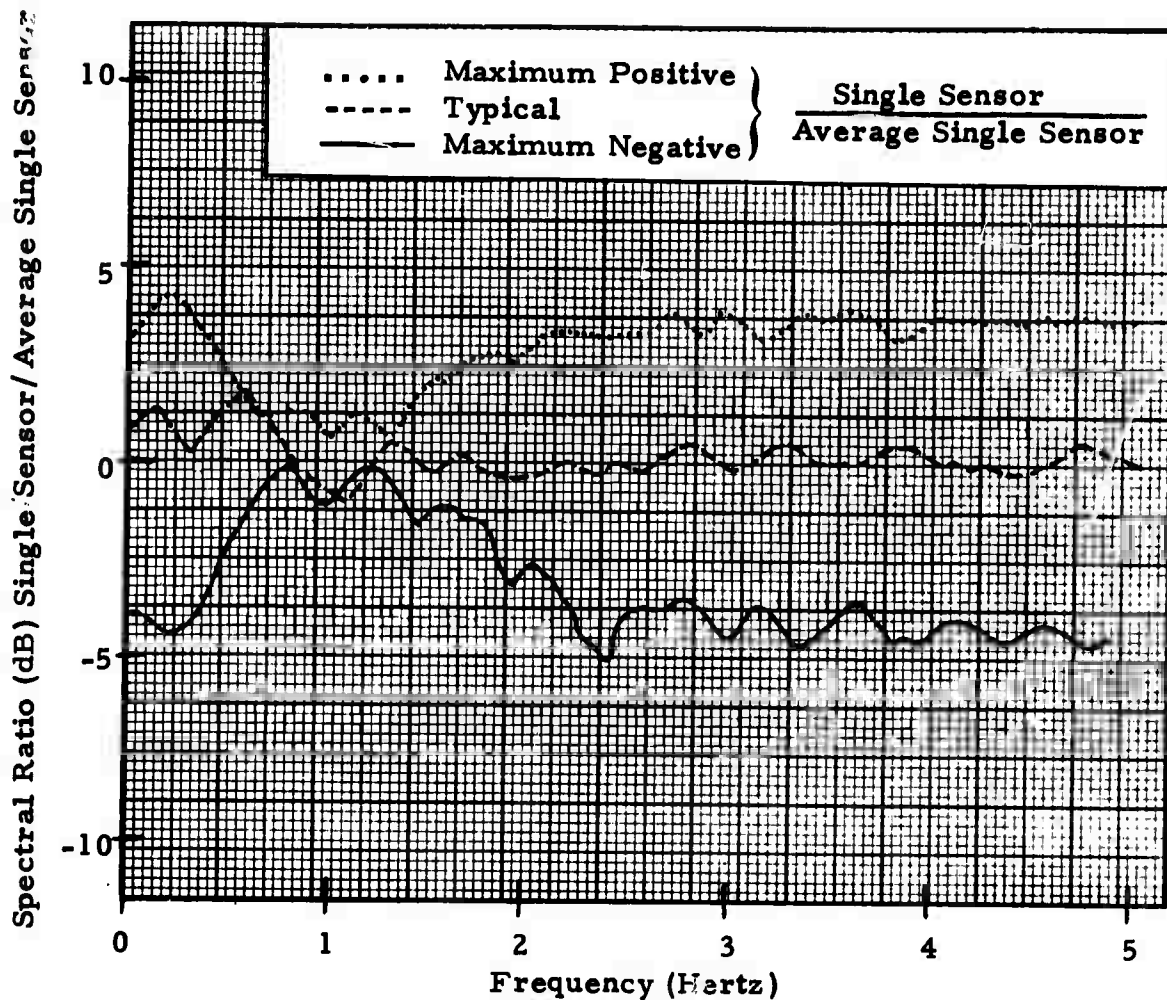


FIGURE II-2  
SINGLE SENSOR NOISE SPECTRAL RATIO VARIATIONS  
GREECE NOISE SAMPLE

Spectral Ratio (dB) Subarray Beam/Average Subarray Beam

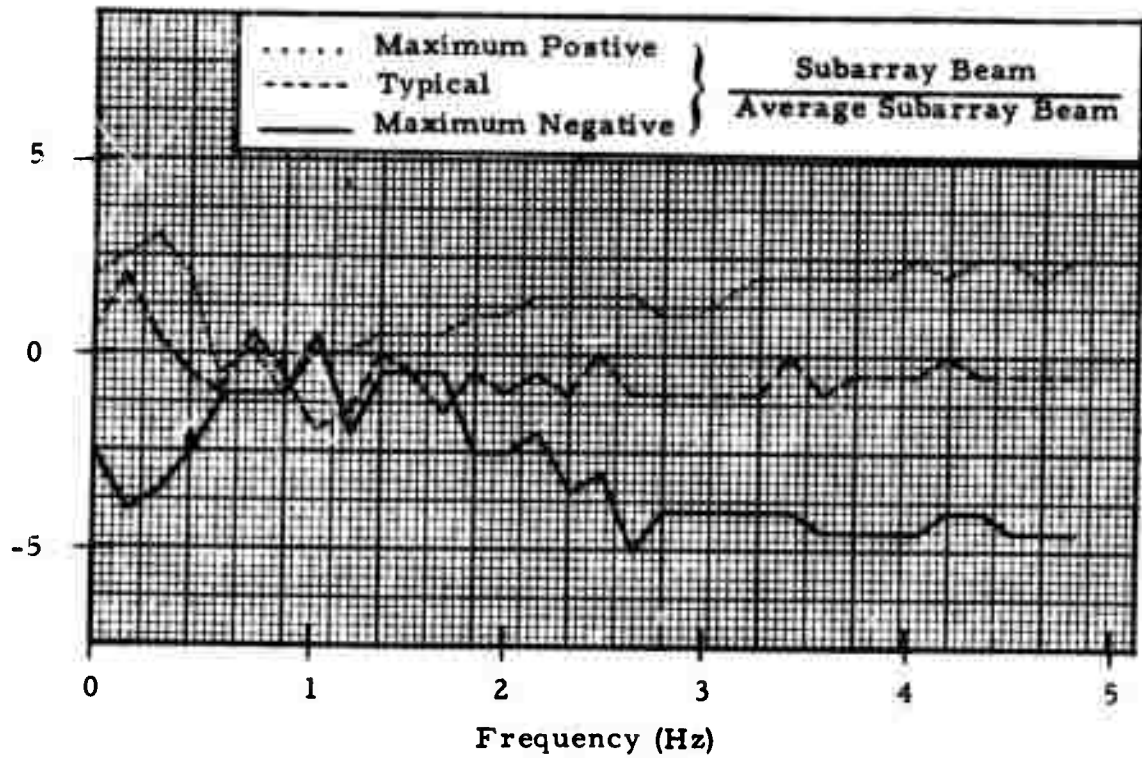


FIGURE II-3

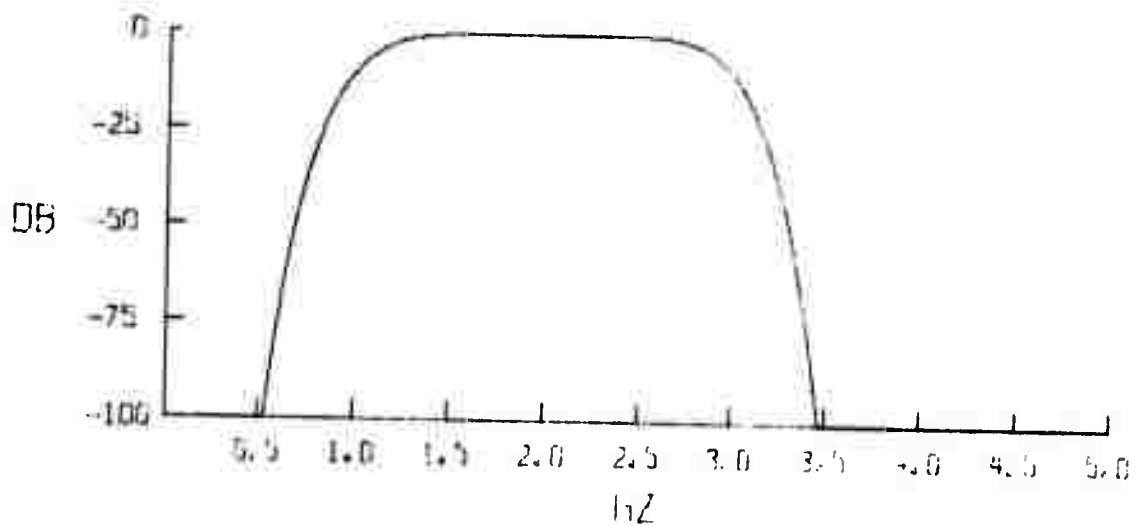
SUBARRAY BEAM NOISE SPECTRAL RATIO VARIATIONS  
 GREECE NOISE SAMPLE

after application of two bandpass filters (Figure II-4); the "standard" filter, which is a filter that appears to be optimum for improving the signal-to-noise ratio on the array beam; and the SDL filter, which has been used at several other short-period arrays. Thus the "standard" filter RMS noise levels represent minimum levels that can be achieved (without significantly attenuating the signal). The SDL noise levels can be compared with RMS values obtained at other short-period arrays such as LASA. It should be noted that the system response has not been removed prior to calculating an RMS level, but that the levels have been normalized to 1.0 Hz, using the  $42 \times 10^{-3} \text{ m}\mu / \text{count}$  conversion factor.

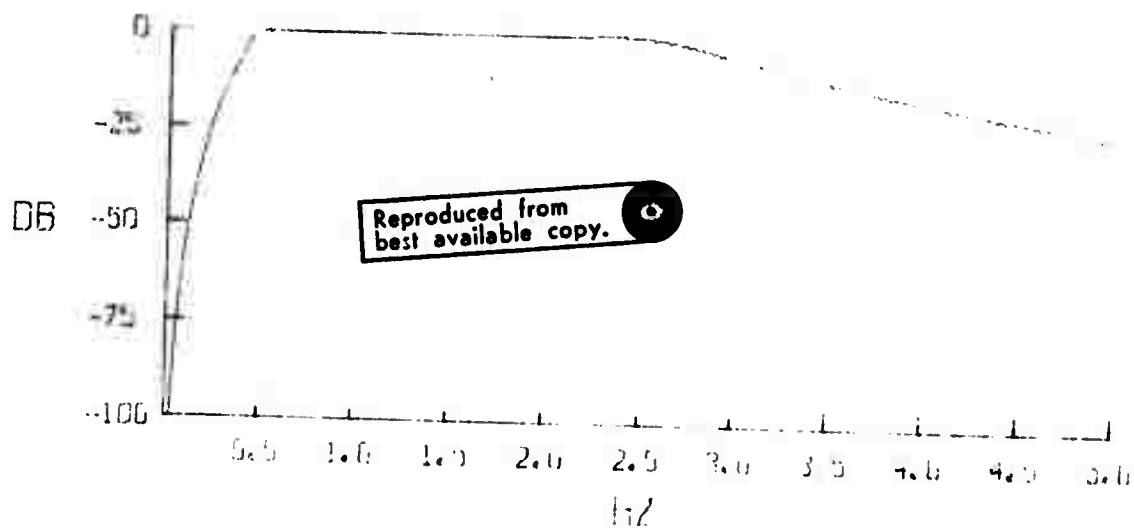
Figure II-5 is a histogram of wide-band single sensor RMS noise levels for three noise samples; two (TAD/188/04N and KM2/073/12N) were taken during relatively quiet periods, one (KUR/193/06N) was taken during a relatively noisy period. For the quiet noise samples the mode is about 6 m $\mu$ , a few values as low as 3 and a few as high as 10 were observed. The total spread is  $\pm 6$  dB, which is consistent with the spectral variations shown previously. For the noisy sample the mode is about 12 m $\mu$ ; values range from 5 to 17 (close to  $\pm 6$  dB), however the histogram is less peaked. Of interest is whether the low (or high) values are associated with the same sensors for all samples and if so, if the low (or high) noise values correspond to low (or high) signal amplitudes. We will be studying this aspect in the future.

Figures II-6 and II-7 show the wide-band, SDL-filtered and standard-filtered RMS values for the reference subarray beam and the adjusted-delay beam respectively for all 72 noise samples. For the reference subarray, which has noise typical of all subarrays, wide-band RMS noise levels range from about 0.8 to 6 m $\mu$ , and typically are 1.5 m $\mu$ . There is evidence of a seasonal dependence in the levels as summertime levels (days 130 to 270) are somewhat lower than wintertime levels. Analysis of the long-period NORSAR data (Texas Instruments, 1972) showed that the 3 to 6 second microseismic peak, which dominates these wide-band RMS measurements, increases significantly during the winter; thus this

# STANDARD FILTER RESPONSE



# SDL FILTER RESPONSE



Reproduced from  
best available copy.

FIGURE II-4  
FREQUENCY RESPONSE OF STANDARD FILTER  
AND SDL FILTER

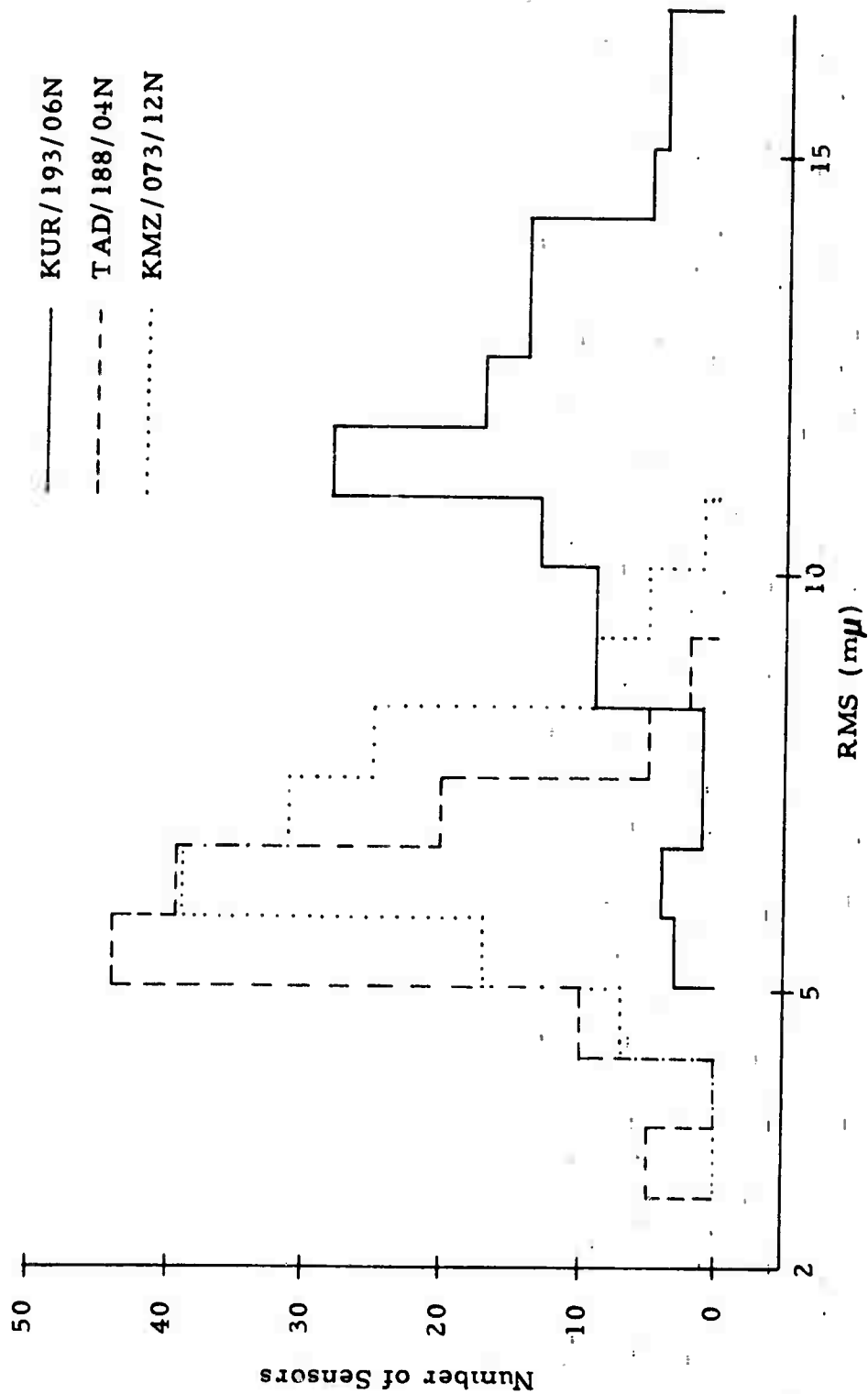


FIGURE II-5  
HISTOGRAM OF SINGLE SENSOR NOISE LEVELS FOR THREE  
NOISE SAMPLES

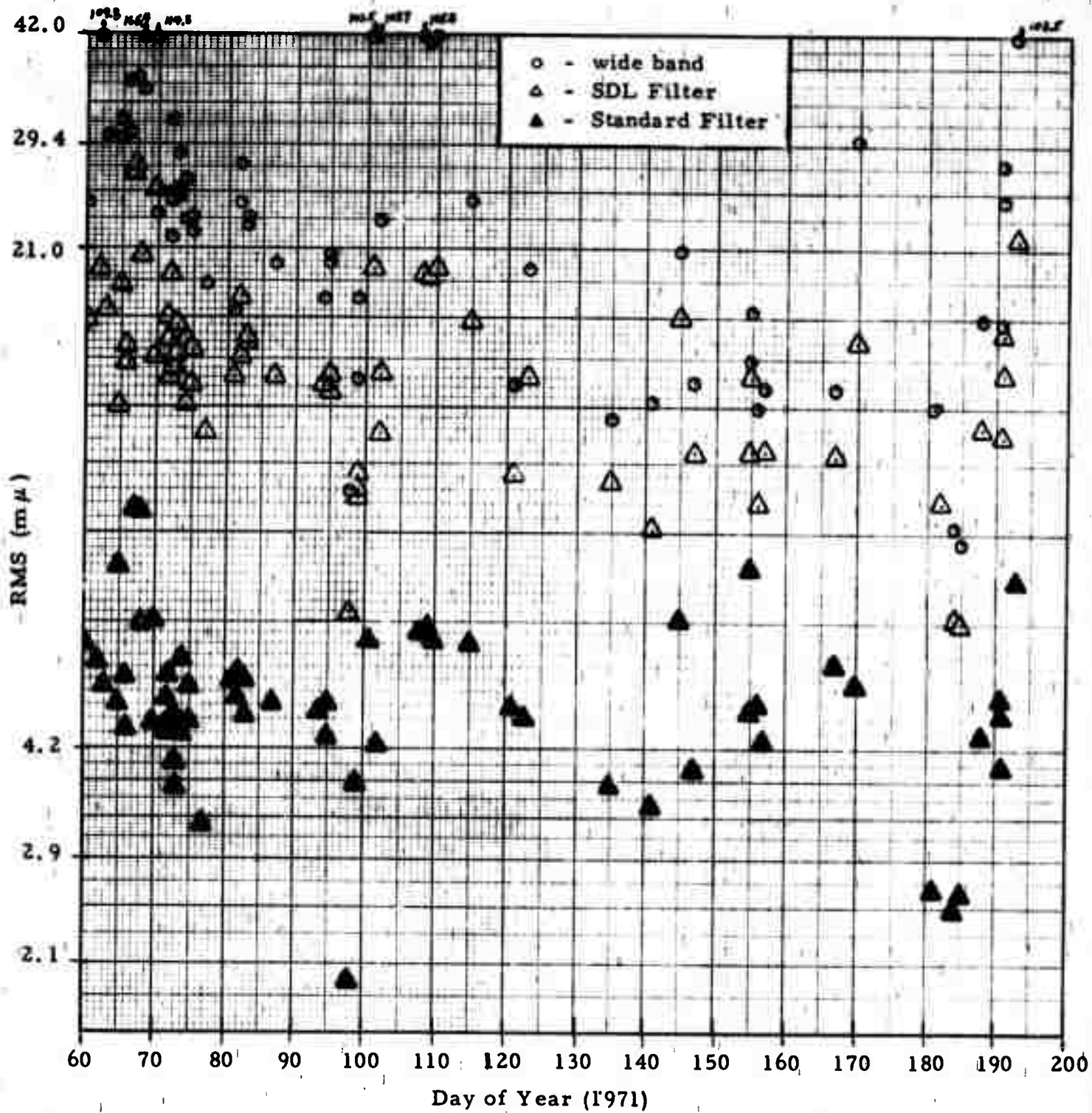


FIGURE II-6(a)  
REFERENCE SUBARRAY NOISE LEVELS

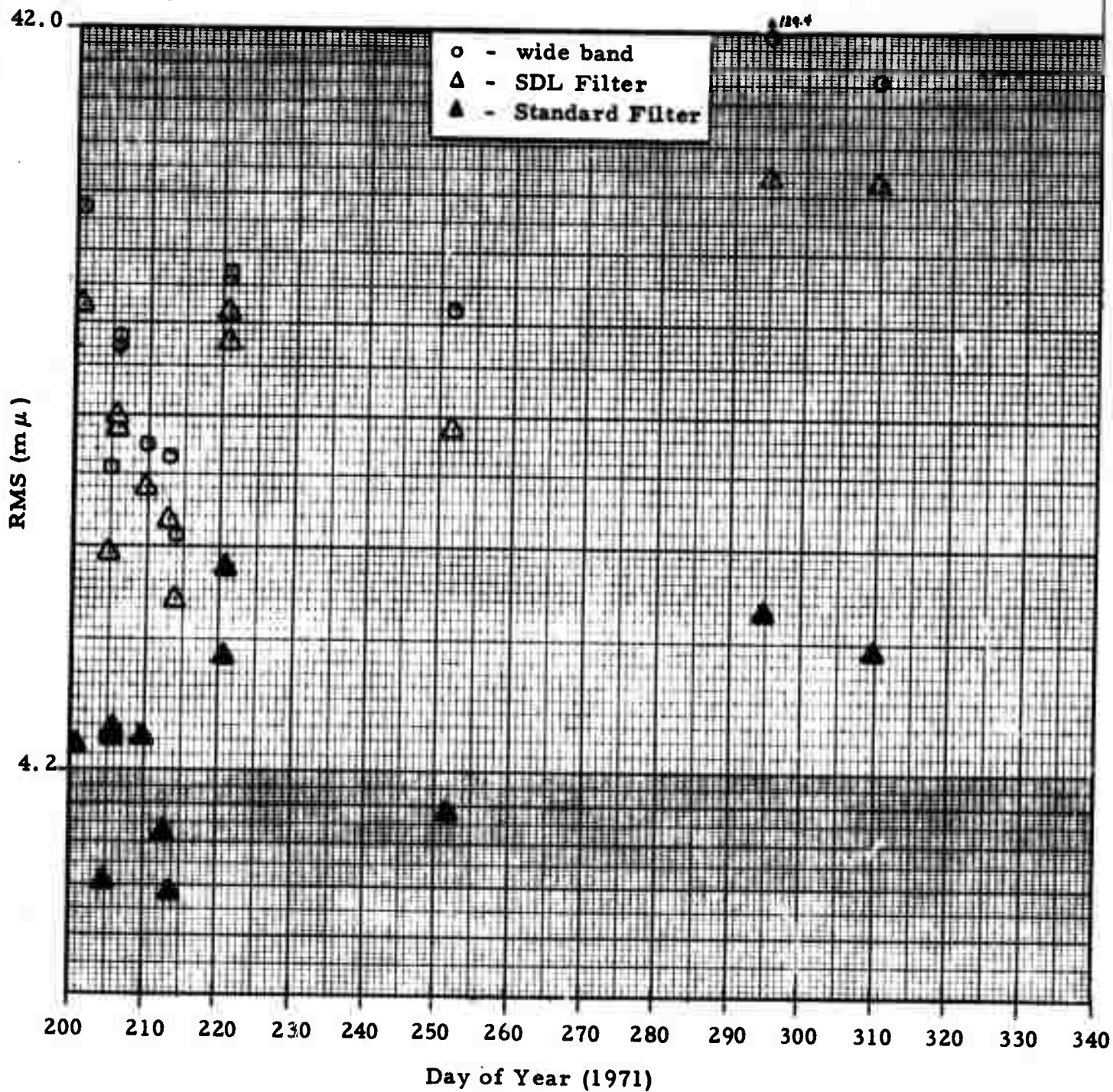


FIGURE II-6(b)  
REFERENCE SUBARRAY RMS NOISE LEVELS

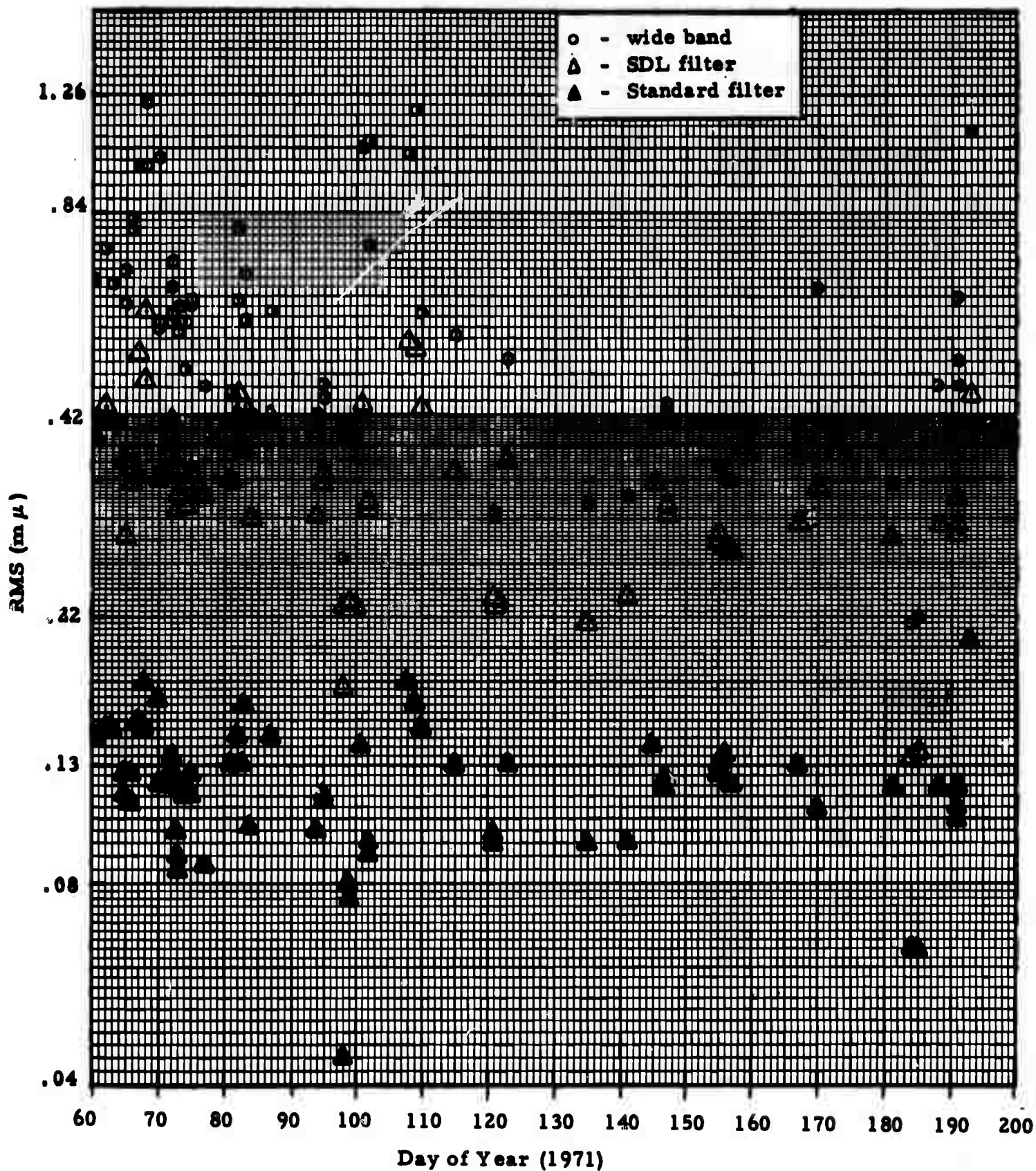


FIGURE II-7(a)

ADJUSTED-DELAY ARRAY BEAM RMS NOISE LEVELS

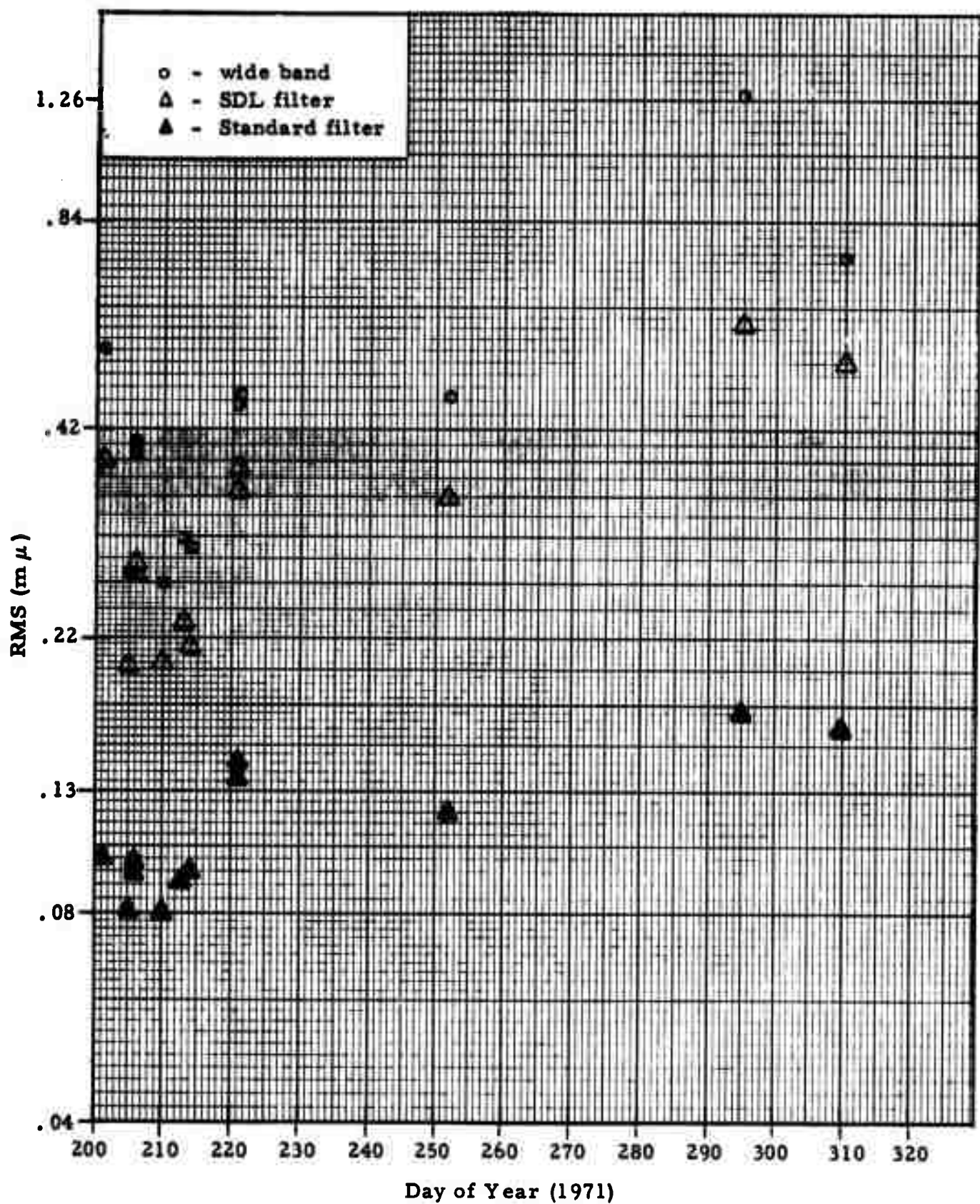


FIGURE II-7(b)  
ADJUSTED-DELAY ARRAY BEAM RMS NOISE LEVELS

seasonal dependence would be expected. The SDL filter, with its low corner frequency, does not reduce the reference subarray beam RMS noise levels very much. RMS levels range from 0.6 to 3 m $\mu$ , and typically are 1 m $\mu$ . The "standard" filter, which has a very severe low-frequency roll-off, attenuates the subarray beam RMS noise levels significantly, as would be expected. Values range from 0.2 to 0.8 m $\mu$ , and typically are 0.5 m $\mu$ . Thus this filter reduces RMS noise levels by 10 dB, and more on noisy days.

For the adjusted-delay array beam wide-band RMS noise levels range from 0.25 to 1.2 m $\mu$ , and typically are 0.5 m $\mu$ . Again, a seasonal dependence is evident. Note however, that there are occasional summer days (e.g., day 193) when the noise levels are high. RMS levels through the SDL filter range from 0.16 to 0.6 m $\mu$ , and typically are 0.3 m $\mu$ . RMS levels through the "standard" filter range from 0.04 to 0.17 m $\mu$ , and typically are 0.12 m $\mu$ . The "standard" filter is probably close to the best filter for detection purposes (see Section V) and is similar to the filter currently being used on the NORSAR on-line system. RMS levels through this filter are about a factor of 2 higher than those observed at LASA (Dean, 1971) which implies the NORSAR teleseismic detection threshold will be about 0.3 m $\mu$  units higher than the 3.9 (90% incremental) LASA threshold.

Finally, it is interesting to note that the seasonal dependence is less evident on the filtered beams; this implies that the low-frequency microseismic noise peak shifts to longer periods when the levels increase.

#### D. MULTIPLE COHERENCE

Noise multiple coherences within a subarray (five sensors on ring predicting the central sensor of the subarray) were calculated for the 22 subarrays for several noise samples. A typical multiple coherence plot (subarray 10) is given in Figure II-8 for the Greece noise sample. Except for the peak at 3 to 6 seconds, coherence is low at all frequencies where there is significant energy. The 3 to 6 second energy is well below the signal band, and so can be removed by band-pass filtering. Above 2 Hz, there is moderate coherence, but spectral levels are

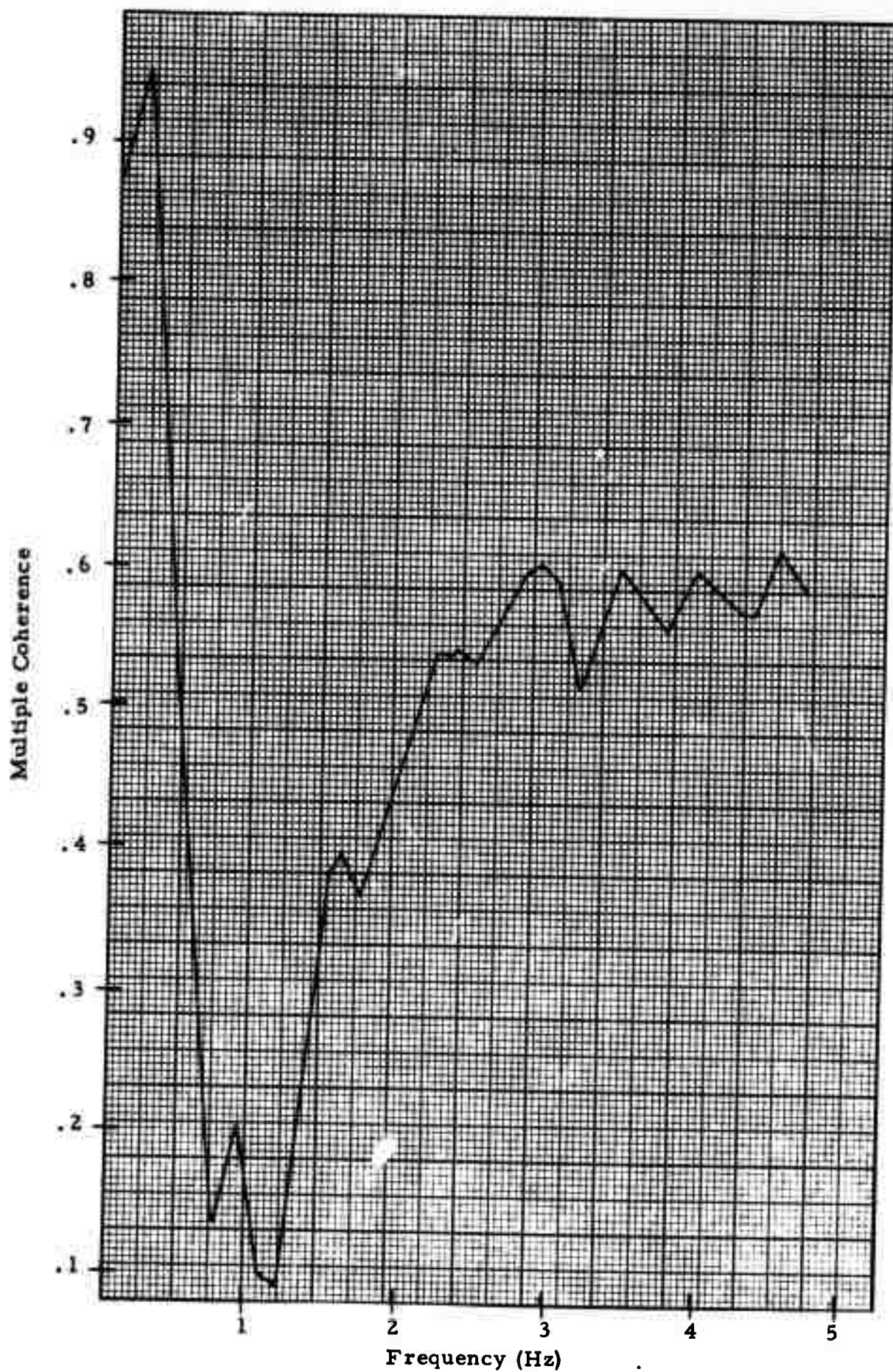


FIGURE II-8

MULTIPLE COHERENCE FOR SUBARRAY 10 NOISE FIELD  
GREECE NOISE SAMPLE

at least 25 dB below the peak. The moderate coherence at high frequencies may be due to the system electronics. In any event it is clear that multichannel processing would not be necessary at the subarray level.

Multiple coherences calculated between subarrays were very low, as expected, because of the large distances involved. Figure II-9 shows the multiple coherence between the reference sensor of subarray 1 and the reference sensors of subarrays 2, 3, 4, 6, and 8 for the Greece noise sample; very low values were obtained over the entire band.

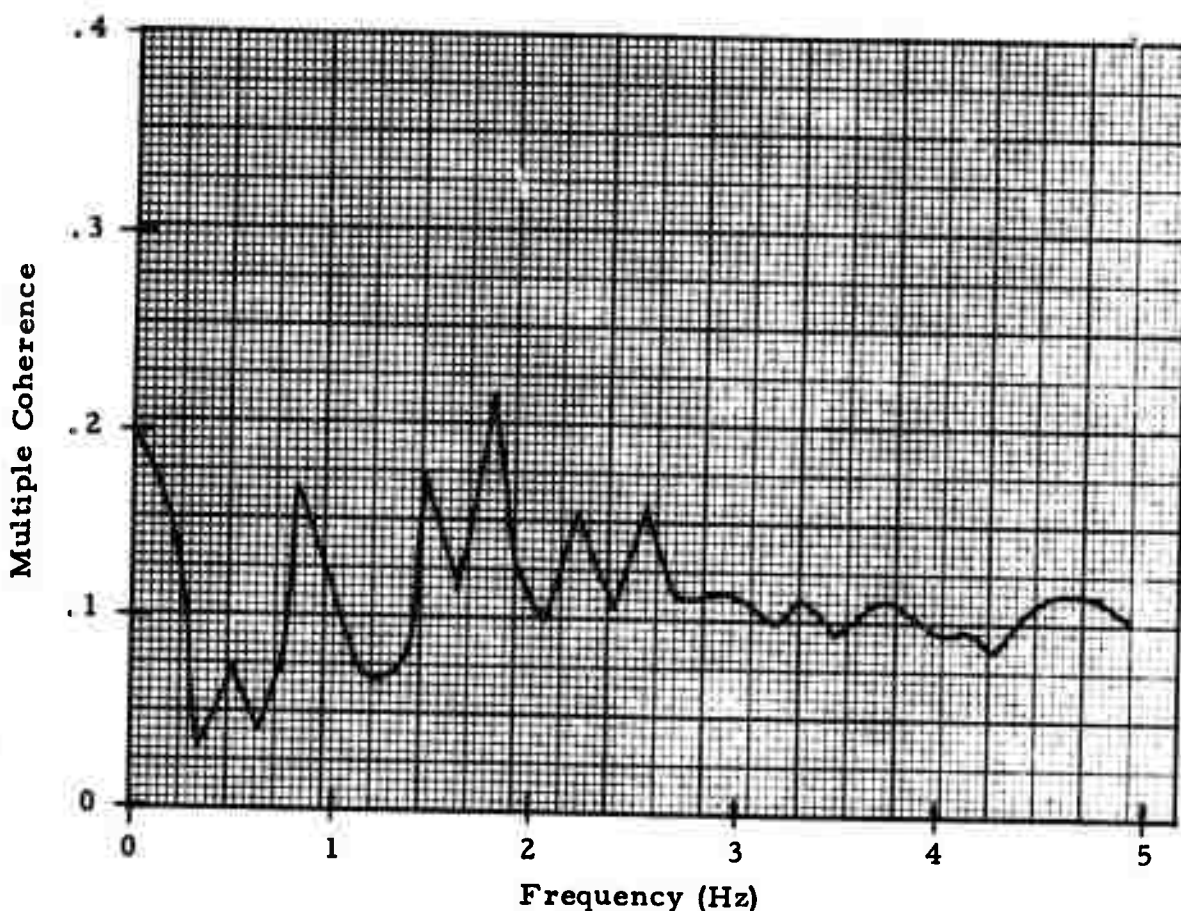


FIGURE II-9

MULTIPLE COHERENCE BETWEEN THE REFERENCE  
SENSOR OF SUBARRAY 1 AND THE REFERENCE  
SENSORS OF SUBARRAYS 2, 3, 4, 6 AND 8  
GREECE NOISE SAMPLE

### SECTION III

#### SIGNAL ANALYSIS

##### A. INTRODUCTION

Several large signals recorded by the entire array were analyzed in order to study signal characteristics. The following analyses were performed:

- Qualitative review of signal similarity among sensors at a subarray and among subarrays
- Subarray beam amplitude variations
- Spectral content
- Time delay anomalies (deviation from plane wave propagation)
- Comparison of NORSAR magnitudes ( $m_b$ ) with PDE (or LASA) magnitudes

Results of these analyses are discussed in subsequent subsections.

##### B. SIGNAL SIMILARITY

Qualitative estimates of the single sensor signal similarity within a subarray were made by comparing the single sensor waveforms of the Greece and Vancouver Island events for all 22 subarrays. In general, waveforms were quite similar within a subarray (In Section IV data are presented which shows that the signal loss in subarray beamforming typically was 1 dB; this small loss is consistent with the above qualitative observations). Some nearby ( $\Delta < 30^\circ$ ) Eurasian events contained significant amounts of high-frequency energy ( $f > 2.0$  Hz) which was not preserved by the subarray beam, probably because the time delay anomaly corrections were not precise enough for these events.

Signal similarity among subarrays was quite variable from event to event. For predominantly low-frequency events (Figure III-1) similarity was

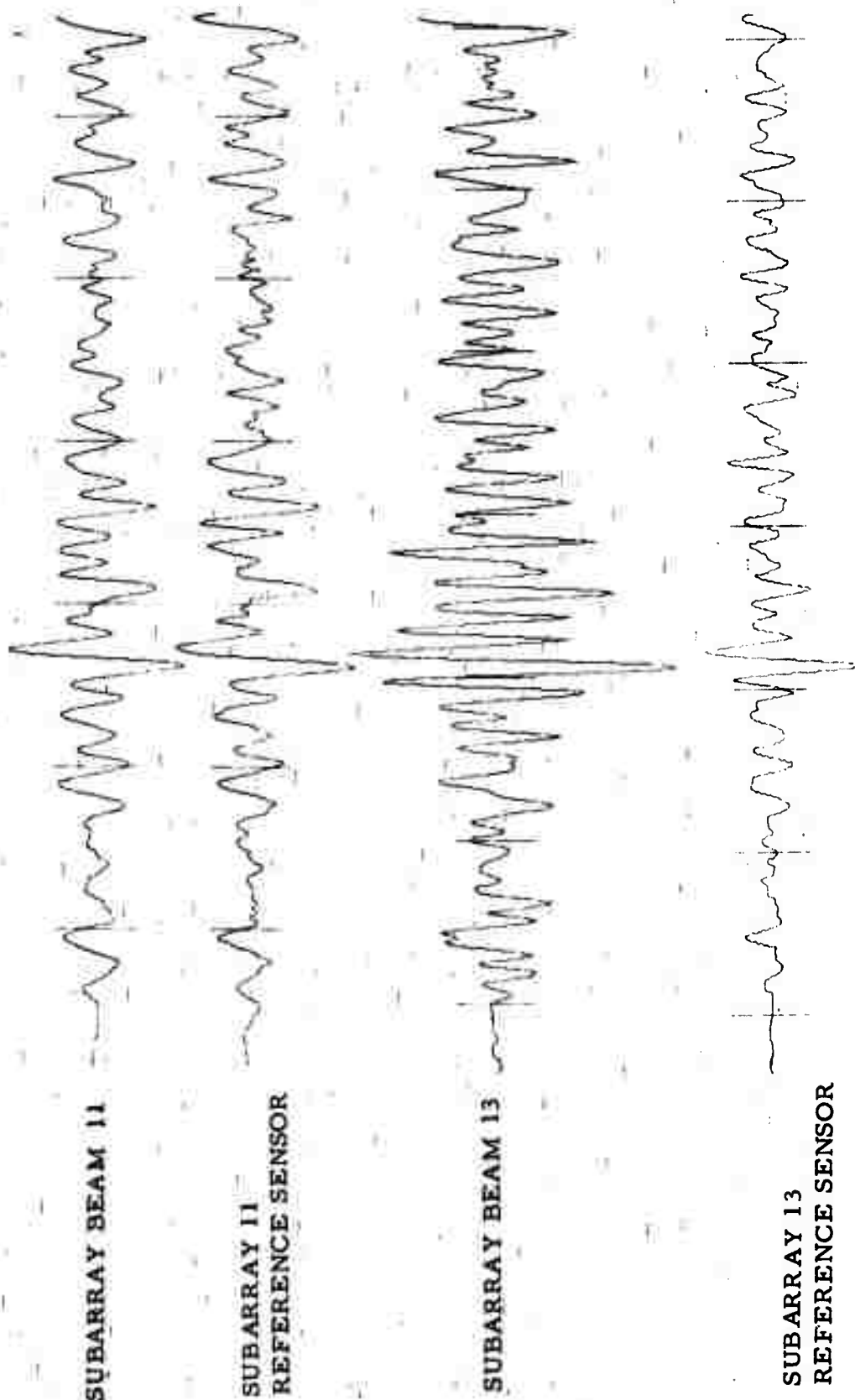


FIGURE III-1  
 SELECTED SUBARRAY BEAM AND SINGLE SENSOR TRACES OF EVENT IRA/221/02N  
 SCALE FACTOR = 0.0002 INCHES/COUNT  
 (PAGE 1 OF 2 PAGES)

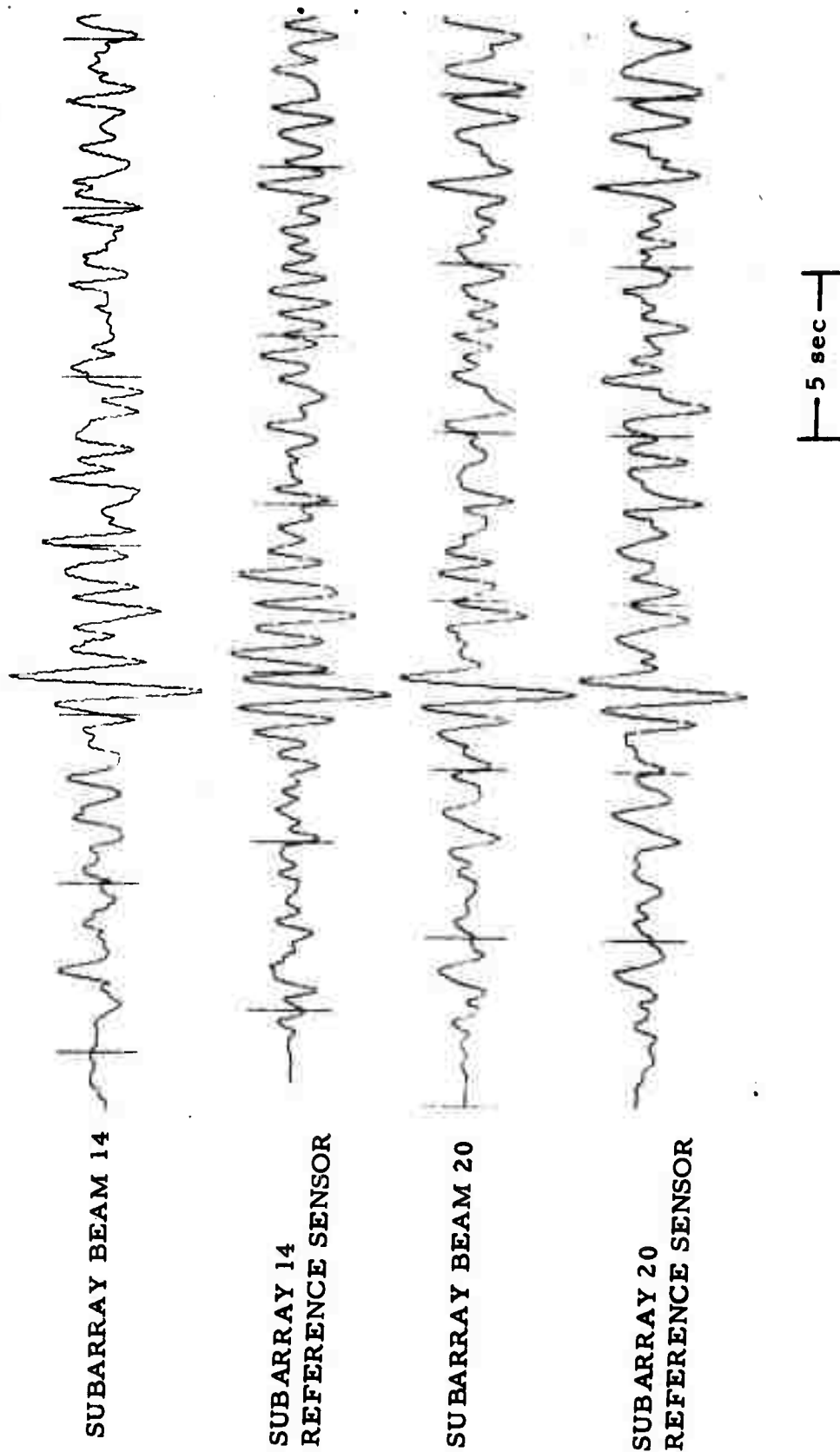


FIGURE III-1

SELECTED SUBARRAY BEAM AND SINGLE SENSOR TRACES OF EVENT IRA/221/02N  
 SCALE FACTOR = 0.0002 INCHES/COUNT  
 (PAGE 2 OF 2 PAGES)

generally good over the entire wavetrain. For events with substantial high-frequency energy (Figure III-2), however, subarray wavetrains often were quite different after the first few cycles (usually the low-frequency part of these signals was not significantly attenuated in array beamforming, implying that signal similarity at low frequencies was reasonably good). A detailed discussion of array beamforming loss is given in Section IV.

### C. SUBARRAY BEAM AMPLITUDE VARIATIONS

Signal amplitude variations among subarray beams are striking (note that the seismometers appear to be well-equalized). For the GRE/068/04N event, the peak-to-peak/2 values are shown in Figure III-3. These values vary from 84 m $\mu$  at subarray 12 to 24 m $\mu$  at subarray 6 (10.8 dB variation). For this event, the southwest quadrant of the NORSAR array (subarrays 6, 7, 15, 16, 17, 18, 19, 20, and 21) exhibits peaks below 42 m $\mu$ , while the northeast section (subarrays 12, 13, and 14) has peaks above 63 m $\mu$ . For the URA/082/06N event, the corresponding zero-to-peak values are shown in Figure III-4. These values vary from 330 m $\mu$  at subarray 11 to 228 m $\mu$  at subarray 7 (3.2 dB variation). Subarray 12 also had the highest signal amplitude for this event.

Table III-1 shows the ratio (in dB) of the strongest to weakest subarray RMS signal level for events having  $m_b > 5.0$ . The signal RMS calculations were made over a 6.4 second gate which began just prior to the P-wave arrival. The events are grouped by region, and the subarrays having the strongest and weakest signal respectively also are listed.

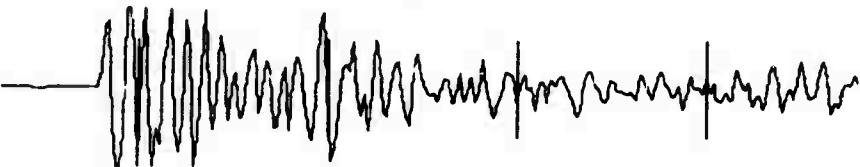
The average spread in signal amplitudes was 11.8 dB (a factor of 4), however the spread shows strong regional dependence. The largest spreads were for the Kazakh events (about 10:1), the lowest for the Ural events (about 2:1); events from both these areas were presumed explosions.

Note also that within a region the spread varies considerably; this is true even for the Kazakh events which are all located very close together.

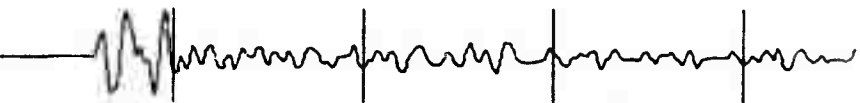
SUBARRAY 11 BEAM



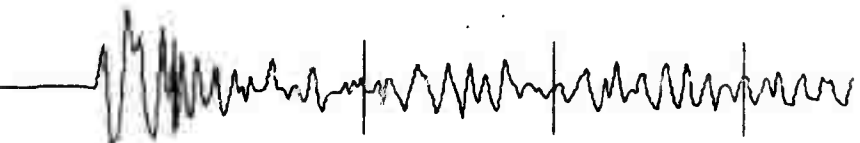
SUBARRAY 11 REFERENCE



SUBARRAY 13 BEAM



SUBARRAY 13 REFERENCE



SUBARRAY 14 BEAM



SUBARRAY 14 REFERENCE



SUBARRAY 20 BEAM



SUBARRAY 20 REFERENCE

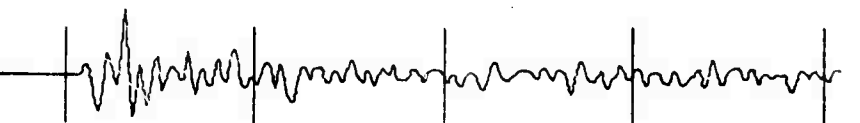


FIGURE III-2

— 5 sec —

SELECTED SUBARRAY BEAM AND SINGLE SENSOR TRACES  
OF EVENT KAZ/115/03N  
SCALE FACTOR = 0.00005 INCHES/COUNT

III-4

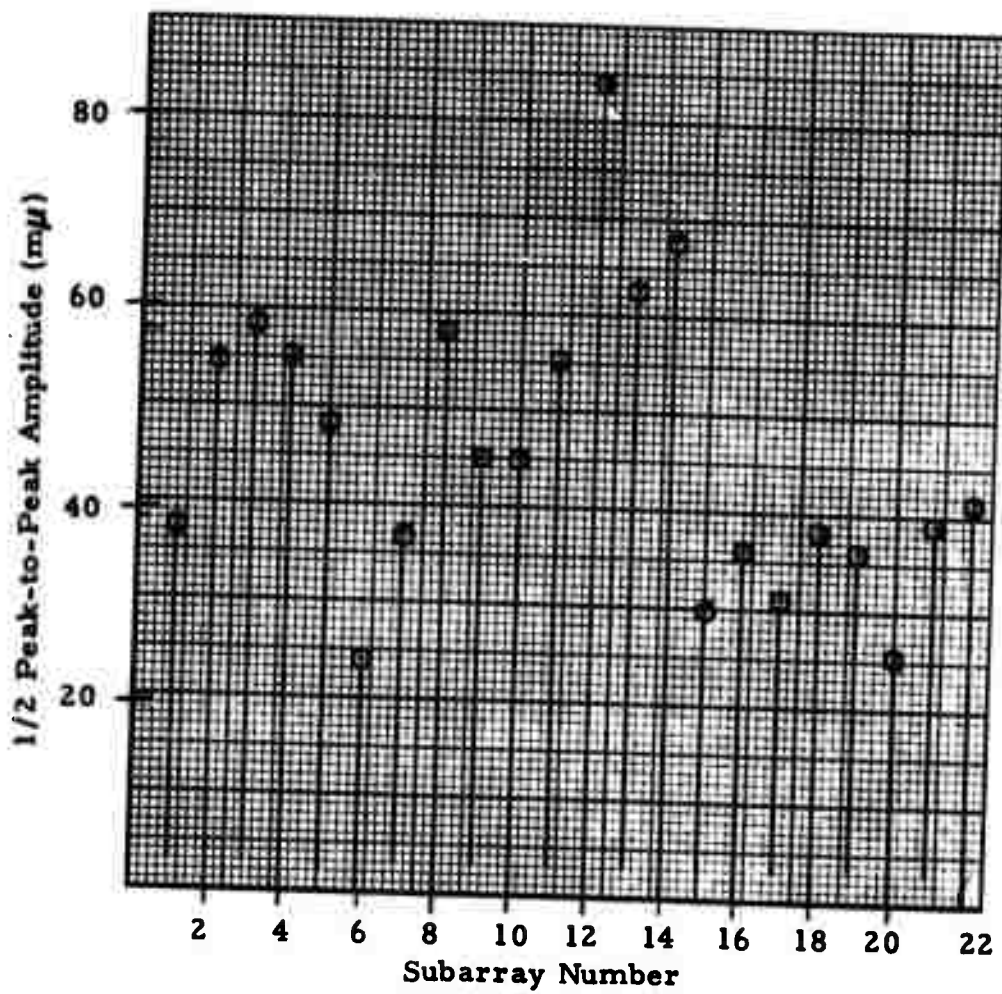


FIGURE III-3  
SUBARRAY SIGNAL AMPLITUDES FOR GRE/068/04N

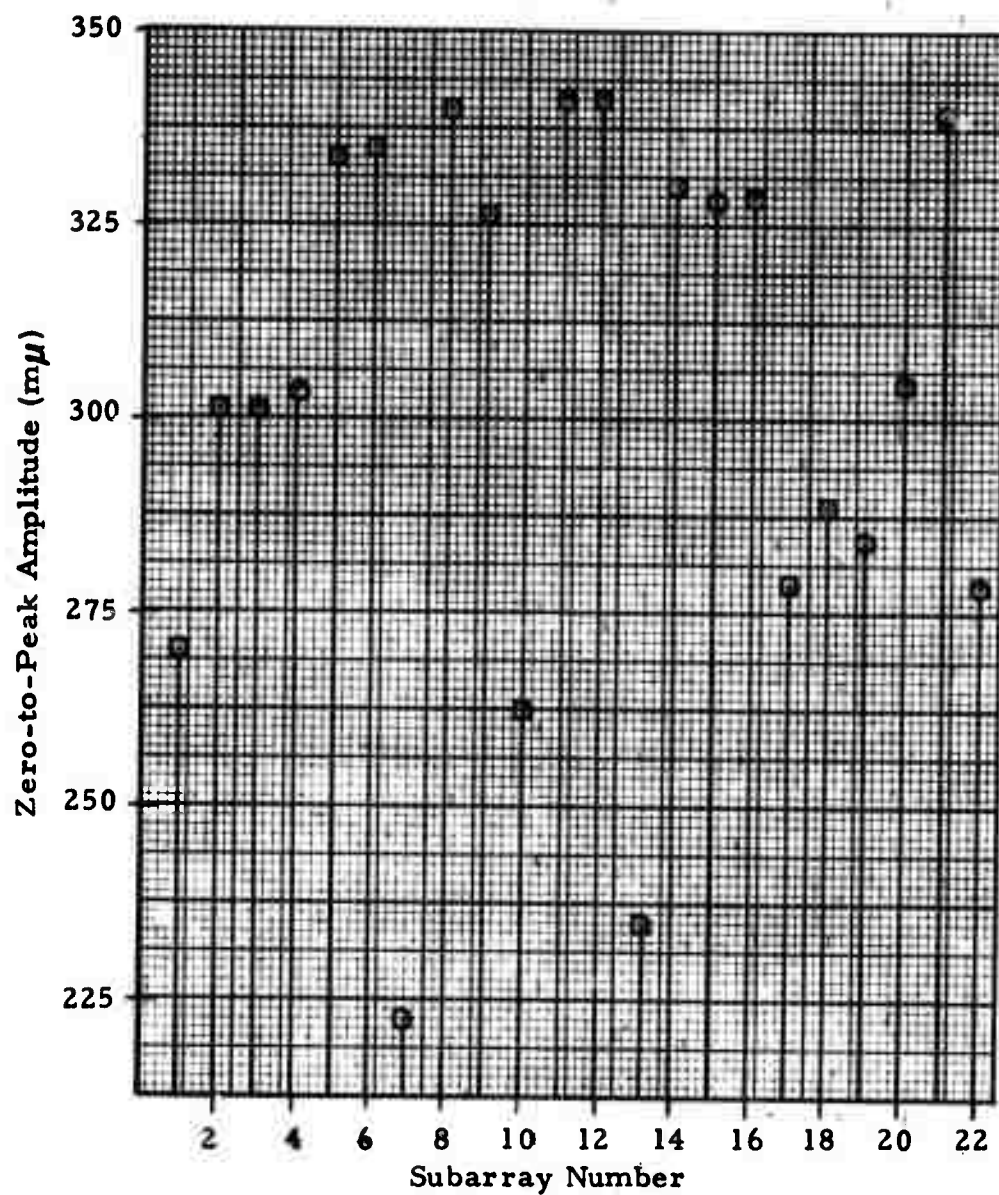


FIGURE III-4  
SUBARRAY SIGNAL AMPLITUDES FOR URA/082/06N

TABLE III-1  
MAXIMUM VARIATION OF SUBARRAY BEAM SIGNAL  
RMS LEVELS ACROSS NORSAR  
(PAGE 1 OF 2)

Event	$m_b$	$\Delta^\circ$	Azimuth $^\circ$	RMS Variation Max/Min (dB)	Maximum Subarray	Minimum Subarray
KUR/099/15N	5.1	69.0	32.1	18.2	3	15
KUR/077/03N	5.1	66.5	23.8	9.8	9	15
KUR/095/17N	5.1	69.1	28.1	6.9	3	21
KUR/213/02N	5.6	65.5	23.1	12.4	3	19
JAP/063/07N	5.2	71.4	36.0	11.5	9	16
JAP/072/03N	5.1	71.6	37.1	10.6	9	6
KMI/073/12N	5.3	62.8	19.6	14.5	3	15
KIR/082/09N	5.7	44.6	83.2	10.4	12	7
KIR/082/20N	6.0	44.6	83.2	9.3	12	7
KIR/083/20N	5.3	44.7	83.0	15.1	11	7
SIN/207/01N	6.0	44.8	86.4	9.7	11	7
KAZ/181/04N	5.4	38.3	74.5	16.1	14	20
KAZ/081/04N	5.8	38.1	75.5	20.7	14	20
KAZ/170/04N	5.5	37.6	75.5	25.3	14	20
KAZ/115/03N	5.9	38.0	75.4	23.3	11	20
KAZ/145/04N	5.2	38.0	75.4	20.6	14	20
KAZ/157/04N	5.5	37.7	75.4	19.7	14	20
SZE/070/04N	5.1	66.6	72.7	4.8	10	12
TIB/093/07N	5.1	59.6	77.5	5.9	9	20
TIB/123/00N	5.4	55.6	87.3	9.7	10	7
TIB/155/14N	5.0	59.6	77.5	10.0	9	7
TSI/083/13N	5.8	58.3	72.9	8.1	10	7
IRA/102/19N1	6.0	44.1	110.9	8.8	18	9
IRA/221/02N	5.2	36.0	113.7	11.9	4	22
URA/082/06N	5.6	21.6	68.6	5.2	12	7
URA/191/16N	5.3	20.3	61.2	6.5	9	10

TABLE III-1  
 MAXIMUM VARIATION OF SUBARRAY BEAM SIGNAL  
 RMS LEVELS ACROSS NORSAR  
 (PAGE 2 OF 2)

Event	$m_b$	$\Delta^\circ$	Azimuth $^\circ$	RMS Variation Max/Min (dB)	Maximum Subarray	Minimum Subarray
WRS/295/05N	5.3	25.4	91.4	9.4	22	7
WRS/277/10N	5.1	17.3	71.5	11.3	5	7
GRE/109/02N	5.1	22.6	160.2	11.1	3	20
TUR/252/15N	5.3	26.5	143.8	9.2	8	13
VAN/072/23N	5.7	64.2	333.5	10.2	1	13

Average Variation (All Events) = 11.8

The subarrays having the largest and smallest signal amplitudes tend to repeat for a given region, especially if general rather than detailed amplitude values are considered. That is, for the Kuriles - Kamchatka - Japan region, subarrays 3 and 9 had high amplitudes for all the events and subarrays 6, 15, 16, 19, and 21 had low amplitudes. Thus diversity-stack weights (for array beamforming) calculated from large events should be satisfactory for application to small events, although they probably won't be exactly correct.

Finally, it is interesting to note that the largest-amplitude subarrays for some events are the smallest-amplitude for others. For example, subarray 9 has large signal amplitudes for the Kuriles - Kamchatka - Japan region, and small signal amplitudes for Iran.

#### D. SIGNAL SPECTRAL CONTENT

Signal spectral content was studied by computing power density spectra over a 6.4 second gate beginning just before the P-wave arrival for several large signal-to-noise ratio events. Figures III-5 to III-8 show the reference subarray and adjusted delay array beam for two earthquakes and two presumed explosions. The system response has not been removed, but the spectra have to be normalized to  $\text{dB re } 1(\text{m}\mu)^2/\text{Hz}$  at 1.0 Hz.

Figures III-5 and III-6 are spectra for two presumed explosions, URA/082/06N ( $\Delta = 22^\circ$ ) and KAZ/115/03N ( $\Delta = 36^\circ$ ). The spectra are essentially flat out to about 2.5 Hz, then drop off rapidly at higher frequencies. The lower spectral values on the adjusted-delay beam are not because of signal loss, since the reference subarray beam is the subarray with the largest signal amplitude. The reference subarray signal RMS levels are 3 to 13 dB, and typically 6 dB above the average subarray level. Thus the average subarray beam spectra for these two events would be about 6 dB lower than the reference subarray spectra and hence it can be seen that there was little signal loss out to 2.5 Hz for both URA/082/06N and KAZ/115/03N. It also should be pointed out that some Eurasian earthquakes, especially those with  $\Delta < 30^\circ$ , have significant high-frequency energy.

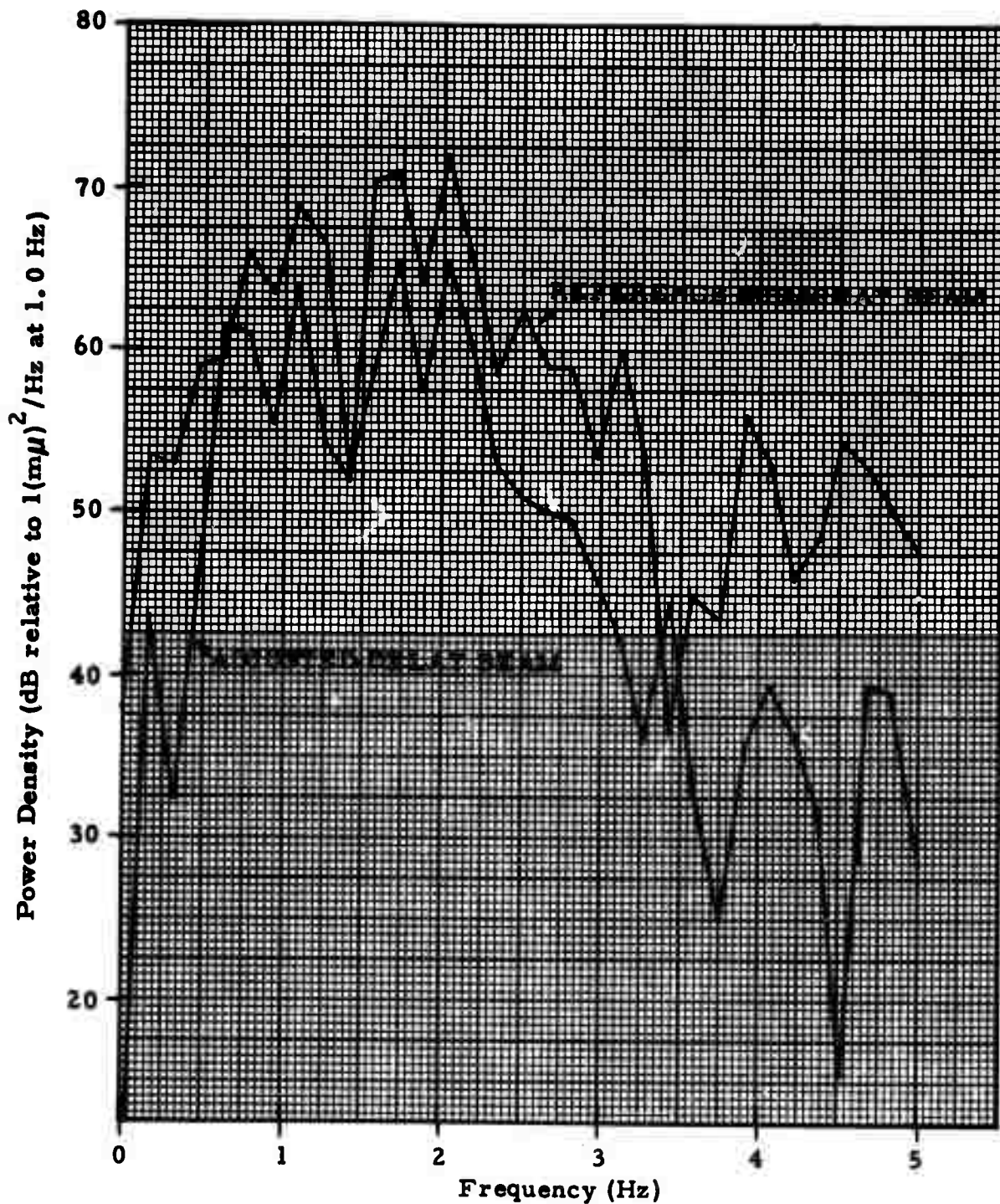


FIGURE III-5  
REFERENCE SUBARRAY AND ARRAY BEAM SIGNAL SPECTRA  
OF EVENT URA/082/06N

42c

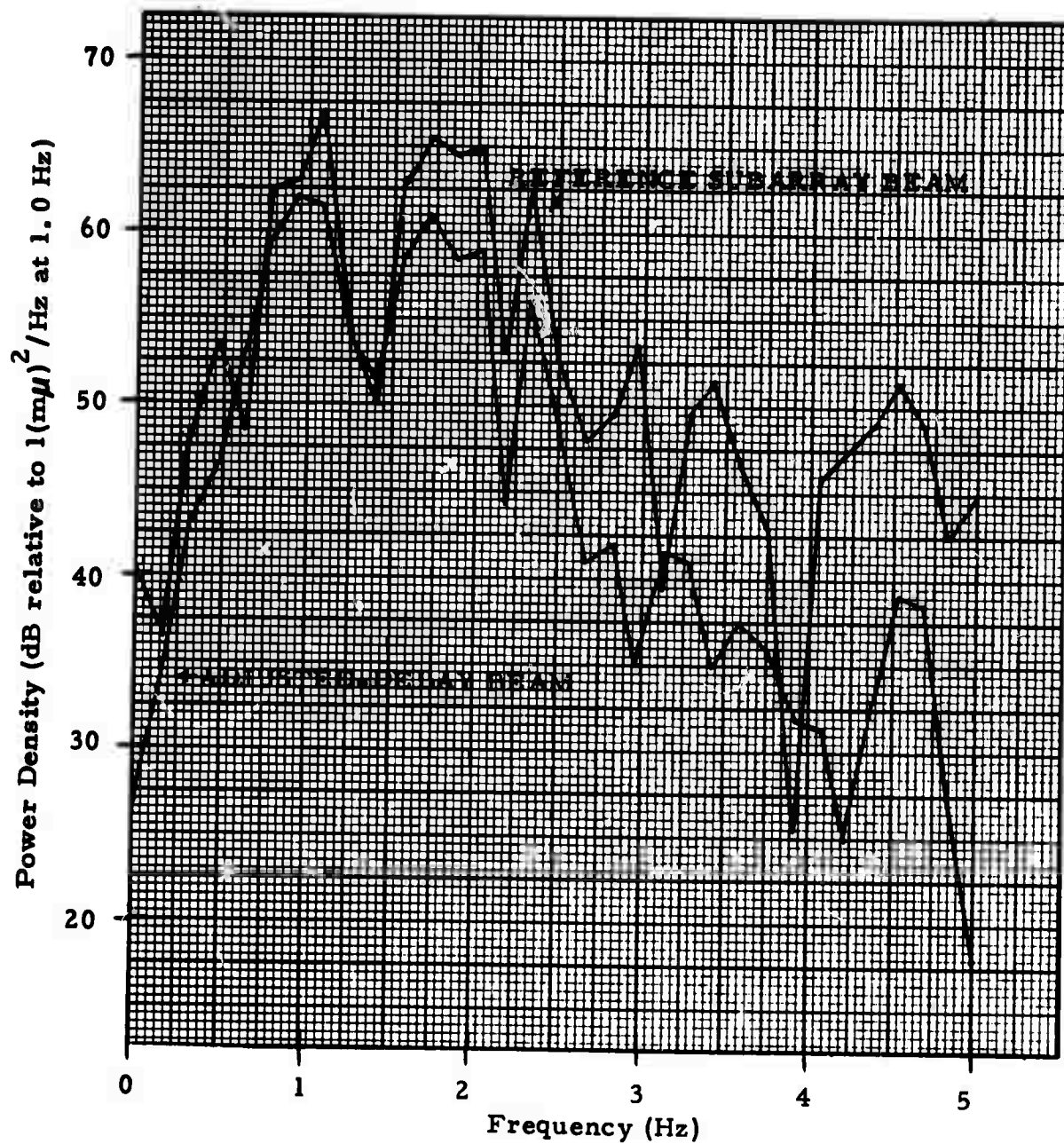


FIGURE III-6  
REFERENCE SUBARRAY AND ARRAY BEAM SIGNAL SPECTRA  
OF EVENT KAZ/115/03N

Figures III-7 and III-8 are spectra for two earthquakes, KIR/082/20N ( $\Delta = 45^\circ$ ) and TSI/083/13N ( $\Delta = 58^\circ$ ). Both events have spectral peaks at about 0.8 Hz; KIR/082/20N has a secondary peak at 1.4 Hz whereas TSI/083/13N drops off uniformly at higher frequencies. Again, array beamforming signal loss appears to be small for both events.

There appears to be a significant difference in signal energy content for events from the western hemisphere as compared with those from Eurasia. For our limited ensemble of western hemisphere events, spectral content generally is of a lower frequency for both earthquakes and presumed explosions. Figure III-9 shows the spectrum for an event from the Nevada test site ( $\Delta = 73^\circ$ ); this presumed explosion spectrum drops off at about 1.4 Hz.

We do not have enough data as yet to make comments about spectral content as a function of region in Eurasia, except to say that, not unexpectedly, Eurasian signals (both earthquakes and presumed explosions) from  $\Delta < 30^\circ$  generally have higher frequency content. Regional characteristics of signal spectra will be studied in the future.

#### E. TIME DELAY ANOMALIES

It was established early in the analysis that standard plane-wave delays generally were adequate for subarray beamforming, but that time delay anomalies (deviations from plane wave propagation along the great circle azimuth) had to be accounted for in array beamforming.

Inter-subarray time delay anomalies were calculated by computing the crosscorrelation functions between the reference subarray beam and the remaining subarray beams for all large SNR events. A short signal gate (generally 6.4 seconds) was used in the computations. In cases where inconsistent or uncertain delays were obtained, results were hand checked by measuring delay anomalies from the time traces. After computation, the delay anomalies were adjusted so that they were all relative to subarray 1 at the center of NORSAR.

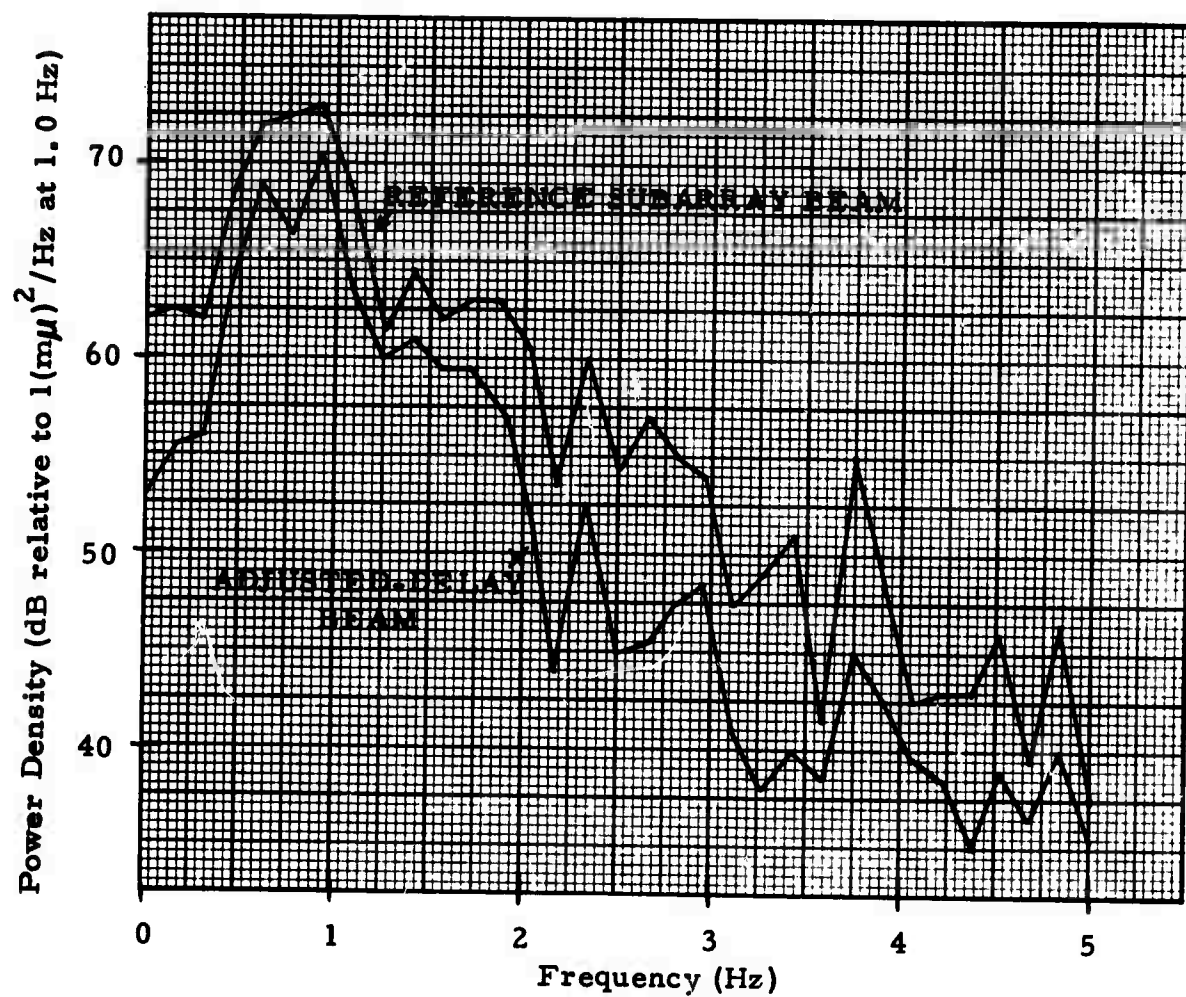


FIGURE III-7  
REFERENCE SUBARRAY AND ARRAY BEAM SIGNAL SPECTRA  
OF EVENT KIR/082/20N

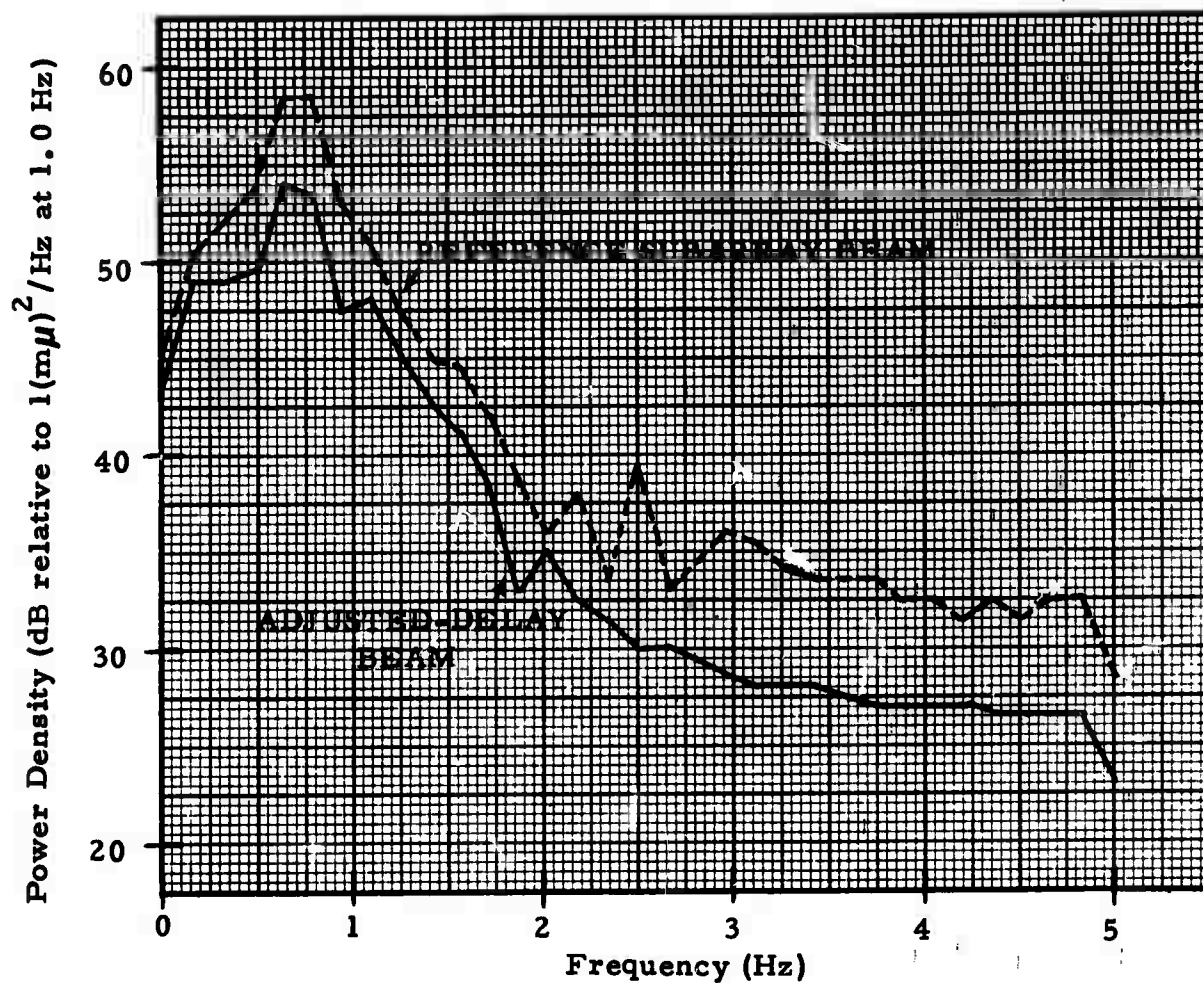


FIGURE III-8  
REFERENCE SUBARRAY AND ARRAY BEAM SIGNAL SPECTRA  
OF EVENT TSI/083/13N

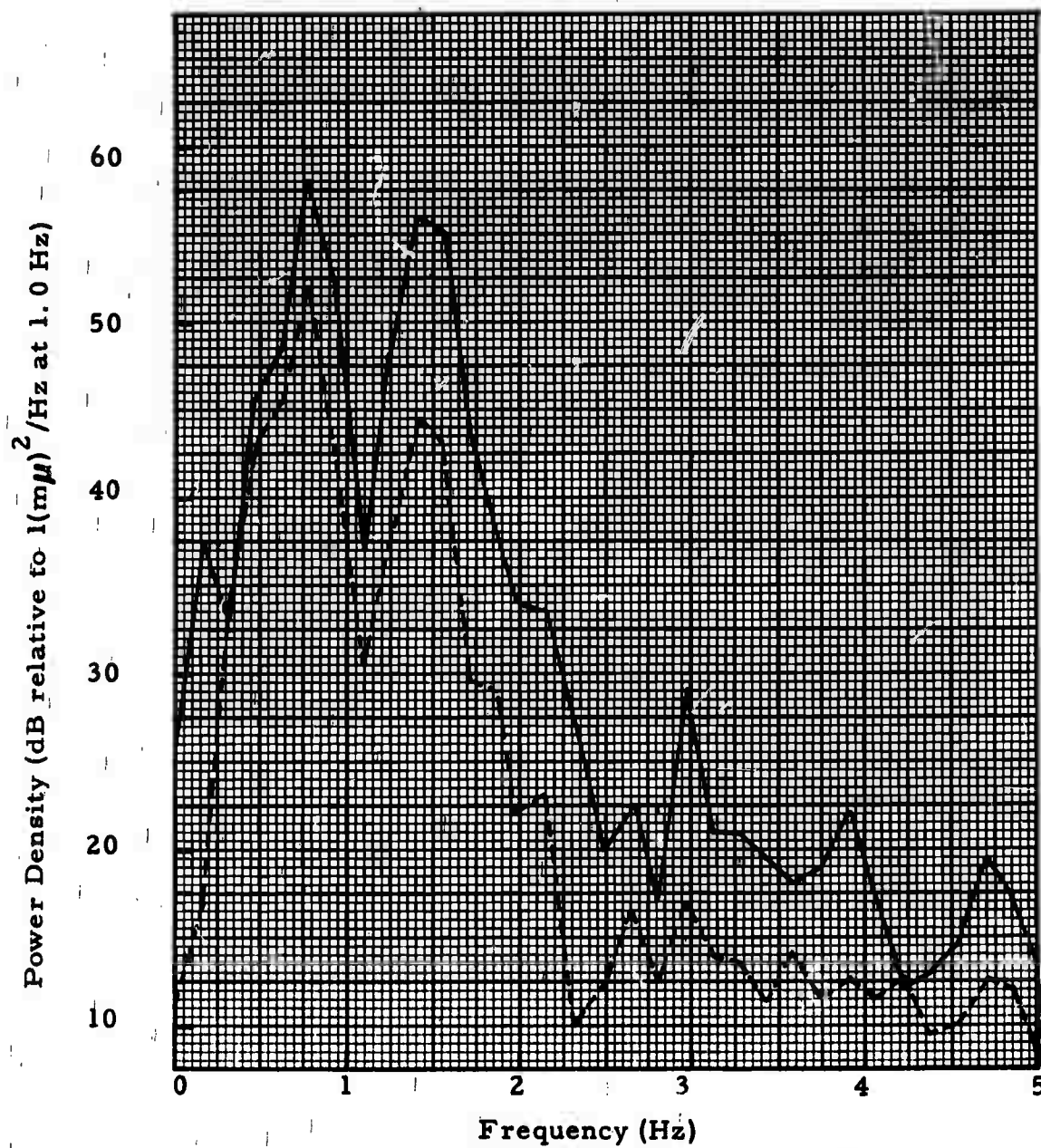


FIGURE III-9  
REFERENCE SUBARRAY AND ARRAY BEAM SIGNAL SPECTRA  
OF EVENT NEV/189/14N

For each subarray the delay anomalies obtained for all events were plotted on a map of the Eurasian continent at the geographic locations (epi-centers) of the events. The anomalies then were reviewed to determine the absolute value of the anomalies and their consistency for events in the same region. The following was observed:

- Anomalies typically were (+) a few tenths but occasionally reached a full second. Anomalies generally were larger for subarrays on the outer ring.
- Consistent delays could be obtained for Kamchatka/ Kuriles, Eastern Kazakh, South Central Russia, and China. Table III-2 shows the anomalies for four large South Central Russia events; the individual event values differ from the average value by more than 0.1 seconds only for subarray 7. Because the absolute value of delay anomalies over all other subarrays is 0.7 seconds or less, it appears that the subarray 7 delays determined for the Kirgiz events are erroneous. Delay anomalies obtained from other smaller events more widely scattered throughout the area agreed closely with those shown in Table III-2. It is interesting to note that all anomalies were zero or negative; this implies that the signal was early (relative to all other subarrays) at subarray 1.
- Consistent delays could not be obtained from close-in events from the Mediterranean and Western Russia. Table III-3 shows the delays for four moderate Mediterranean events which are located in a circle with a radius of  $5^{\circ}$ . Delay anomalies vary by as much as 1.0 second at some subarrays event to event. Anomalies are not consistent even for GRE/109/02N and GRE/068/04N, which have essentially the same epicenter. The difficulty is obtaining consistent delays for the close-in events results because the

TABLE III-2

## DELAY ANOMALIES FOR FOUR SOUTH CENTRAL RUSSIAN EVENTS

Subarray	Delay Anomalies (tenths of seconds)			Average
	-KIR/082/09N $\Delta = 44.6$ Azimuth=83.2	KIR/082/20N $\Delta = 44.6$ Azimuth=83.2	KIR/083/20N $\Delta = 44.7$ Azimuth=83.0	SIN/083/20N $\Delta = 44.8$ Azimuth=86.4
2	-2	-2	-2	-2
3	-4	-4	-3	-4
4	-3	-3	-3	-2
5	-2	-2	-1	-1
6	-1	-1	-1	0
7	-18(?)	-18(?)	-18(?)	-2
8	-1	-1	0	-1
9	-4	-4	-4	-4
10	-4	-4	-4	-4
11	-7	-7	-7	-7
12	-6	-6	-6	-6
13	-5	-5	-5	-5
14	-3	-3	-3	-3
15	-1	-1	-1	-1
16	0	0	0	0
17	-1	-1	-1	-2
18	-3	-3	-3	-3
19	-5	-5	-5	-4
20	-5	-5	-5	-6
21	-4	-4	-4	-5
22	-2	-2	-3	-2
				-2.0
				-3.8
				-2.8
				-1.7
				-0.8
				-14.0
				-0.8
				-4.0
				-4.0
				-7.0
				-6.0
				-5.0
				-3.0
				-1.0
				0.0
				-1.3
				-3.0
				-4.8
				-5.2
				-4.2
				-2.2

TABLE III-3

## DELAY ANOMALIES FOR FOUR MEDITERRANEAN EVENTS

Subarray	Delay Anomalies (tenths of seconds)			
	GRE/109/02N $\Delta = 22.6$ Azimuth=160.2	GRE/068/04N $\Delta = 22.4$ Azimuth=160.7	GRE/074/15N $\Delta = 25.0$ Azimuth=154.6	TUR/067/23N $\Delta = 26.2$ Azimuth=144.4
2	0	1	-1	1
3	1	1	0	3
4	0	1	0	0
5	-7	-6	-4	3
6	-5	-5	-2	3
7	-3	-3	0	-1
8	0	-2	0	-2
9	-2	-1	1	0
10	-2	-2	1	1
11	2	2	5	5
12	3	4	5	7
13	5	6	3	-1
14	-3	-1	0	2
15	12(?)	-3	2	7
16	3	3	2	6
17		4	3	6
18	5	4	2	6
19	7	-3	1	6
20	-2	-6	-1	6
21	-1	-1	1	7
22	0	0	2	6

events are rich in high frequencies. These higher frequency arrivals may have different paths (perhaps because of local crustal effects) or be incoherent among subarrays; either case would make obtaining consistent delays very difficult. More work is needed to determine appropriate delays for these close-in events.

#### F. COMPARISON OF NORSAR $m_b$ VALUES WITH PDE AND LASA $m_b$ 's

NORSAR  $m_b$  values were measured for the 85 detected events using the formula:

$$m_b = \log \frac{A}{T} + B$$

where: A is the maximum peak-to-peak signal amplitude in  $m\mu$  on the adjusted delay array beam

T is the period of the cycle with the maximum amplitude

B is the distance factor

Values for B are shown in Table III-4; these also are used for calculation of LASA  $m_b$ 's.

Figure II-10 is a plot of NORSAR  $m_b$ 's versus either PDE  $m_b$ 's (circles) or LASA  $m_b$ 's (crosses). Note that on the average LASA and PDE  $m_b$ 's are the same (Dean, 1971) so that the data points can be considered together. Values for presumed explosions are circled.

In general the NORSAR  $m_b$ 's are somewhat smaller than the LASA and PDE  $m_b$ 's; the difference is somewhat more pronounced for  $m_b \leq 5.3$ . We do not have an explanation for the apparently larger difference at lower magnitudes; it is neither distance- nor region-dependent. Further, our data do not indicate that beamforming loss is lower for large events. It may be simply statistical scatter, or it may be related to the fact that several of the larger events were presumed explosions. The most likely explanation is that the PDE magnitudes for small events are based on the quieter stations in the PDE net (e.g., TFO), which tend to give lower than average magnitudes. We plan to investigate this difference in more detail in the future.

TABLE III-4  
DISTANCE FACTOR (B) FOR COMPUTING NORSAR  $m_b$  VALUES

Distance Degrees	B	Distance Degrees	B	Distance Degrees	B
0					
1	0.50	35	3.34	69	3.48
2	1.50	36	3.34	70	3.49
3	2.50	37	3.34	71	3.50
4	2.55	38	3.33	72	3.50
5	2.76	39	3.33	73	3.51
6	2.90	40	3.32	74	3.51
7	3.02	41	3.32	75	3.52
8	3.10	42	3.32	76	3.53
9	3.15	43	3.33	77	3.53
10	3.20	44	3.33	78	3.54
11	3.23	45	3.34	79	3.54
12	3.25	46	3.34	80	3.55
13	3.26	47	3.35	81	3.56
14	3.26	48	3.36	82	3.57
15	3.25	49	3.36	83	3.58
16	3.21	50	3.37	84	3.59
17	3.10	51	3.37	85	3.61
18	2.98	52	3.38	86	3.64
19	2.79	53	3.39	87	3.66
20	2.77	54	3.39	88	3.68
21	2.80	55	3.40	89	3.72
22	2.85	56	3.40	90	3.76
23	2.94	57	3.41	91	3.80
24	3.04	58	3.42	92	3.85
25	3.15	59	3.42	93	3.90
26	3.24	60	3.43	94	3.96
27	3.34	61	3.44	95	4.02
28	3.42	62	3.44	96	4.11
29	3.44	63	3.45	97	4.19
30	3.42	64	3.45	98	4.28
31	3.38	65	3.46	99	4.40
32	3.36	66	3.46	100	4.56
33	3.36	67	3.47		
34	3.35	68	3.48		

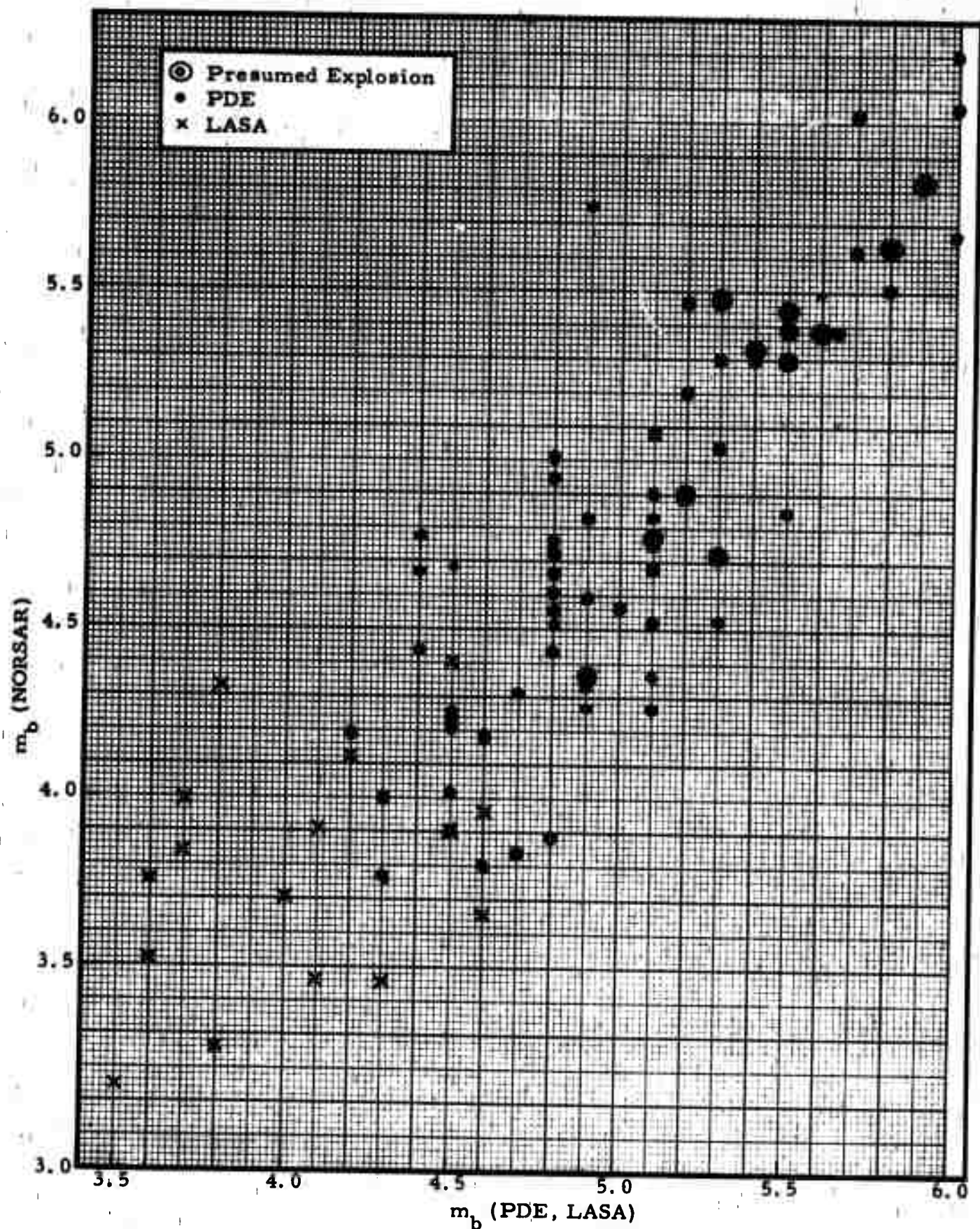


FIGURE III-10

NORSAR MAGNITUDE VERSUS PDE OR LASA MAGNITUDE

Figure III-11 is a histogram of the magnitude difference (NORSAR minus PDE or LASA). The shaded area of the histogram corresponds to LASA  $m_b$ 's. There is a 0.2 magnitude unit negative bias; this could be accounted for by signal loss in beamforming, which typically is 3 to 4 dB (0.15 to 0.2 magnitude units). Note that the LASA magnitudes are corrected for beamforming loss but our NORSAR magnitudes are not. The distribution about this bias appears to be approximately normal and reflects normal variance in signal amplitude due to radiation patterns and/or propagation effects. It appears that, if signal loss in beamforming is accounted for, NORSAR  $m_b$ 's would be equivalent to PDE or LASA  $m_b$ 's. Still to be explained, however, is the apparent magnitude-dependence of the NORSAR/PDE (or LASA)  $m_b$  difference.

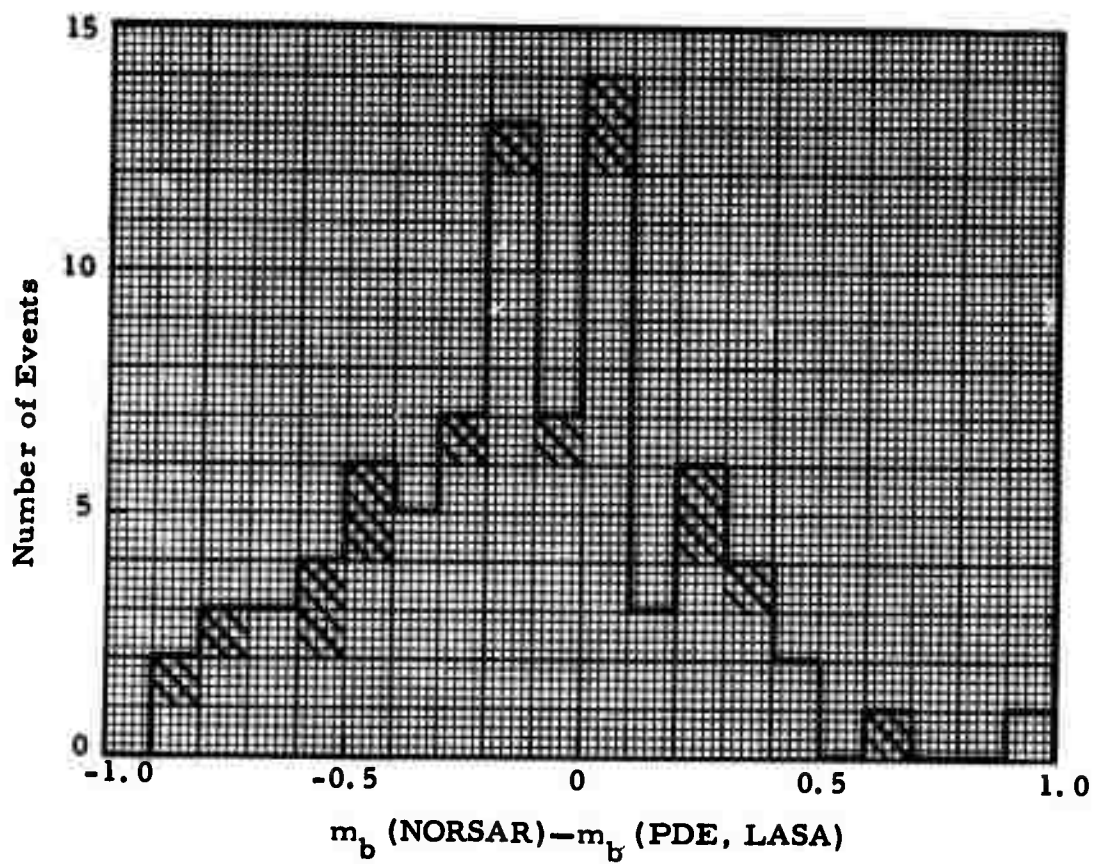


FIGURE III-11  
HISTOGRAM OF DIFFERENCES BETWEEN NORSAR AND  
PDE OR LASA  $m_b$  FOR 85 EVENTS

## SECTION IV

### ARRAY BEAMFORMING RESULTS

#### A. INTRODUCTION

This section covers signal-to-noise ratio improvement achieved by NORSAR short-period array beamforming. Subsection B covers noise reduction both at the subarray level and at the array level, while subsection C analyzes signal degradation at both these levels. Subsection D presents direct signal-to-noise ratio measurements for subarray beams and the various types of array beams and combines these with the results of the two previous subsections in an attempt to specify where noise reduction and signal degradation occur. In addition, the signal-to-noise ratio on the subarray with the strongest signal arrival is compared with that of the adjusted-delay beam. Finally, the amount of signal-to-noise ratio improvement obtained by the diversity-stack beamforming technique is examined.

#### B. NOISE REDUCTION

Noise reduction in forming subarray beams and the array beam at NORSAR was only slightly below the  $\sqrt{N}$  reduction expected from summing  $N$  uncorrelated, equal-strength traces.

Figure IV-1 shows noise reduction from single sensor to subarray as a function of frequency for typical five-minute noise sample preceding an event from northeastern China. At the top are the average single-sensor power spectrum and the average subarray beam power spectrum. The reduction in noise level from single sensor to subarray beam is shown at the bottom. At frequencies above 0.5 Hz, it is remarkably close to the 7.8 dB expected for six equalized traces.

Figure IV-2 gives the corresponding noise reduction from subarray to array beam. At the top, the average subarray beam power spectrum is plotted

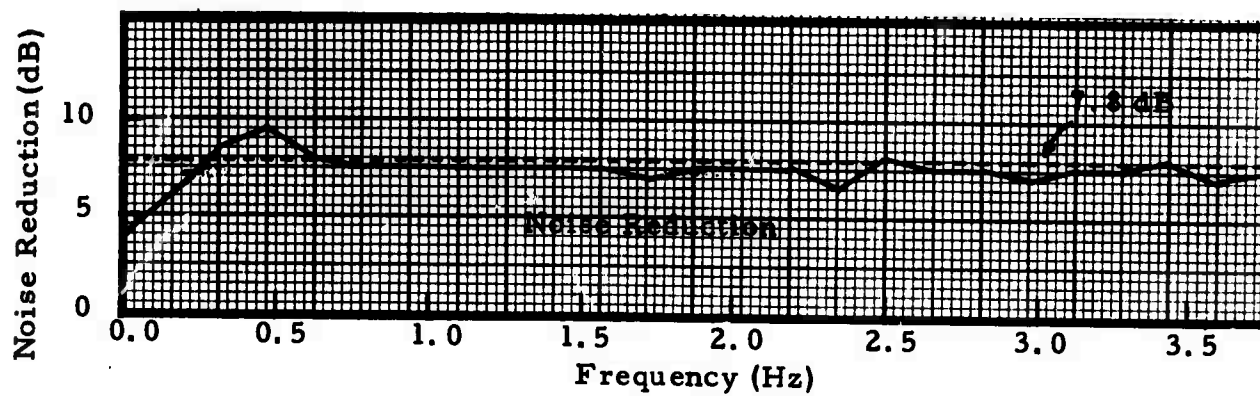
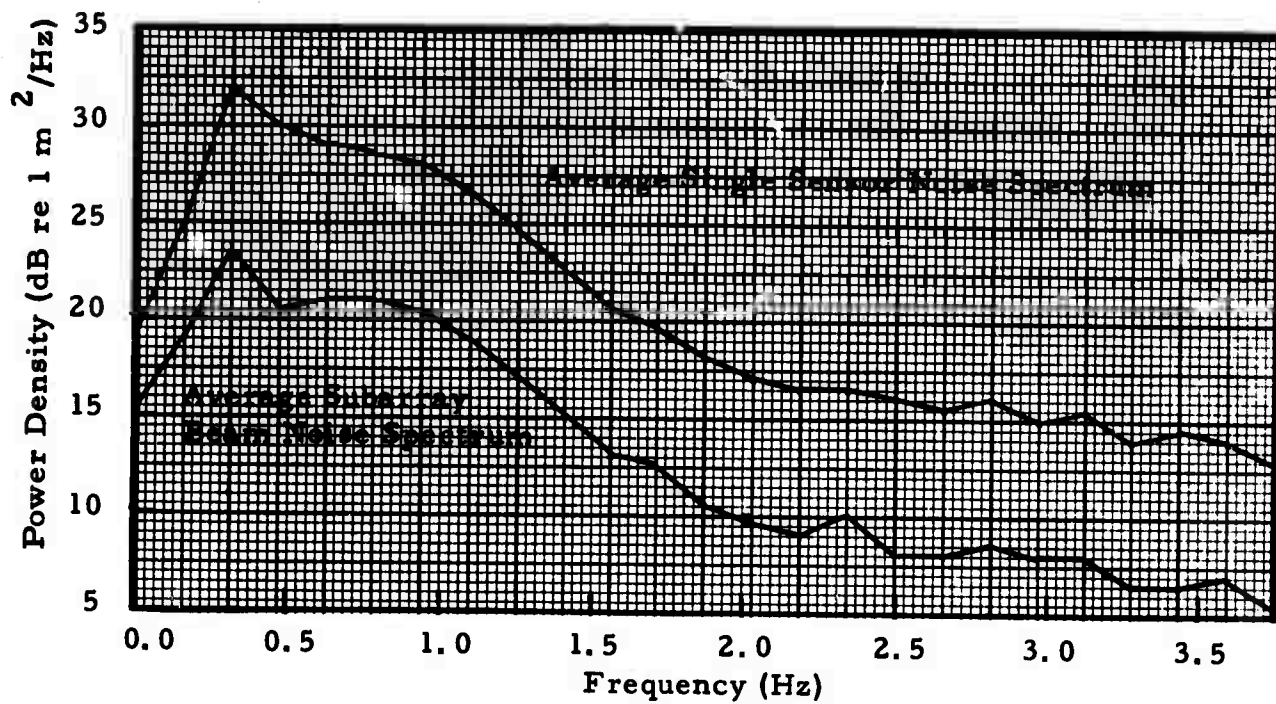


FIGURE IV-1  
SINGLE SENSOR TO SUBARRAY NOISE REDUCTION  
FOR NOISE SAMPLE BEFORE EVENT NEC/156/10N

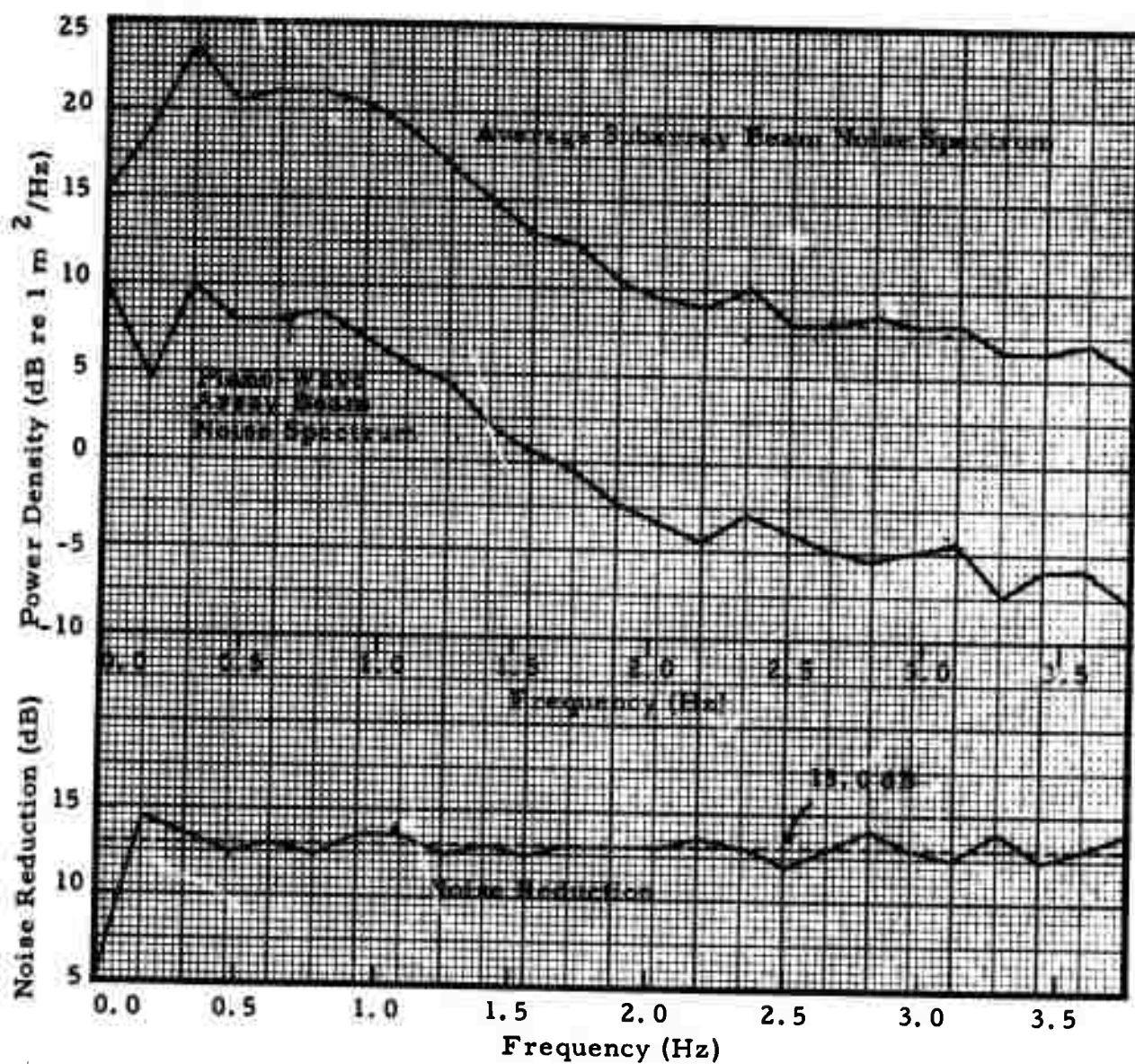


FIGURE IV-2  
 SUBARRAY TO ARRAY NOISE REDUCTION  
 FOR NOISE SAMPLE BEFORE EVENT NEC/156/10N

together with the plane-wave array beam spectrum for the same noise sample. Noise reduction is shown at the bottom. At all frequencies except 0 Hz, it closely follows the 13.0 dB level expected for the twenty subarrays operational during this sample.

Figure IV-3 is a histogram of the drop in noise level from reference subarray to adjusted-delay beam over the band 0.55 to 1.5 Hz for 45 events in which all 22 subarrays were operational. The purpose of this figure is to indicate the amount of noise reduction which can be expected from subarray to array beam. The most common reduction was about 13 dB, slightly below the 13.4 dB level expected for 22 perfectly equalized subarrays. Since one subarray was used instead of all 22 subarrays, part of the spread in values is due to fluctuations of the reference subarray relative to the average subarray power in the band 0.55 to 1.5 Hz.

Noise reduction of 7.8 dB at the subarray level together with 13 dB at the array level yields a total noise reduction of slightly below 21 dB.

In addition to demonstrating that  $\sqrt{N}$  noise reduction is achieved at NORSAR, these results indicate that noise levels from sensor to sensor do not vary significantly.

#### C. SIGNAL DEGRADATION

To determine single sensor to subarray signal degradation, hand measurements were made of peak-to-peak displacement in the reference sensor and subarray beam for each subarray. Corresponding cycles in the traces were used in these measurements. Amplitude degradation ratios were averaged across all subarrays. To find subarray to array signal degradation, peak-to-peak variation was also measured on the adjusted-delay beam and compared with the average peak-to-peak displacement across the subarray beams. Table IV-1 gives the subarray level and array level signal degradation obtained in this way for seven large events. The WRS/295/05N adjusted delays are suspect. The subarray beam to adjusted-delay beam degradation for this event is probably the worst encountered

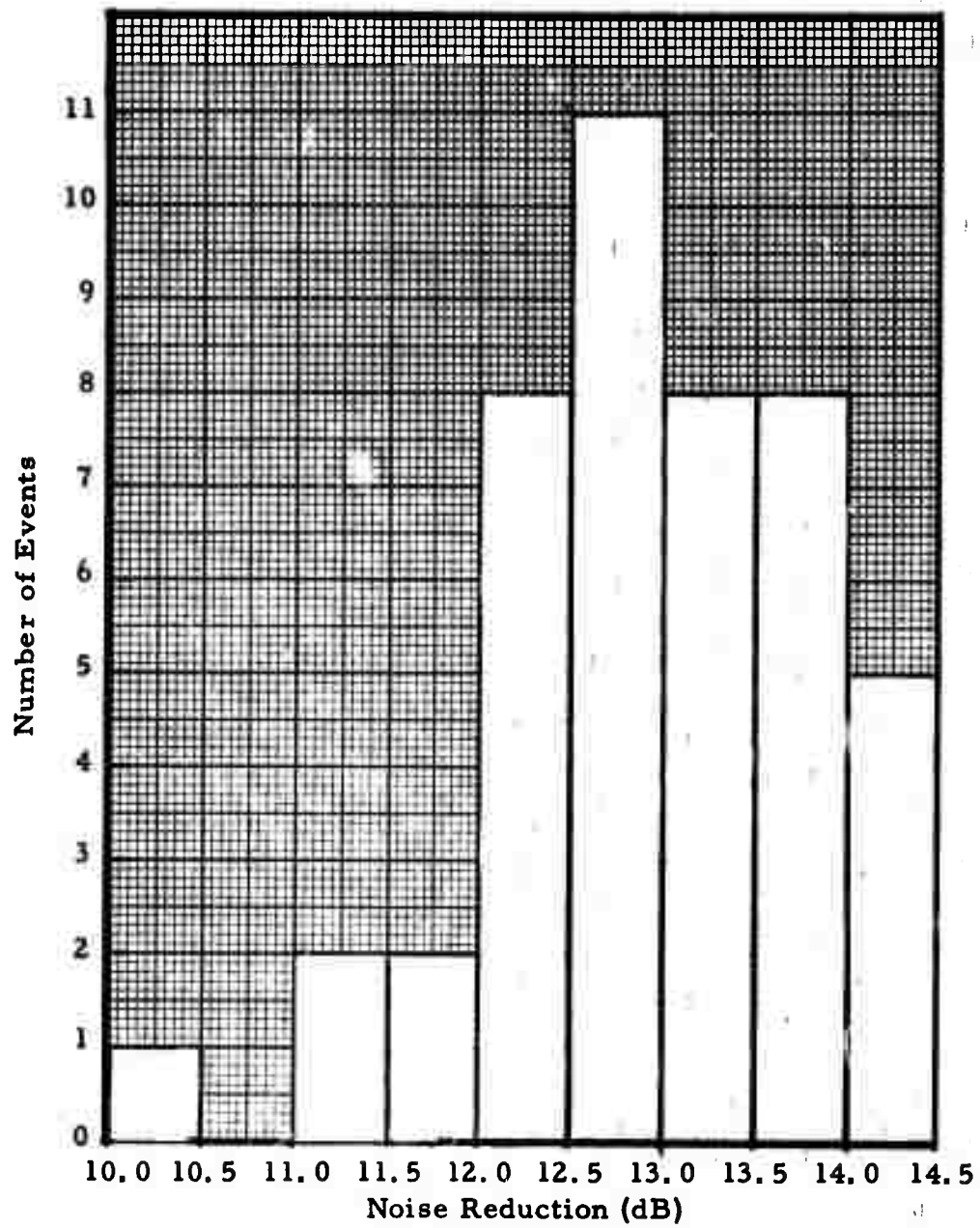


FIGURE IV-3  
NOISE REDUCTION FROM REFERENCE SUBARRAY  
TO ADJUSTED-DELAY BEAM (0.55 TO 1.5 Hz)

**TABLE IV-1**  
**SUBARRAY-LEVEL AND ARRAY-LEVEL SIGNAL DEGRADATION**  
**(FROM HAND MEASUREMENTS)**

Event	Single Sensor to Subarray Beam Degradation (dB)	Subarray Beam to Adjusted-Delay Beam Degradation (dB)	Single Sensor to Adjusted-Delay Beam Degradation (dB)
KAZ/115/03N	1.4	0.3	1.7
TIB/123/00N	1.1	3.1	4.2
TSI/083/13N	0.4	0.3	0.7
VAN/072/03N	0.8	0.4	1.2
IRA/221/02N	1.9	0.3	2.2
WRS/295/05N	1.8	11.0	12.8
KAZ/081/04N	1.4	1.0	2.4

out of all 85 signals detected. Typical signal degradation in forming subarray beams appears to be slightly higher than 1 dB. Degradation in peak-to-peak displacement from subarray to adjusted-delay beam appears to be a surprisingly low 1 to 3 dB (ignoring WRS/295/05N).

Signal degradation from subarray beam to adjusted-delay beam also was computed using RMS measurements over a 6.4 second gate starting a few deciseconds before the signal arrival. RMS values were averaged over all subarray beams and compared with the adjusted-delay beam RMS. Table IV-2 shows subarray beam to adjusted-delay beam degradation for six events whose average subarray beam signal-to-noise ratio was greater than 10 dB. Results are for unfiltered traces and traces passed through the "standard" detection filter (see Figure II-4). Broadband degradation is not given for the event BLS/210/19N because the signal-to-noise ratio for the average subarray beam was less than 10 dB. On a broadband basis, signal degradation was 1 to 3 dB, except for the two events from western Russia (which probably have inaccurate adjusted-delays). These values agree reasonably well with the amplitude measurements made directly from the time traces.

For beams passed through the "standard" detection filter signal degradation from subarray to adjusted-delay beam is 3 or 4 dB. Slightly higher degradation is observed because the low frequency energy, which is generally more coherent across the array, is attenuated by the detection filter and hence is not as significant in the RMS calculations from which signal degradation was estimated.

#### D. SIGNAL-TO-NOISE IMPROVEMENT

##### 1. Improvement from Single Sensor to Subarray Beam

In forming subarray beams, noise levels were reduced about 7.5 dB, slightly less than the 7.8 dB expected from 6 equalized sensors. Signals were degraded anywhere from 0 dB to 2 dB, with an average degradation of about 1 dB. Thus signal-to-noise improvement was approximately 6.5 dB, with variations of about 1 dB above or below this figure.

**TABLE IV-2**  
**SIGNAL DEGRADATION FROM AVERAGE SUBARRAY BEAM TO**  
**ADJUSTED-DELAY BEAM**

Event	Broadband Degradation (dB)	Degradation for Filtered Beams (dB)
KUR/185/15N	2.2	2.9
WRS/277/10N	8.6	8.4
WRS/295/05N	7.3	11.8
AND/087/08N	0.9	2.8
SIN/207/01N	3.0	3.6
BLS/210/19N	—	4.3

## 2. Improvement from Subarray Beam to Adjusted-Delay Beam

For twenty-five events, subarray signal powers over a short gate starting just before the signal arrival were averaged over all operating subarrays. Gate length varied from 6.4 seconds to 19.2 seconds, but was normally 6.4 seconds. Noise powers for the same subarrays over a longer gate starting about 75 seconds and ending about 5 seconds before the signal arrival also were averaged. From these figures, an average subarray beam signal-to-noise ratio was computed and compared with a similarly computed signal-to-noise ratio for the adjusted-delay beam. Figure IV-4 is a histogram of the signal-to-noise ratio improvement from average subarray beam to adjusted-delay beam (where all the beams have been passed through the standard detection filter). Most commonly, signal-to-noise improvement is about 11 dB. In the case of three events from western Russia and southwestern Russia, improvement is below 3.5 dB, probably because adjusted-delays are inaccurate.

Signal-to-noise improvement of 11 dB from subarray to adjusted-delay beam is somewhat higher than would be expected with the 3.4 dB signal degradation figure derived from the events KUR/185/15N, AND/087/08N, SIN/207/01N and BLS/210/19N. In fact, the improvement for these events was 10.6 dB, 10.4 dB, 10.5 dB and 9.0 dB, respectively. It appears that the 3.4 dB signal degradation figure for these events is about 1 dB higher than normal.

Single sensor to subarray signal-to-noise ratio improvement of 6.5 dB together with subarray to adjusted-delay beam improvement of 11 dB yields a total signal-to-noise ratio improvement of 17.5. Without signal degradation, the single-sensor to adjusted-delay beam noise reduction would have given an improvement of 21 dB. It appears that about 1 dB was lost at the subarray level and about 2.5 dB in forming the array beam from the subarray beams.

## 3. Comparison of Signal-to-Noise Ratios for the Reference Subarray and Adjusted-Delay Beam

Because of the large variation in signal amplitudes from subarray to subarray, it is useful to compare the reference subarray signal-to-noise ratio

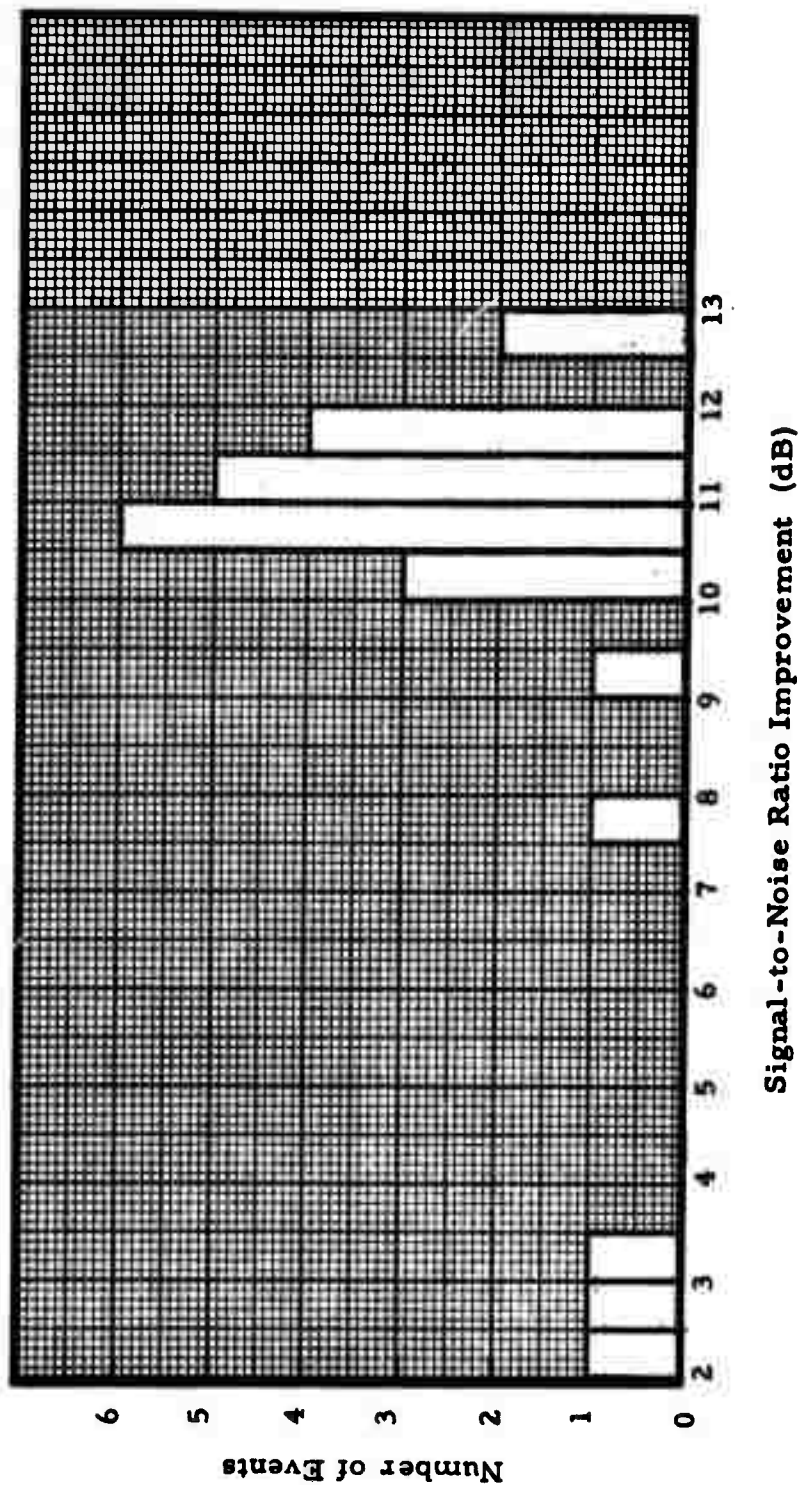


**FIGURE IV-4**  
**SIGNAL-TO-NOISE RATIO IMPROVEMENT OF ADJUSTED-DELAY BEAM**  
**RELATIVE TO AVERAGE SUBARRAY BEAM**  
**(DATA PROCESSED THROUGH STANDARD FILTER)**

with that of the adjusted-delay beam. Note that the reference subarray is the subarray with the highest signal-to-noise ratio. Figure IV-5 is a histogram, for data passed through the standard detection filter, of the signal-to-noise ratio improvement from the reference subarray beam to the adjusted-delay beam for 26 events. In four cases, the signal-to-noise ratio is higher at the reference subarray. Two of these events are from western Russia and two are from southwestern Russia. The remaining 22 events vary from 0 to 7.5 dB increase in signal-to-noise ratio on the adjusted-delay beam. Two peaks in improvement, at 1 dB and 5 dB, are observed, of which the second is the most common. If the subarray with the highest signal-to-noise ratio were used as the array beam instead of the adjusted-delay beam, it is interesting that no more than 7.5 dB in signal-to-noise ratio would be lost. In a few cases, the signal-to-noise ratio would be increased. This fact, however, does not mean that all but one subarray could be eliminated from the array with signal-to-noise ratio loss no higher than that indicated by the figure, because the subarray with the strongest signal changes with event location.

#### 4. Signal-to-Noise Ratio Improvement Obtained by Diversity-Stack Beamforming

Selective weighting of the subarray beams according to the signal-to-noise ratio on each prior to the time-shift-and-sum process provides some improvement in the signal-to-noise ratio of the resultant beam. Such a beam is called a diversity-stack beam. Figure IV-6 is a histogram of the improvement achieved in this way for 26 events whose subarray beams were filtered using the standard detection filter. In most cases, improvement is close to 1 dB. The two cases that resulted in degradation were caused by inability to determine accurately the signal power on the subarray beam. For both these events, the average subarray signal-to-noise ratio was less than 0 dB.

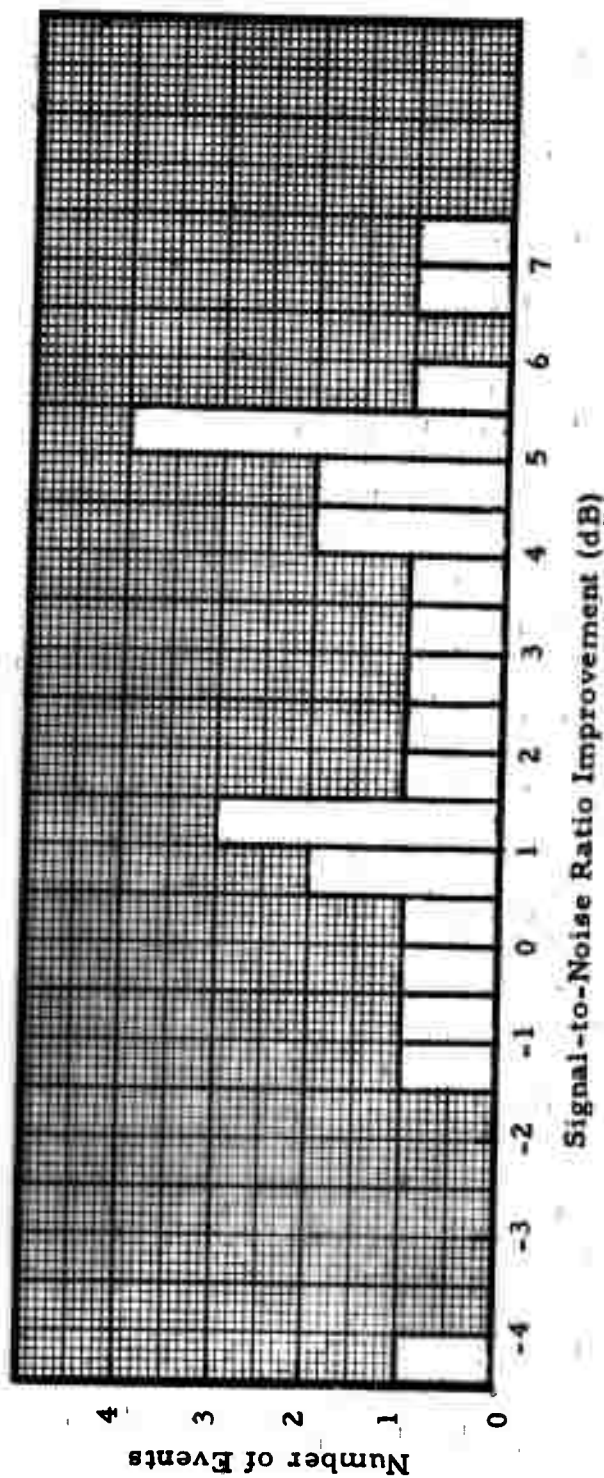


FIGURE IV-5

SIGNAL-TO-NOISE RATIO IMPROVEMENT OF ADJUSTED-DELAY BEAM  
RELATIVE TO REFERENCE SUBARRAY BEAM  
(DATA PASSED THROUGH STANDARD DETECTION FILTER)

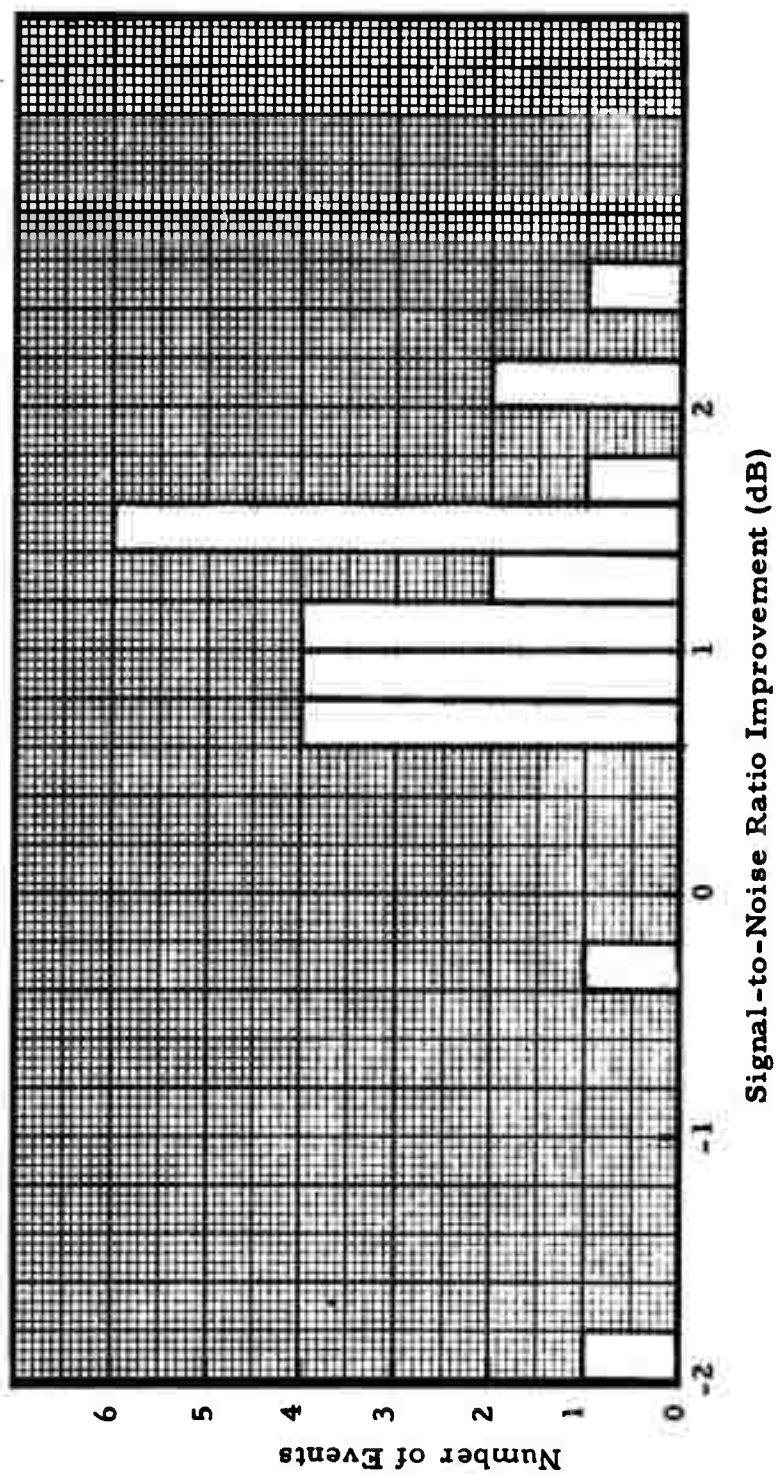


FIGURE IV-6  
 SIGNAL-TO-NOISE RATIO IMPROVEMENT OF DIVERSITY-STACK BEAM  
 RELATIVE TO ADJUSTED-DELAY BEAM  
 (DATA PASSED THROUGH STANDARD FILTER)

## SECTION V

### PRELIMINARY ESTIMATE OF THE NORSAR SHORT-PERIOD TELESEISMIC DETECTION THRESHOLD

A preliminary study of the detectability of teleseismic P-waves using the NORSAR short-period array has been made. The adjusted-delay array beam was used for P-wave detection. In almost all cases where event magnitude was below 4.5, a "standard" detection filter was used (see Figure II-4). The frequency response of this filter was  $-10(f - 2)^6$  dB, where  $f$  is the frequency in Hz. To obtain this filter, a filter was designed to maximize the ratio of the lowest filtered signal power to the highest filtered noise power for an ensemble of about 25 signals and 25 noise samples. From the filter derived in this way, the "standard" detection filter was selected by requiring a flat response near the center frequency and a rolloff rate approximating that of the designed filter. In several cases, detections were made using the "standard" filter when a 0.5 to 5.0 Hz bandpass filter failed to work. There were only one or two cases where a different (narrower band) filter allowed detection; thus the standard filter is close to optimum for detection of Eurasian events.

The data base used in this study consisted of 103 events reported in the LASA and/or the PDE bulletin. Of this population a total of nineteen events ranging in body-wave magnitude from 3.5 to 4.3 were not detected by NORSAR. The detected/not detected status of a subset of this population as a function of  $m_b$  and distance from NORSAR is illustrated in Figure V-1. The expected tendency for detectability to decrease as a function of increasing epicentral distance is not clearly shown by this figure. This is possibly due at least in part to the scarcity of data, but several additional observations should be made. Four events in the epicentral distance range twenty to thirty degrees and ranging in magnitude from 3.8 to 4.1 were not detected. Three of these events occurred in southwest Russia.

V-2

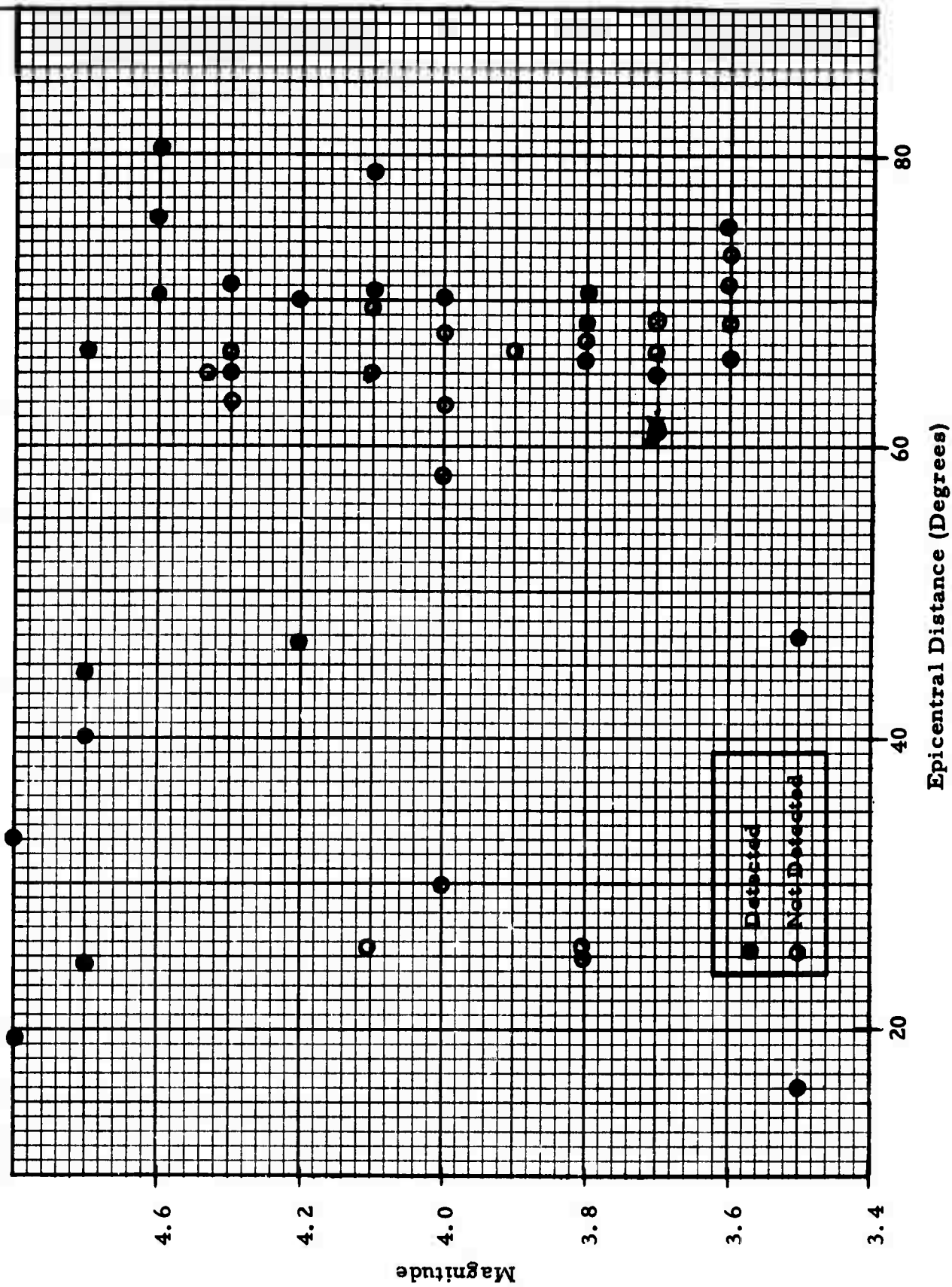


FIGURE V-1

NORSAR P WAVE DETECTIONS/MISSES VS.  $m_b$  AND EPICENTRAL DISTANCE

Considerable difficulty has been encountered in forming beams for this particular source region. Signal degradation by the subarray beams ranges as high as four dB, and additional degradation results from forming the array beam. As a result the signal-to-noise ratio increase provided by array processing for this source region is eight or nine dB lower than for other source regions. Poor detectability then for this region is not surprising.

The second striking feature of Figure V-1 is the mixture of detections and non-detections in the distance range sixty to eighty degrees. Based on these events, the detection probability does not appear to vary as a function of magnitude over the range 3.6 to 4.3. These events are almost exclusively from the Japan-Kuriles-Kamchatka arc. The data were examined in search of a pattern relating to precise epicentral location, depth of source, and background noise level. No such pattern was evident. This seemingly anomalous behavior is not understood at the present time.

In view of these considerations it is desirable to treat detection probability as a function of source region. Unfortunately, the size of the population at the present time does not permit this, and it is necessary to lump the entire population together in order to obtain a reasonably stable estimate of the detection threshold. As more events are processed, it will be possible to refine these results and obtain regional detectability estimates.

Figure V-2 is a histogram representing the magnitude distribution of the 103 events which were processed. For magnitudes at which not all processed events were detected, the number of events detected is indicated by a dashed line. These data were used to obtain the estimates of incremental detection probability given in Figure V-3. In an effort to stabilize these estimates, the events were grouped in bins 0.2 magnitude units wide. The detection probability in each bin is the ratio of the number of events detected to the total number of events processed. As mentioned above, the population is sparse and there is considerable resultant scatter in the figure. It would appear, however, that the 90% detection level is somewhat near  $m_b = 4.3$  or  $4.4$ , which is about  $0.5 m_b$  units above LASA.

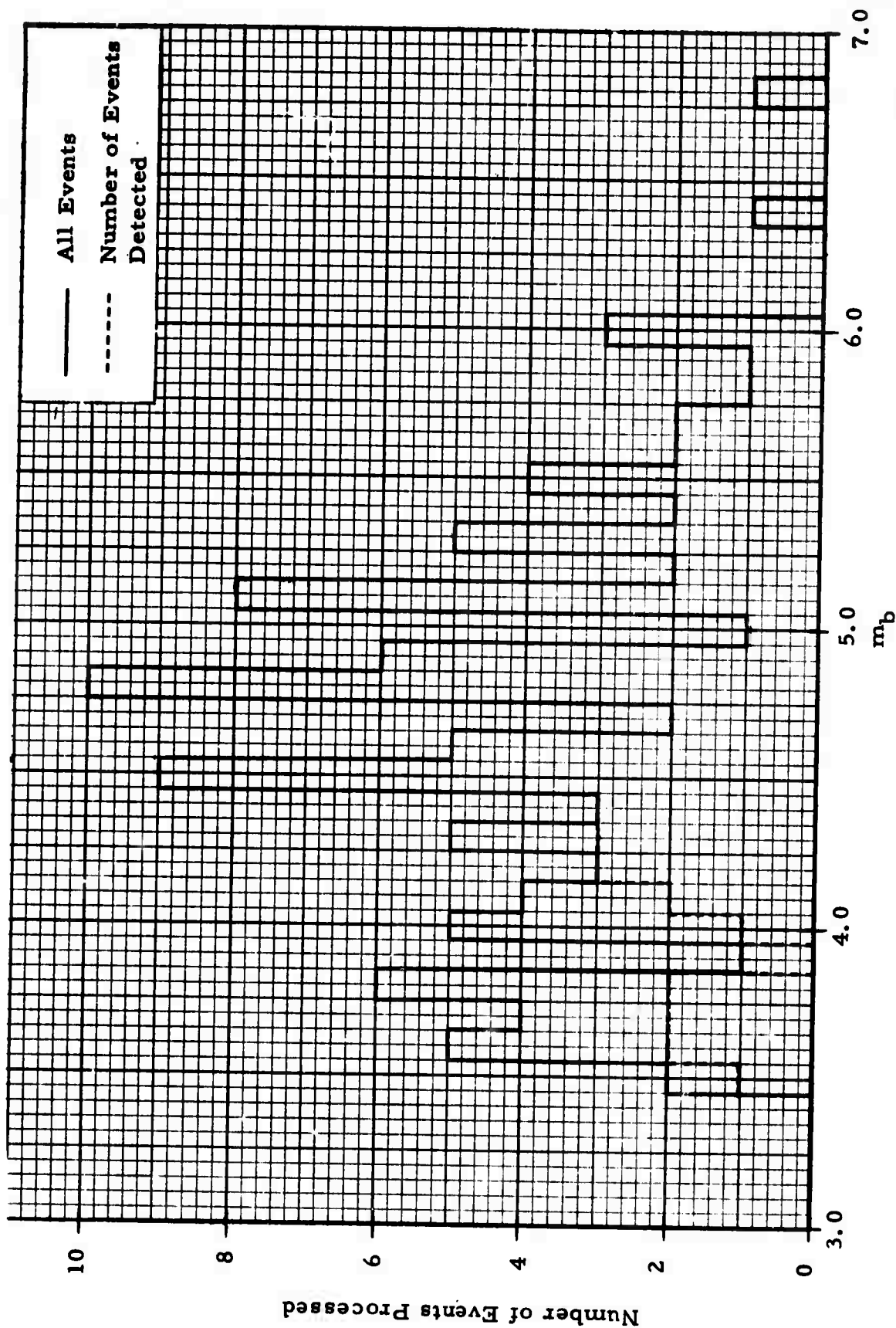


FIGURE V-2  
HISTOGRAM OF P WAVES PROCESSED AND DETECTED BY THE  
NORSAR SHORT-PERIOD ARRAY

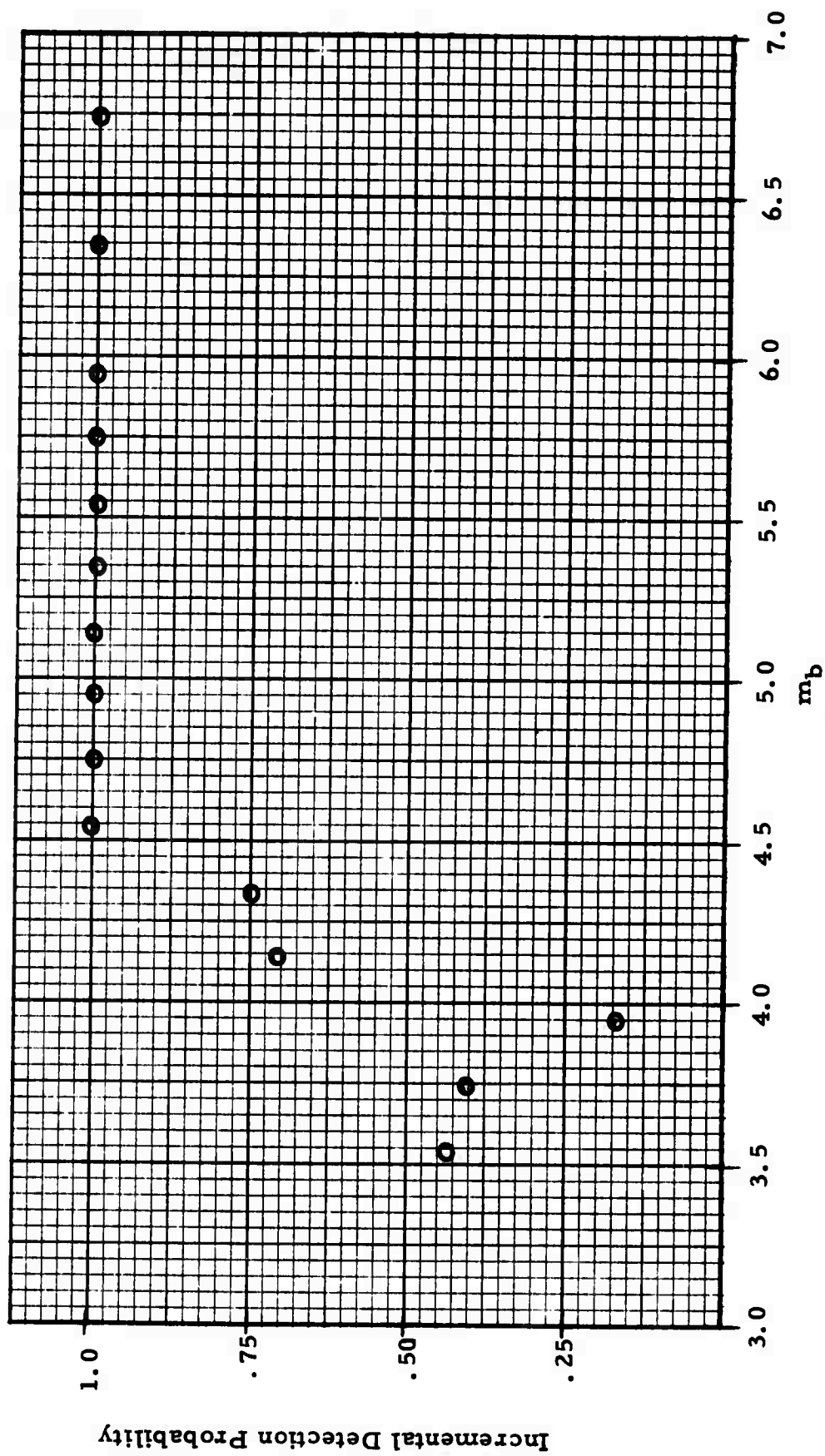


FIGURE V-3  
INCREMENTAL DETECTION PROBABILITY OF THE  
NORSAR SHORT-PERIOD ARRAY

As discussed in Section II, about 0.3  $m_b$  units can be accounted for on the basis of higher NORSAR noise levels in the detection band. The remaining 0.2 units may be real, may be due to the lack of data or may be associated with bias resulting from the four close-in events discussed above.

It should be noted that in most cases the adjusted delays used in beamforming were estimated directly from the event itself. Thus for large events these adjusted delays should be the best available. For the smaller events, however, there exists the possibility of contamination of the adjusted delays by background noise. The question as to whether the use of regional adjusted delays, estimated from an adequate population of large events, will improve or degrade these results at NORSAR has not been fully answered. A second qualification of these results arises from the fact that in all cases the data were beamsteered for a known source location and the detection/no detection decision was made by analyst. Thus the degradation inherent in an automated detection system was not a factor here. In view of these considerations the estimate of detection threshold must be considered as only tentative.

Future work in this area will concentrate on the following goals:

- Expansion of the population of events processed.
- Determination of regional detection thresholds, and resolution of anomalies within the regions.
- Evaluation of the efficacy of regional adjusted delays for use in NORSAR beamforming.

## SECTION VI

### SHORT-PERIOD DISCRIMINATION

#### A. DEFINITION OF DISCRIMINANTS

##### 1. P30 Mean Square

This discriminant, which is a measure of event complexity, is computed by crosscorrelating 4 sec of the waveform (beginning a few points before P-wave onset) with the next 30 seconds of the waveform and with the noise preceding the signal. A mean square, weighted by the lag, is then computed from the correlations over both 30 seconds of the noise and 30 seconds of the signal. The noise mean square is subtracted from the signal mean square to obtain the discriminant used (Texas Instruments Incorporated, 1971).

##### 2. Autocorrelation Mean Square

This discriminant is also a measure of complexity. The autocorrelations of a 30-second noise gate and of a 30-second signal gate are computed and a weighted mean square then derived from these correlations for the noise and signal. The discriminant is derived from the signal mean square minus the noise mean.

##### 3. Envelope Difference

This discriminant is also derived from the P30 correlation by computing the mean-square difference between the envelope correlation and a fixed decaying exponential, the decay rate of which is the average rate for an ensemble of 16 explosions recorded at LASA. As with the first two statistics, envelope difference is a measure of complexity.

##### 4. Dominant Period

This discriminant is computed by finding the cycle in the waveform with the maximum absolute amplitude; the dominant period is the duration of this cycle in seconds. This parameter can be estimated with some confidence, even

for events with a relatively low signal-to-noise ratio. The dominant period discriminant is a rough measure of spectral energy distribution.

## 5. Spectral Ratio

This discriminant is derived from the signal power spectrum over a gate beginning just before the signal arrival. In the original short-period discrimination package, the power spectrum is smoothed over three frequency points, and the power in two bands (0.35 to 0.85 Hz and 1.45 to 1.85 Hz) is computed. Dividing the power in the first band by that in the other band gives the discriminant used. The bands just mentioned appear to produce the best separation of earthquakes and presumed explosions for events processed using LASA data.

Noise spectra from NORSAR short-period data, however, have much higher relative levels at frequencies below 0.5 Hz. Most shallow earthquake spectra, furthermore, drop rapidly at frequencies above 1.5 Hz, while presumed explosions do not begin to fall off significantly until about 2.5 Hz. Thus, the NORSAR spectral ratio discriminant was computed by taking the ratio of energy in the band 1.5 Hz to 5.0 Hz to that in the band 0.55 Hz to 1.5 Hz.

## B. NORSAR SHORT-PERIOD DISCRIMINATION RESULTS

Short-period discriminant values for the discriminants just defined are plotted as a function of body-wave magnitude for all 85 detected events in Figures VI-1 to VI-12. Shallow earthquakes and earthquakes of unknown depth are represented by a cross. Deep earthquakes (of depths greater than 100 km) are denoted by a triangle. Presumed explosions are indicated by an asterisk. All seven events from the Western Hemisphere in these graphs are surrounded by a circle. The figures show that, as has been previously observed (Lacoss 1969), the short period discriminants are not effective for deep earthquakes. The figures also show that the discriminant values are very different for the limited Western Hemisphere earthquake and presumed explosion ensemble than they are for the Eurasian area. This is a very important (and sometimes overlooked) observation;

because the basic separation of the two populations usually is not large (for a given SP discriminant) path effects can "overpower" any separation inherent in the discriminant. Thus, a SP discriminant which works well at a station for source area A may not work at all for source area B. Conversely, an SP discriminant which works well for a source area at station X may not work at all for station Y.

The remainder of this section is confined to a discussion of the performance of the SP discriminants for shallow Eurasian events (crosses in the figures) and presumed explosions (asterisks in the figures).

Figure VI-1 shows the logarithm of the P30 mean square discriminant as a function of body-wave magnitude for the reference subarray beam; there is a wide region of overlap between the earthquake and presumed explosion population. Figure VI-2 shows the same discriminant for the adjusted-delay beam; separation is somewhat better, but there is still a considerable region of overlap.

Figure VI-3 shows the log of the autocorrelation mean square discriminant as a function of body-wave magnitude for the reference subarray beam. Again, there is a wide region of overlap between the earthquakes and presumed explosions. When the same discriminant is plotted for the adjusted-delay beam (Figure VI-4), better separation is apparent, but overlap still occurs.

The last of the discriminants based on event complexity, envelope difference, is presented in Figure VI-5 for the reference subarray beam. Overlap still persists. In Figure VI-6 the same discriminant computed from the adjusted-delay beam is given. Slightly better separation is apparent, but overlap still is severe.

The remaining discriminants to be presented in this section are based on spectral energy distribution. The first of these, the dominant-period discriminant, is shown in Figure VI-7. It would be possible to draw a straight line separating all but one earthquake from the presumed explosions. But the

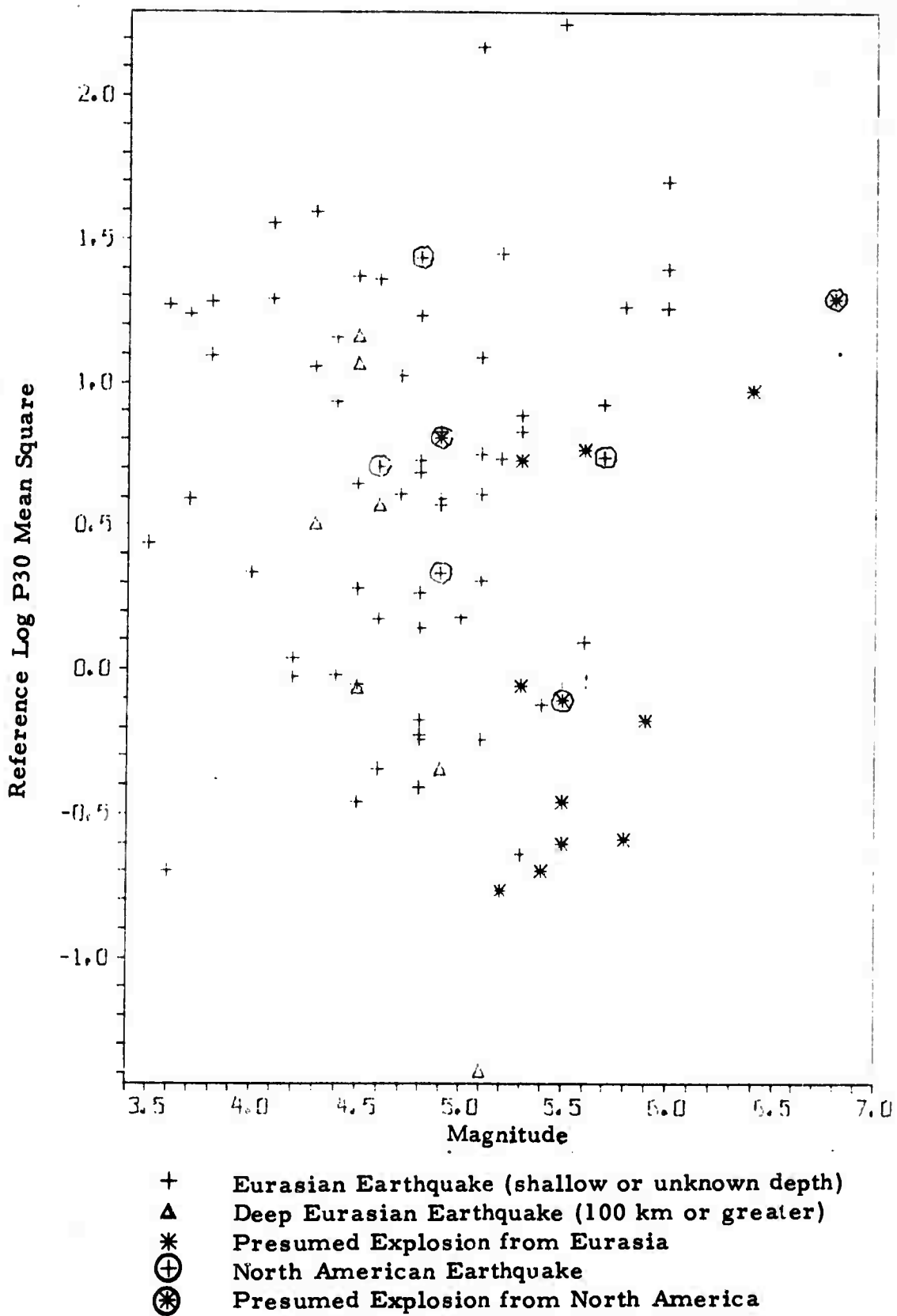


FIGURE VI-1

REFERENCE SUBARRAY P30 MEAN SQUARE DISCRIMINANT

VI-4

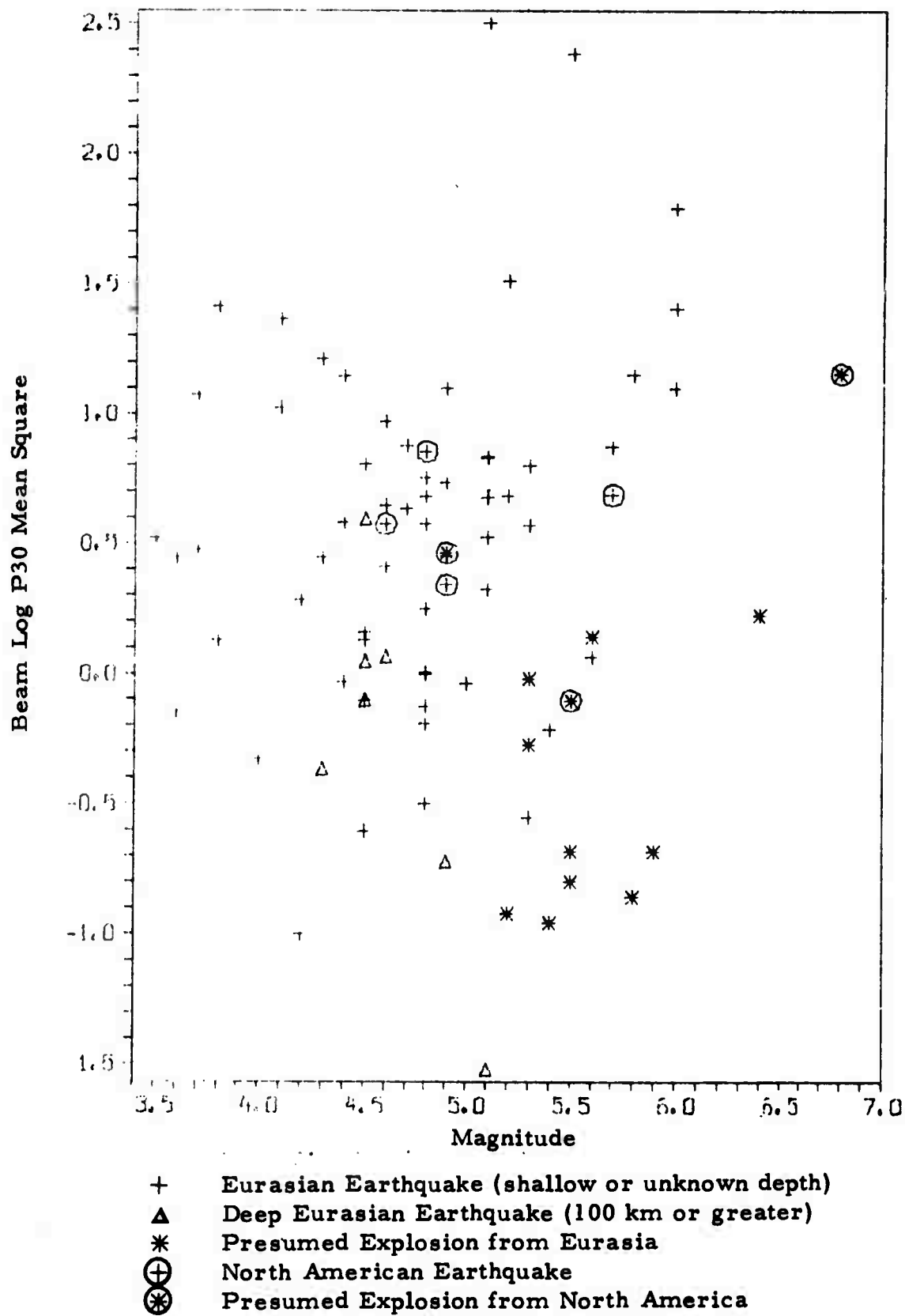
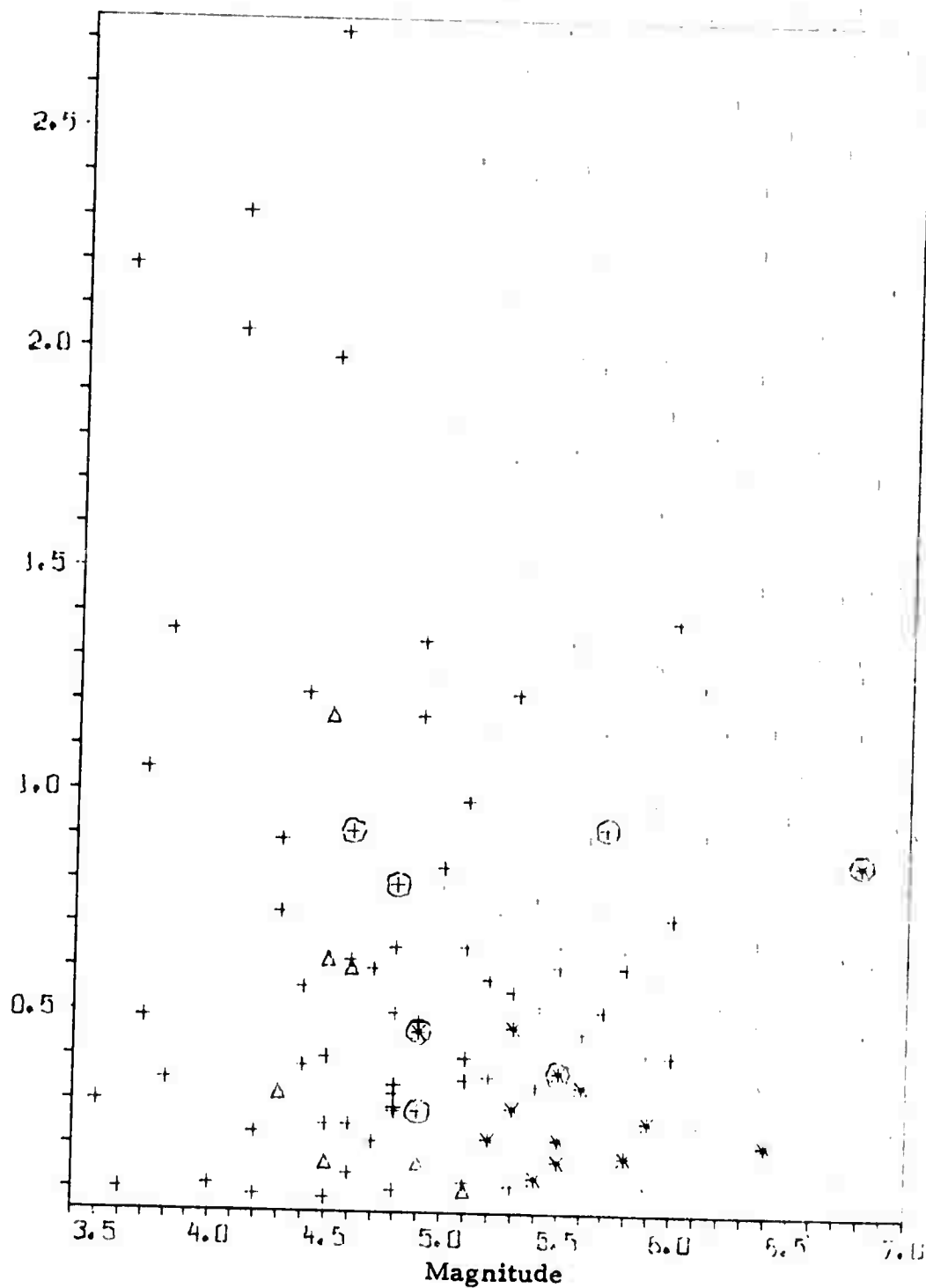


FIGURE VI-2  
ADJUSTED-DELAY BEAM P30 MEAN SQUARE DISCRIMINANT

Reference Log Autocorrelation Mean Square



- + Eurasian Earthquake (shallow or unknown depth)
- Δ Deep Eurasian Earthquake (100 km or greater)
- \* Presumed Explosion from Eurasia
- ⊕ North American Earthquake
- ⊗ Presumed Explosion from North America

FIGURE VI-3  
REFERENCE AUTOCORRELATION MEAN SQUARE



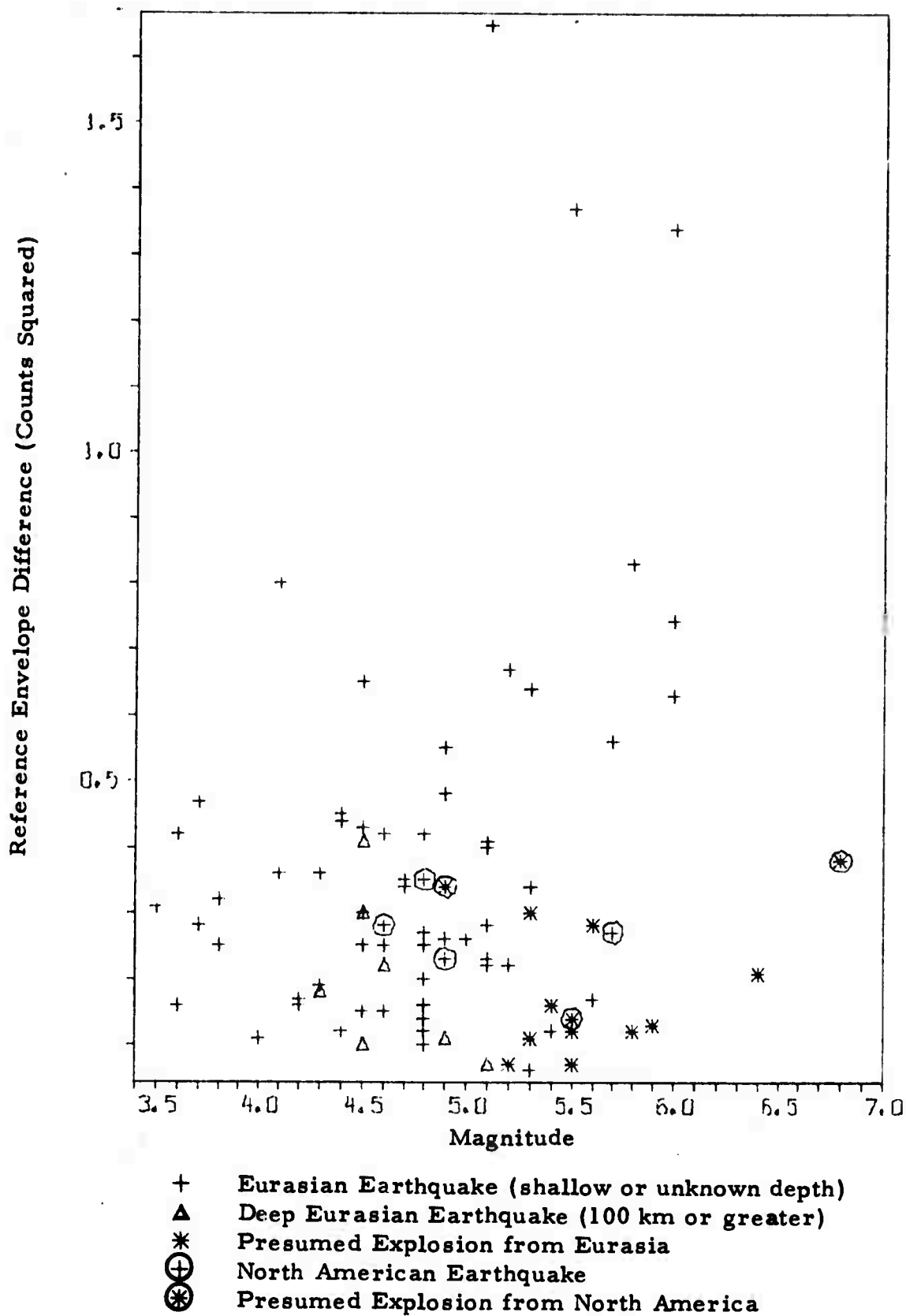
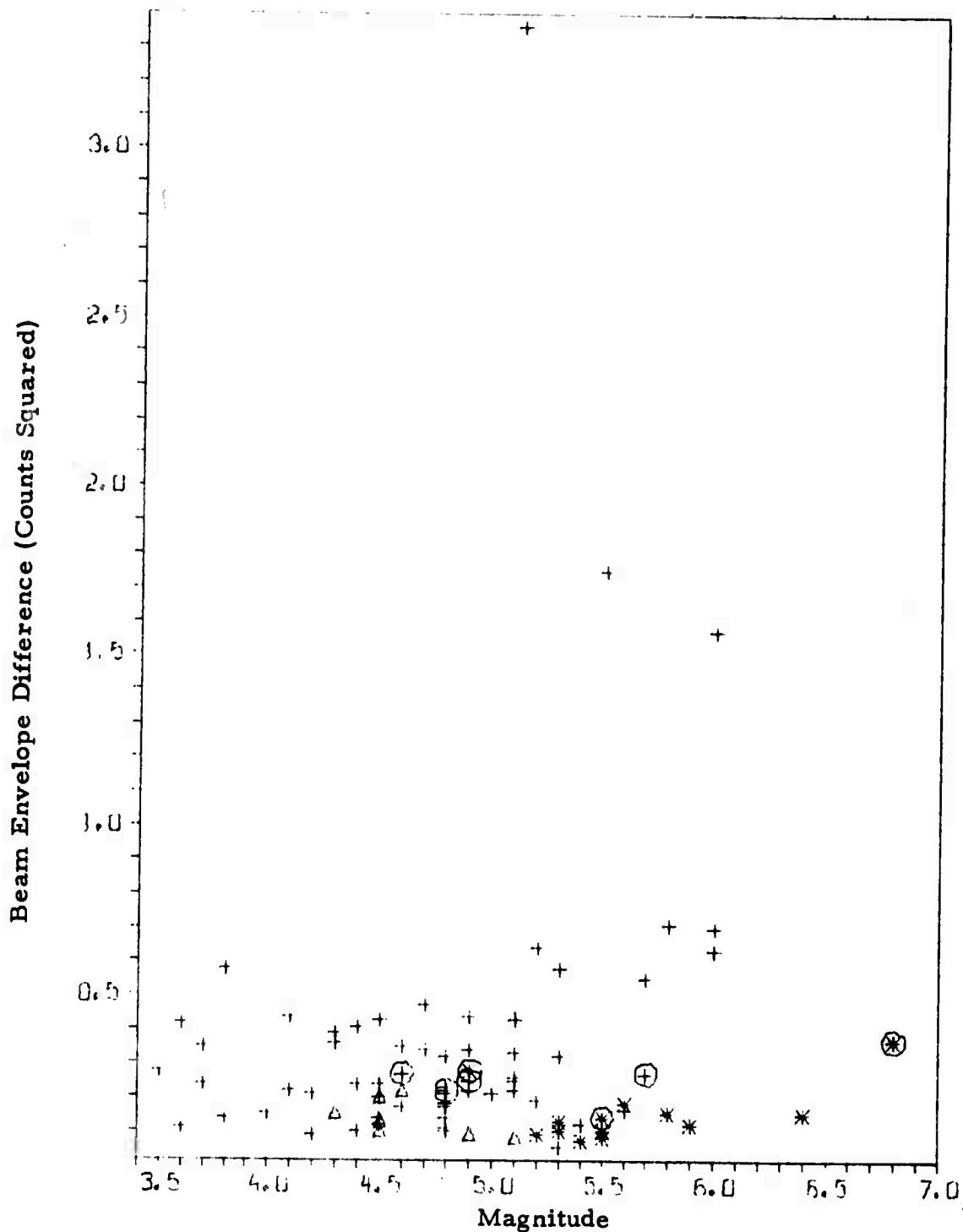


FIGURE VI-5  
REFERENCE ENVELOPE DIFFERENCE (COUNTS SQUARED)



- + Eurasian Earthquake (shallow or unknown depth)
- Δ Deep Eurasian Earthquake (100 km or greater)
- \* Presumed Explosion from Eurasia
- ⊕ North American Earthquake
- ⊗ Presumed Explosion from North America

FIGURE VI-6  
 ADJUSTED-DELAY BEAM ENVELOPE DIFFERENCE (COUNTS SQUARED)  
 VI-9

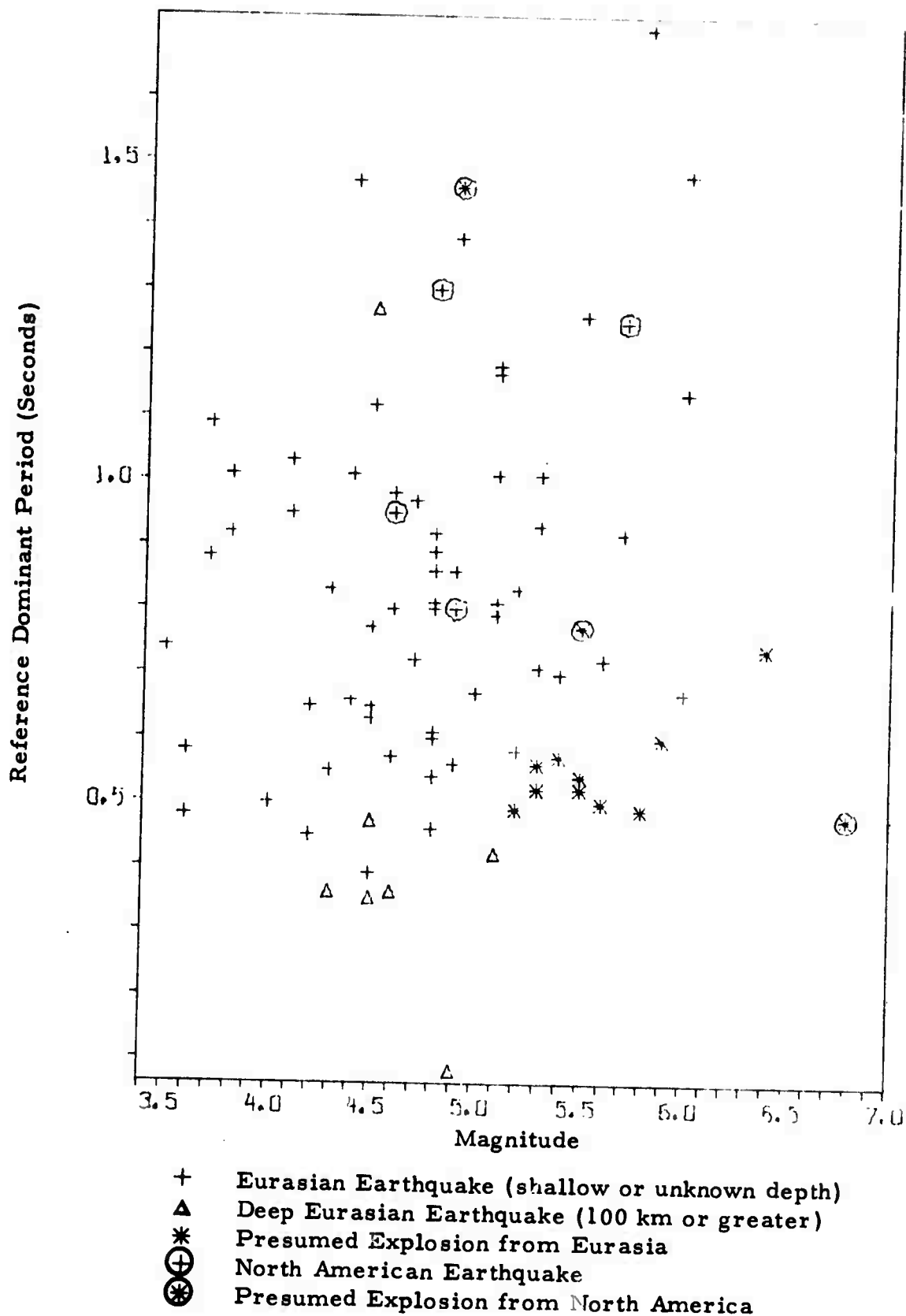


FIGURE VI-7  
REFERENCE DOMINANT PERIOD (SECONDS)

separation, even ignoring the one earthquake, is extremely small. If presumed explosions of smaller magnitude had been processed, it is likely that there would be more overlap. The dominant-period discriminant calculated from the adjusted-delay beam is presented in Figure VI-8. In this case, there is one presumed explosion inside the earthquake population. The reason for this anomalous point will be discussed later. Ignoring this point, there is a noticeable separation between the earthquakes and the presumed explosions.

The spectral ratio of energy in the band 0.3 to 0.8 Hz to that in the band 1.4 to 1.8 Hz is graphed in Figure VI-9 for the reference subarray beam. The choice of bands was based on events processed using LASA data. Two presumed explosions lie within the earthquake population, and one earthquake lies within the presumed explosion population. In Figure VI-10, the same discriminant is plotted for the adjusted-delay beam. Here the overlap is considerably worse.

After examination of spectra for earthquakes and presumed explosions received at NORSAR, the bands 1.5 to 5.0 Hz and 0.55 to 1.5 Hz were selected for use in a spectral ratio discriminant. Figure VI-11 is a plot of the resultant spectral ratios for the reference subarray beam. Two presumed explosions lie within the earthquake population. The corresponding spectral ratios for the adjusted-delay beam are shown in Figure VI-12. The same two presumed explosions lie within the earthquake population. In both figures, all other presumed explosions from the Eurasian area lie along a curve at the top right of the graphs.

One of the two presumed explosions within the earthquake population was a magnitude 5.3 event from Western Russia on day 295 of 1971 (Figure VI-13). It was very difficult to decide on the adjusted delays to be used in forming the array beam for this event. When different portions of the signal trace or different features in the trace were used for determining the adjusted delays, different results were obtained. It is likely that much of the high-frequency

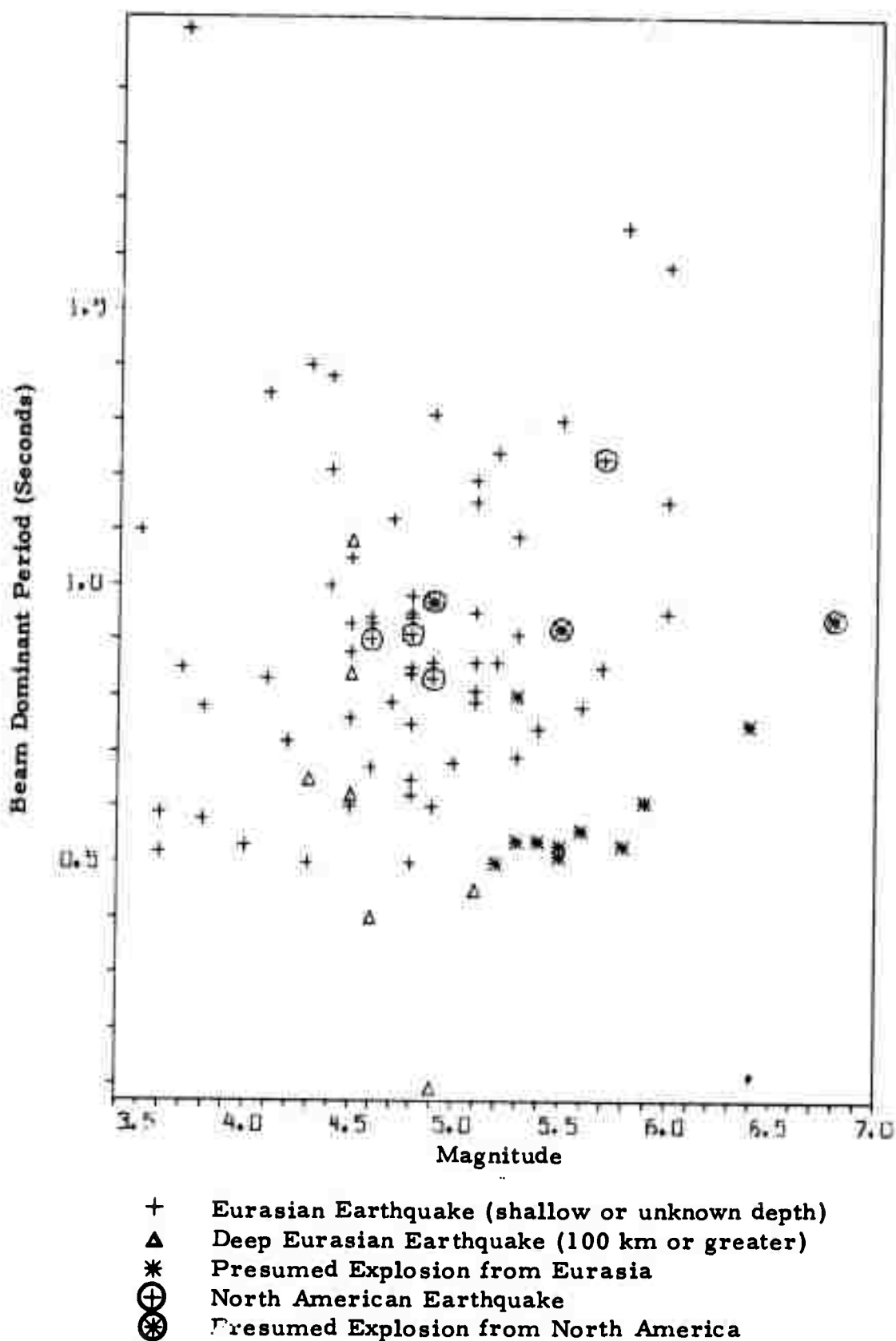


FIGURE VI-8  
ADJUSTED-DELAY BEAM DOMINANT PERIOD (SECONDS)

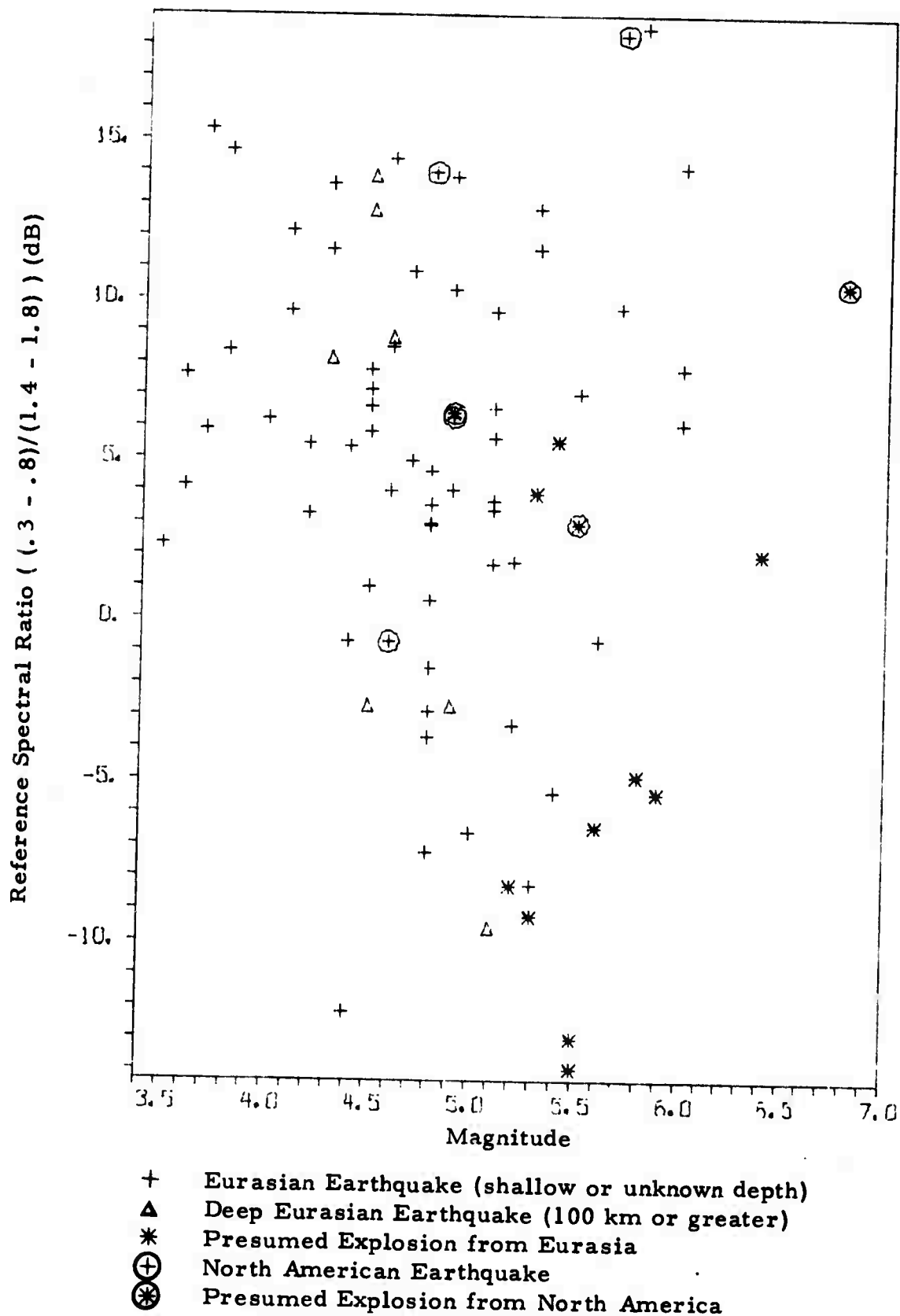


FIGURE VI-9  
REFERENCE SPECTRAL RATIO  $\left[ \frac{(0.3-0.8)}{(1.4-1.8)} \right]$  (dB)

VI-13

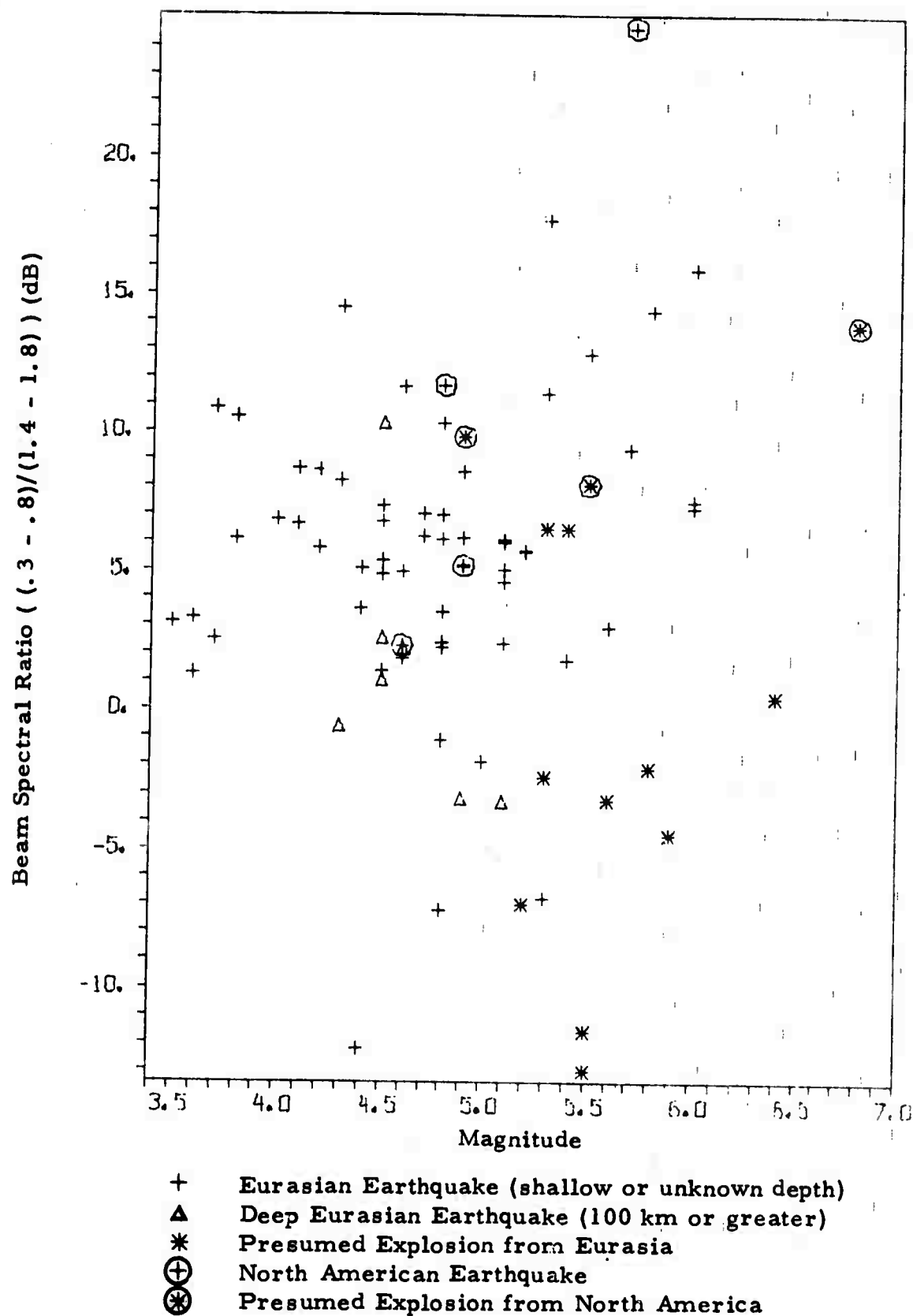
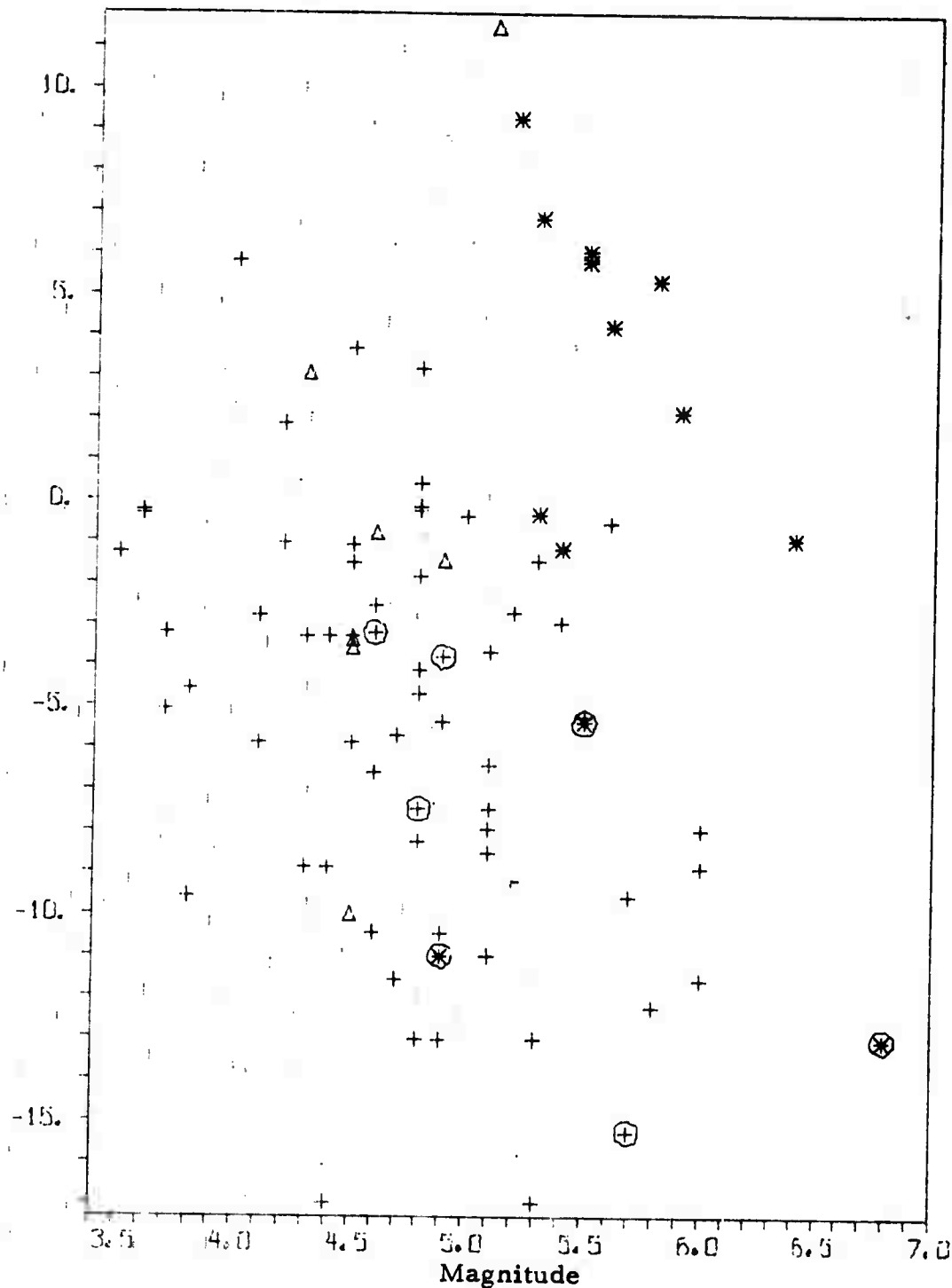


FIGURE VI-10  
ADJUSTED-DELAY BEAM SPECTRAL RATIO  
[(0.3-0.8)/(1.4-1.8)] (dB)

VI-14

Reference Spectral Ratio  $(1.5 - 5) / (0.55 - 1.5)$  (dB)



- + Eurasian Earthquake (shallow or unknown depth)
- Δ Deep Eurasian Earthquake (100 km or greater)
- \* Presumed Explosion from Eurasia
- ⊕ North American Earthquake
- ⊗ Presumed Explosion from North America

FIGURE VI-11

REFERENCE SPECTRAL RATIO  
 $[(1.5-5)/(0.55-1.5)]$  (dB)

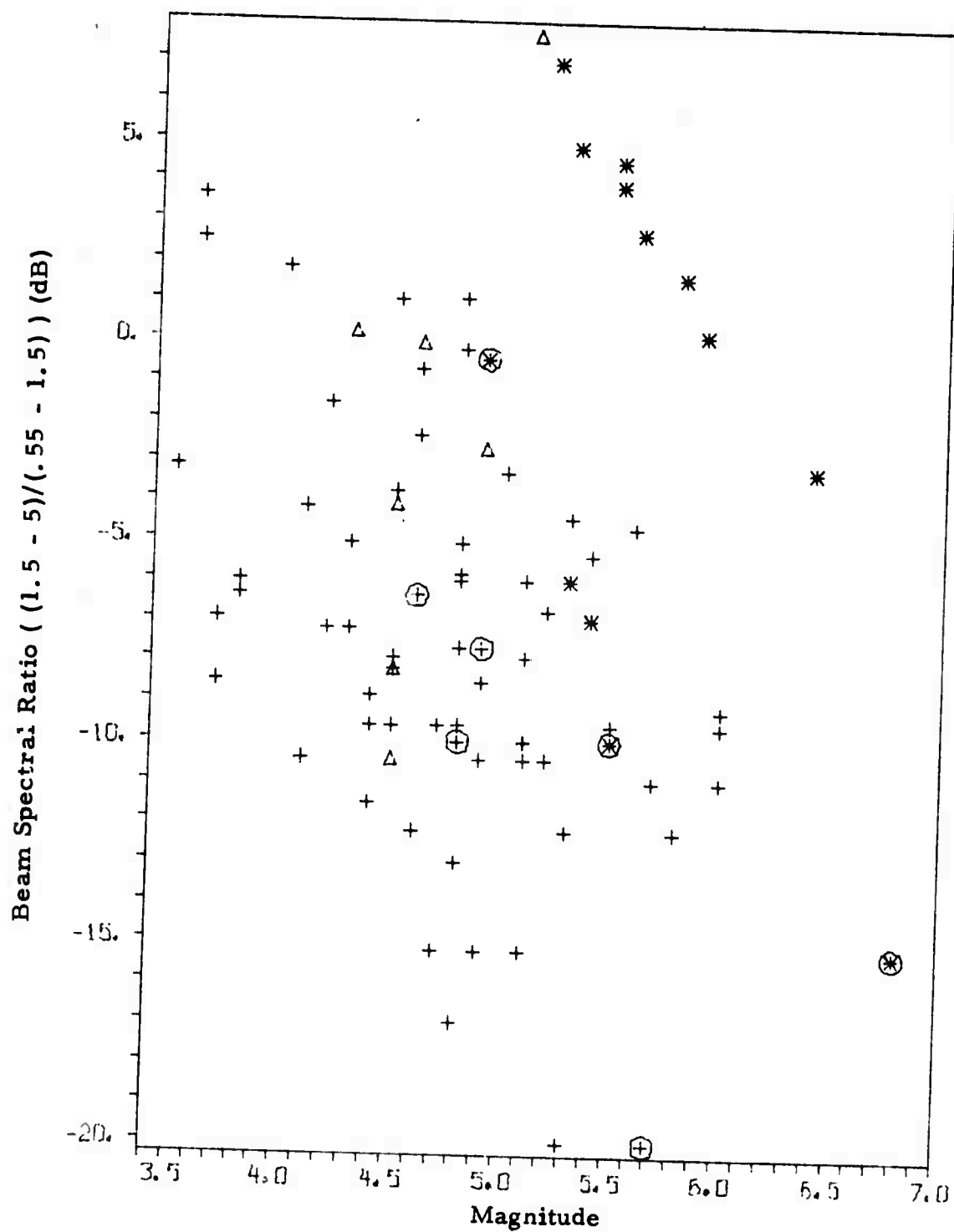


FIGURE VI-12  
ADJUSTED-DELAY BEAM SPECTRAL RATIO  
[(1.5-5)/(0.55-1.5)] (dB)

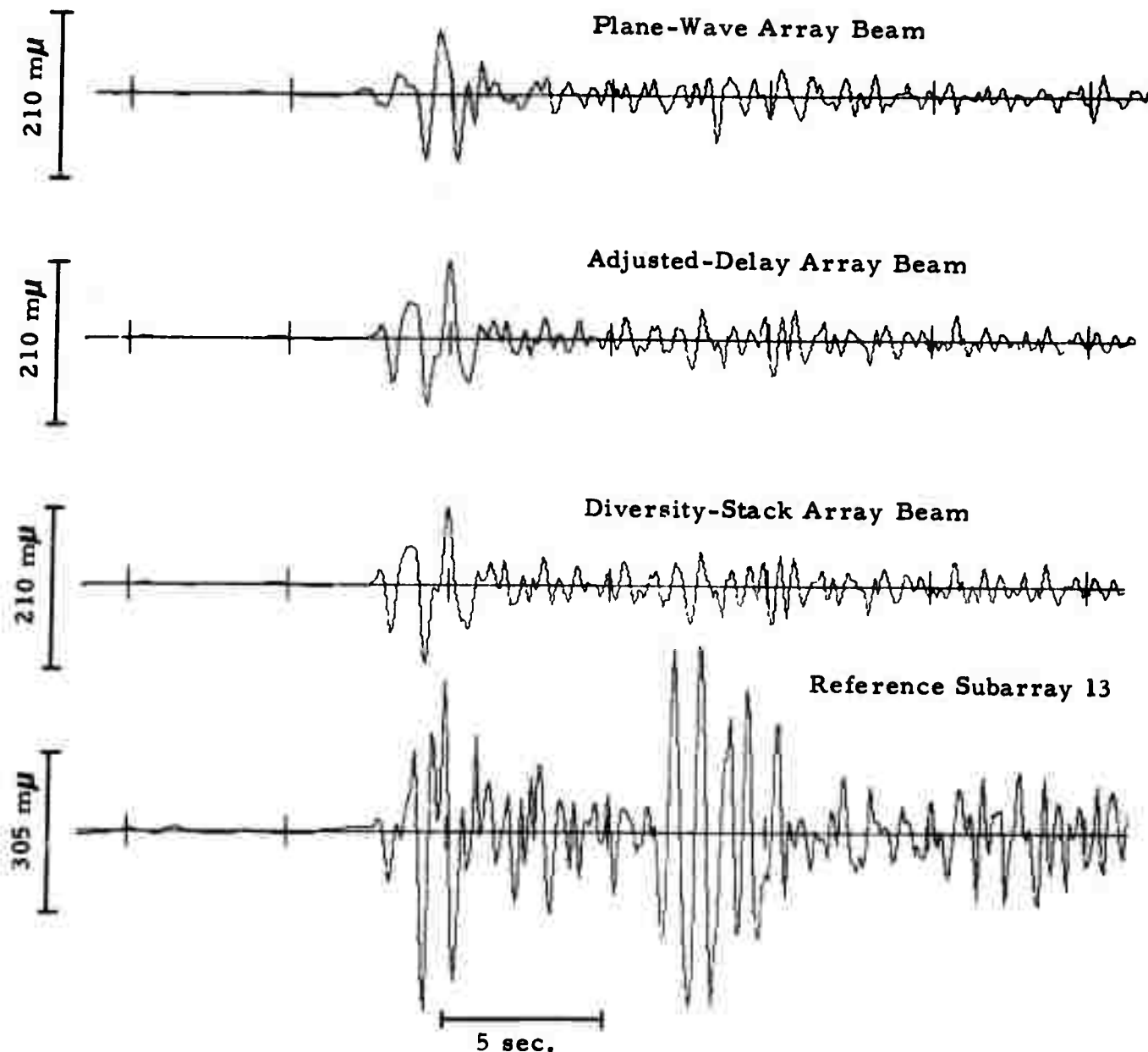


FIGURE VI-13  
MAGNITUDE 5.3 EVENT FROM WESTERN RUSSIA  
(DAY 295 OF 1971, 05:00:00)

energy was lost in forming the array beam. In Figure VI-7 (dominant period for the reference subarray), this event lies at the edge of the presumed explosion population. In Figure VI-8 (dominant period for the adjusted-delay beam), however, this event is the one anomalous point.

The other presumed explosion within the earthquake population was a magnitude 5.4 event from Eastern Kazakh on day 181 of 1971 (see Figure VI-14). The dominant-period discriminant is just able to place this event within the presumed explosion population (see Figures VI-7 and VI-8), whereas the spectral ratio discriminant places this event within the earthquake population. A comparison of the reference subarray beam and the adjusted-delay beam (Figure VI-14) would suggest that the beamforming process was responsible for the loss of high-frequency energy. In the case of the reference subarray beam, the spectral ratio for this event (see Figure VI-11) lies just within the earthquake population. For the adjusted-delay beam, however, the spectral ratio for this event (see Figure VI-12) is buried somewhat more deeply within the earthquake population. The adjusted delays for this area are believed to be well-determined. We cannot explain the reason why so much of the high-frequency energy is lost in the adjusted-delay beam.

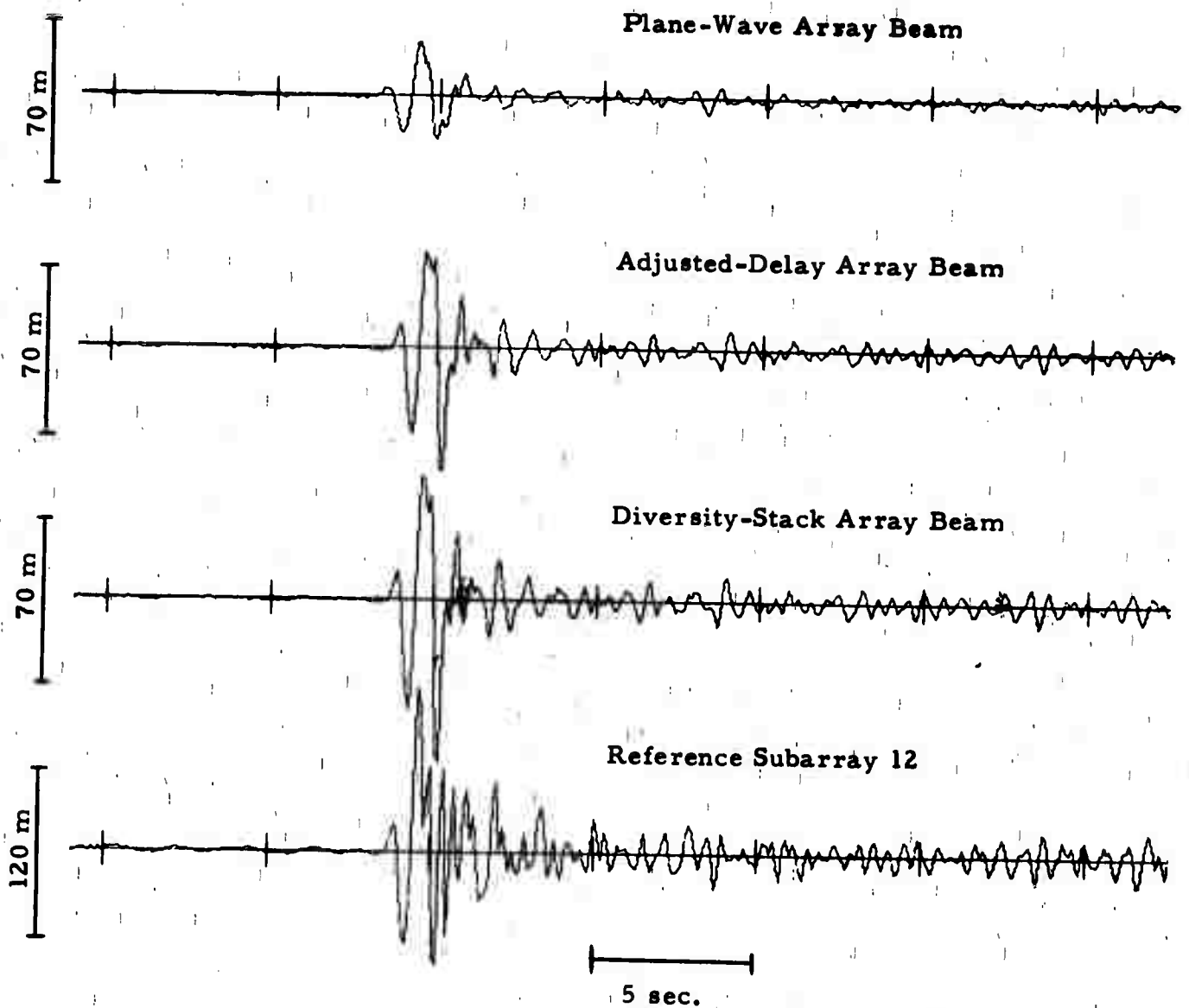


FIGURE VI-14  
MAGNITUDE 5.4 EVENT FROM EASTERN KAZAKH  
(DAY 181 OF 1971, 03:56:57)

## SECTION VII

### CONCLUSIONS AND FUTURE PLANS

#### A. CONCLUSIONS

Conclusions about the performance of the short period NORSAR array, based on analysis of just over 100 signals (primarily from Eurasia) and 72 noise samples, are given below.

Data quality is excellent. For about one-half of the samples all 132 sensors were operational. For most of the rest of the samples one or two subarrays (6 or 12 sensors) were inoperative; the worst data loss was 19 sensors. There were essentially no spikes or glitches in the data.

Conclusions from the noise analysis are based on 72 samples and can be stated with good confidence. Major results are:

- The noise spectral shape is very simple. The peak occurs at 3 to 6 seconds and the spectra decrease rapidly at shorter periods. The spectral shape does not change significantly either across the array or with time.
- Noise levels are very similar across the array. Maximum single sensor variations typically are  $\pm 6$  dB, and most sensors are within  $\pm 3$  dB of the average single sensor level. Variation among subarray beam noise levels in the region of significant power (0 to 2.0 Hz) is  $\pm 2$  dB.
- Wideband RMS noise levels show a definite seasonal dependence; wintertime levels are 6 dB higher. The increased wintertime level results because the 3 to 6 second microseismic peak is stronger in the winter. Application of the "standard" bandpass filter, which rolls off sharply at high frequencies, reduces the difference between summertime and wintertime noise levels.

Preceding page blank

- RMS levels on the "standard"-filtered adjusted-delay array beam range from 0.04 to 0.17  $m\mu$ , and typically are 0.12  $m\mu$ . This is about a factor of two higher than LASA detection-filtered beam noise levels.
- Multiple coherence levels within a subarray are low except at the 3 to 6 second microseismic peak. Inter-subarray multiple coherencies are low over the entire 0 to 5.0 Hz band.

Major conclusions from the signal analysis are:

- Except for a few close-in, high-frequency events signal similarity is good within a subarray. Among subarrays, however, similarity is quite variable.
- Amplitude variations across the array typically are 4:1. Some regions (e.g., Kazakh) show variations as high as 10:1.
- Eurasian signals usually have a substantial amount of high frequency energy (out to about 2 Hz). Spectral shapes are quite variable, but the close-in events ( $\Delta < 30^\circ$ ) generally have more high-frequency content. The limited ensemble of Western hemisphere events processed show substantially less high frequency energy than the Eurasian events.
- Time-delay anomalies (deviation from plane wave propagation along the great circle path) are not significant for subarray beamforming, except perhaps for a few close-in events. Anomalies are significant however, among subarrays and corrections are essential for array beamforming. Consistent subarray delay anomalies could be obtained for all regions except those within  $30^\circ$  epicentral distance of NORSAR.
- NORSAR  $m_b$ 's averaged about 0.2 units less than PDE (and LASA)  $m_b$ 's. This discrepancy can be explained as signal loss in array beamforming, and thus it appears that NORSAR  $m_b$ 's, if corrected

for signal loss, are about the same as PDE  $m_b$ 's. The PDE-NORSAR  $m_b$  differences do appear to be larger at low magnitudes; this may be because the low magnitude PDE  $m_b$ 's are obtained from the quieter stations in the PDE network (e.g., TFO), which normally have lower than average signal amplitudes.

Major conclusions from the array processing performance study are:

- $\sqrt{N}$  noise rejection is achieved over the entire 0 to 5 Hz band for both subarray and array beamforming. Thus noise rejection totals about 21 dB (8 for subarray and 13 for array beamforming).
- Signal degradation for subarray beamforming typically is 1 dB but for some close-in high-frequency signals loss appears to be about 3 or 4 dB.
- Signal degradation for array beamforming is quite variable, but generally appears to be only about 2 to 4 dB. On some events, however, degradation appears to be as high as 11 dB. It should be pointed out that it is quite difficult to estimate array beamforming signal degradation, especially when it is large, because of the dissimilarity of subarray waveforms.
- Net signal-to-noise ratio (SNR) typically is 15 to 18 dB. For the problem close-in events gains drop as low as about 10 dB. For these events the reference subarray beam often has a higher SNR than the array beam. (Usually the array beam SNR is about 1 to 5 dB higher than the reference subarray beam SNR).
- Diversity stack beamforming provides 0 to 2.5 dB, and typically 1 dB, better SNR improvement than the adjusted-delay beam.
- For detection of Eurasian events, a bandpass filter with corner frequencies at about 1.2 and 2.8 Hz and a very sharp rolloff at low frequencies appears to be about optimum. The relatively high bandpass is desirable because event SNR's generally peak at about 1.5 Hz.

This filter may not be best for Western hemisphere events which appear to have somewhat lower signal spectral content.

A preliminary estimate of the NORSAR detection threshold for Eurasian events gives a 90% incremental value of  $m_b \sim 4.3$ . Much more data are required to obtain a reliable estimate, however.

Standard short-period discriminants were calculated for all detected events, and the conclusions are:

- Discriminants based on event complexity (P30 mean square, autocorrelation mean square, and envelope difference) do not appear to be very effective in separating shallow earthquakes or earthquakes of unknown depth from presumed explosions for Eurasian events.
- Discriminants based on spectral energy distribution (dominant period and spectral ratio) appear to work reasonably effectively, although complete separation between Eurasian earthquakes and presumed explosions was not achieved. Surprisingly, the very simple dominant period measurement gave the best results. The spectral ratio of energy in the bands 0.3 to 0.8 Hz and 1.4 to 1.8 Hz was clearly inferior to the ratio of energy in the bands 0.55 to 1.5 Hz and 1.5 to 5.0 Hz. This fact is not surprising, since the first two bands were based on events processed using LASA data.
- The short period discriminant values for Eurasian events are significantly different than those obtained for a limited ensemble of Western hemisphere earthquakes and presumed explosions. This observation points out that the effectiveness of short-period discriminants depends on the source and station location.

## B. FUTURE PLANS

Future NORSAR short-period evaluation efforts will concentrate on increasing the Eurasian event ensemble, emphasizing low-magnitude events, in order to improve estimates of the array detection capability. Close-in events will be analyzed in detail in an attempt to find techniques for improving array SNR gain.

## SECTION VIII

### REFERENCES

- Dean, W.C., R.O. Ahner, E.F. Chiburis, 1971, Evaluation of the SAAC-LASA System; SAAC Special Report No. 1 AFTAC Contract F33657-71-C-0510, August.
- Lacoss, R.T., 1969, A Large Population LASA Discrimination Experiment; Technical Note 1969-24, Lincoln Laboratory Report No. 862-5500, MIT, Lexington, Mass., April.
- Swindell, W.H., 1972, Preliminary Evaluation of the Norwegian Long Period Array, prepared for AFTAC, Contract No. F33657-71-C-0843, Texas Instruments Incorporated, Dallas, Texas, April.
- Texas Instruments, Incorporated, 1971, Documentation of NORSAR Short Period Array Evaluation Software Package, prepared for AFTAC, Contract Number F33657-69-C-1063, Dallas, Texas, March.